AD_____

Award Number: W81XWH-08-1-0037

TITLE: Bone Marrow Microenvironmental Control of Prostate Cancer Skeletal Localization

PRINCIPAL INVESTIGATOR: Laurie McCauley

CONTRACTING ORGANIZATION: The University of Michigan
Ann Arbor, MI 48109

REPORT DATE: May 2011

TYPE OF REPORT: Final

PREPARED FOR: U.S. Army Medical Research and Materiel Command
Fort Detrick, Maryland 21702-5012

Final

REPORT DOCUMENTATION PAGE

Form Approved
OMB No. 0704-0188

1. REPORT DATE *(DD-MM-YYYY)*	2. REPORT TYPE	3. DATES COVERED *(From - To)*
01-05-2011		21 APR 2008-20 APR 2011

4. TITLE AND SUBTITLE
Bone Marrow Microenvironmental Control of Prostate Cancer Skeletal Localization

5a. CONTRACT NUMBER

5b. GRANT NUMBER
W81XWH-08-1-0037

5c. PROGRAM ELEMENT NUMBER

6. AUTHOR(S)
Laurie McCauley

E-Mail: lauriemccauley@gmail.com

5d. PROJECT NUMBER

5e. TASK NUMBER

5f. WORK UNIT NUMBER

7. PERFORMING ORGANIZATION NAME(S) AND ADDRESS(ES)
The University of Michigan
Ann Arbor, MI 48109

8. PERFORMING ORGANIZATION REPORT NUMBER

9. SPONSORING / MONITORING AGENCY NAME(S) AND ADDRESS(ES)
U.S. Army Medical Research and Materiel Command
Fort Detrick, Maryland 21702-5012

10. SPONSOR/MONITOR'S ACRONYM(S)

11. SPONSOR/MONITOR'S REPORT NUMBER(S)

12. DISTRIBUTION / AVAILABILITY STATEMENT
Approved for Public Release; Distribution Unlimited

13. SUPPLEMENTARY NOTES

14. ABSTRACT

The purpose of this study is to analyze the role of prostate cancer derived PTHrP and its ability to impact the bone marrow microenvironment of the skeletal metastasis. During the second year of the project, prostate cancer cells expressing altered levels of PTHrP were used to show that PTHrP prevents anoikis (a form of cell death) in tumor cells contributing to tumor growth in vivo. PTHrP was also associated with increased macrophage recruitment to tumors. Altering the bone marrow microenvironment with a chemotherapeutic agent (cyclophosphamide) increased tumor engraftment. This promotion of tumor growth was attributed to altered vascular architecture and the production of CCL2 (MCP-1) in the bone marrow microenvironment. These studies provide strong support that there are key and controllable events that can be triggered in the bone marrow to prevent tumor growth.

15. SUBJECT TERMS
No subject terms provided.

16. SECURITY CLASSIFICATION OF:			17. LIMITATION OF ABSTRACT	18. NUMBER OF PAGES	19a. NAME OF RESPONSIBLE PERSON
a. REPORT	b. ABSTRACT	c. THIS PAGE			USAMRMC
U	U	U	UU	117	19b. TELEPHONE NUMBER *(include area code)*

Table of Contents

INTRODUCTION:

Prostate carcinoma metastasizes to skeletal sites where bone remodeling is active and engages the bone marrow niche in an unstable cascade with dysregulated bone resorption and formation. Numerous factors in the bone marrow niche have been implicated that support tumor growth. This proposal is focused on parathyroid hormone related protein (PTHrP), a tumor-derived factor that increases angiogenesis and enriches the bone marrow complement of hematopoietic stem cells (HSCs) and hematopoietic progenitor cells (HPCs). The overall hypothesis is that: Prostate cancer-derived PTHrP increases hematopoietic cells which in turn support tumor localization and growth in the bone marrow microenvironment. Two specific aims will validate this hypothesis using novel but well characterized animal models accompanied by *in vitro* cell biologic approaches. The first aim will determine the contribution of prostate cancer-derived PTHrP acting as a stem cell factor to facilitate prostate cancer residency in the bone microenvironment. Aim two will identify a pro-angiogenic impact of prostate cancer-derived PTHrP and elucidate its role in prostate carcinoma residency in the bone microenvironment. Prostate cancer lines expressing varying levels of PTHrP will be used in models where angiogenesis is measured and then altered to verify the PTHrP angiogenic response and dependence for the tumor impact on hematopoietic cells and the osteoblastic response.

BODY:

Task 1: Aim 1: Impact of PTHrP on hematopoietic cells (HCs)

Prostate cancer tumor cells that express varied levels of PTHrP have been utilized to determine the impact of prostate cancer derived PTHrP on hematopoietic cells in the tumor as well as in the bone marrow. Figure 1,2 shows that higher PTHrP producing tumors have higher levels of CD11b+Gr-1+ hematopoietic cells in the tumors as well as in the bone marrow of mice bearing tumors. These hematopoietic cells share markers with cells termed myeloid derived suppressor cells (MDSCs) which have been found to be tumor promoting cells. These data implicate PTHrP derived from prostate cancer in the pathogenesis of prostate cancer metastasis to bone. This aspect of the project is complete.

Task 2: Aim 1: Altered hematopoietic microenvironment and tumor localization (Cyclosphosphamide)

This work was largely completed and reported with a previous annual review and will be summarized briefly here. It was submitted for publication to a high impact journal during year 3 but was not accepted. It was recently revised in response to reviewer critique and submitted to Cancer Research where it is conditionally accepted and revisions are nearly complete. The effects of cyclophosphamide, a bone marrow-suppressive chemotherapeutic drug, were investigated on the development and growth of metastatic tumors in bone using an experimental prostate cancer metastasis model. Priming the murine host with cyclophosphamide prior to intra-cardiac tumor cell inoculation was found to significantly promote tumor localization and subsequent growth in bone (Figure 3). Abrupt expansion of myeloid lineage cells in the bone marrow and the peripheral blood was observed shortly after cyclophosphamide treatment, associated with increases in cytokines with myelogenic potentials such as C-C chemokine ligand (CCL) 2, interleukin (IL)-6 and vascular endothelial growth factor (VEGF)-A (Figure 5). More importantly, neutralizing host-derived murine CCL2, but not IL-6, in the pre-metastatic murine host significantly reduced the pro-metastatic effects of cyclophosphamide. These data suggest that bone marrow perturbation by cytotoxic chemotherapy contributes to bone metastasis, mediated by a transient increase of bone marrow myeloid cells and myelogenic cytokines that can be clinically intervened by blocking CCL2. This aspect of the project is complete.

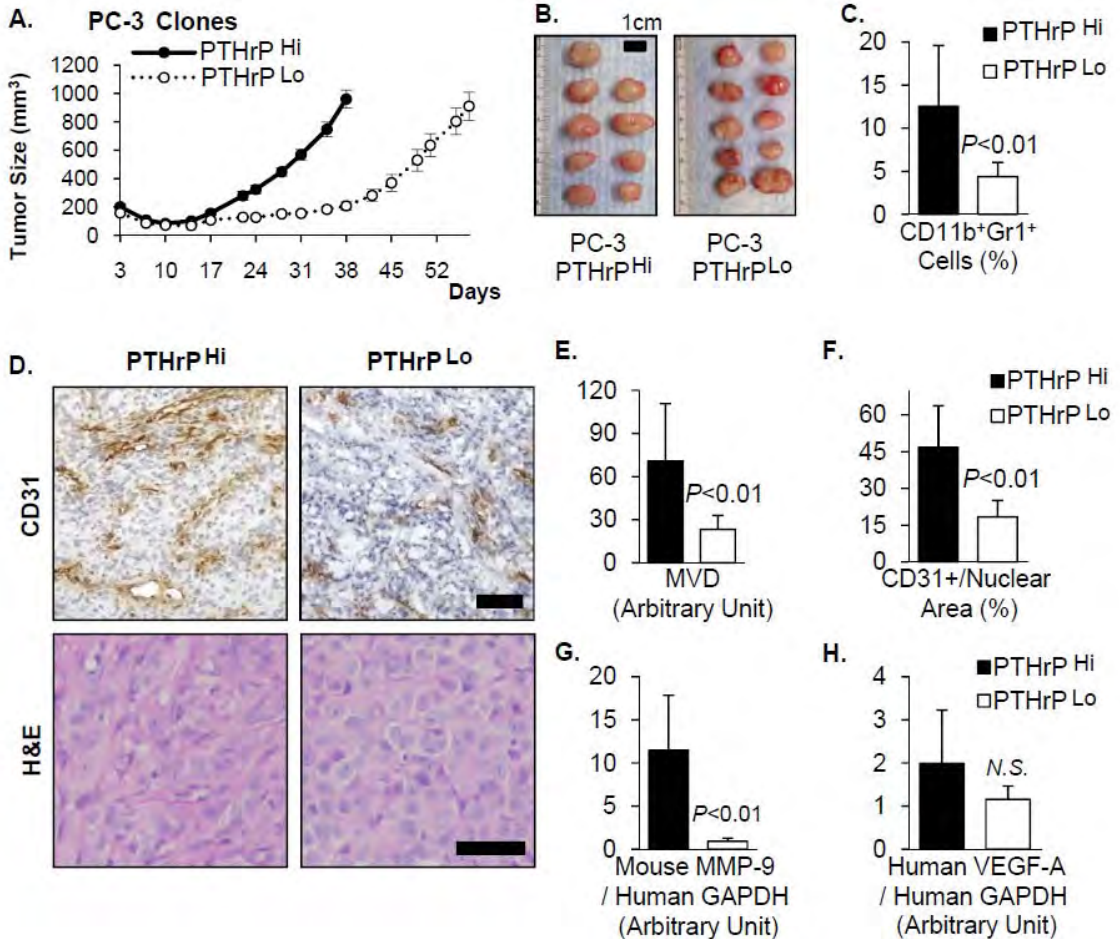

Figure 1 Reduction of PTHrP expression in PC-3 prostate cancer cells decreased CD11b^{+}Gr1^{+} cell recruitment and tumor angiogenesis. PC-3 cells expressing two different levels of PTHrP (961.8±12.8 *vs.* 457.8±4.1 pg ml^{-1} 1×10^{6}cells^{-1} 48h^{-1}; designated PTHrP^{Hi} and PTHrP^{Lo}, respectively) were selected and injected subcutaneously into male athymic mice (*n*=9 for PTHrP^{Hi} and *n*=10 for PTHrP^{Lo}). **A**. PTHrP^{Lo} tumors were grown for an extended period (i.e. 57 days) to reach the similar mean tumor volume as PTHrP^{Hi} tumors (grown for 38 days). **B**. PTHrP^{Hi} and -^{Lo} tumors were surgically dissected on the same day and photographed. Mean tumor volume between two groups was not significantly different (*P*=0.68, Student's t-test). Scale bar: 1cm. **C**. Tumor tissues were mechanically and enzymatically dissociated in order for flow cytometric analyses of CD11b^{+}Gr1^{+} double-positive cells. PTHrP^{Lo} tumors had significantly reduced percentage of CD11b^{+}Gr1^{+} cells compared with PTHrP^{Hi} tumors. *P*<0.05, Student's t-test. **D**. Tumor tissues were sectioned for H&E staining and murine CD31/PECAM immunohistochemical staining. Representative images were selected to show from 3~4 randomly selected fields from each tissue (*n*=9~10 per group). Original magnification, ×20. Scale bars: 50μm. **E and F**. Microscopic images were analyzed for quantification of tumor vasculature (brown stain) normalized to total nuclear area (blue stain). PTHrP^{Lo} tumors had significantly reduced mean vessel density (MVD) and CD31-positive vascular area, compared with PTHrP^{Hi} tumors (*P*<0.01 and *P*<0.05, respectively, Student's t-test). **G and H**. mRNA levels were measured by quantitative RT-PCR using species specific probes (*n*=9~10 per group). PTHrP^{Lo} tumors had significantly reduced host-derived (i.e. murine) *MMP-9* gene expression (*P*<0.01, Student's t-test), but not tumor-derived (i.e. human) *VEGF-A* (*P*=0.42, Student's t-test). Data in all graphs are mean ± SEM.

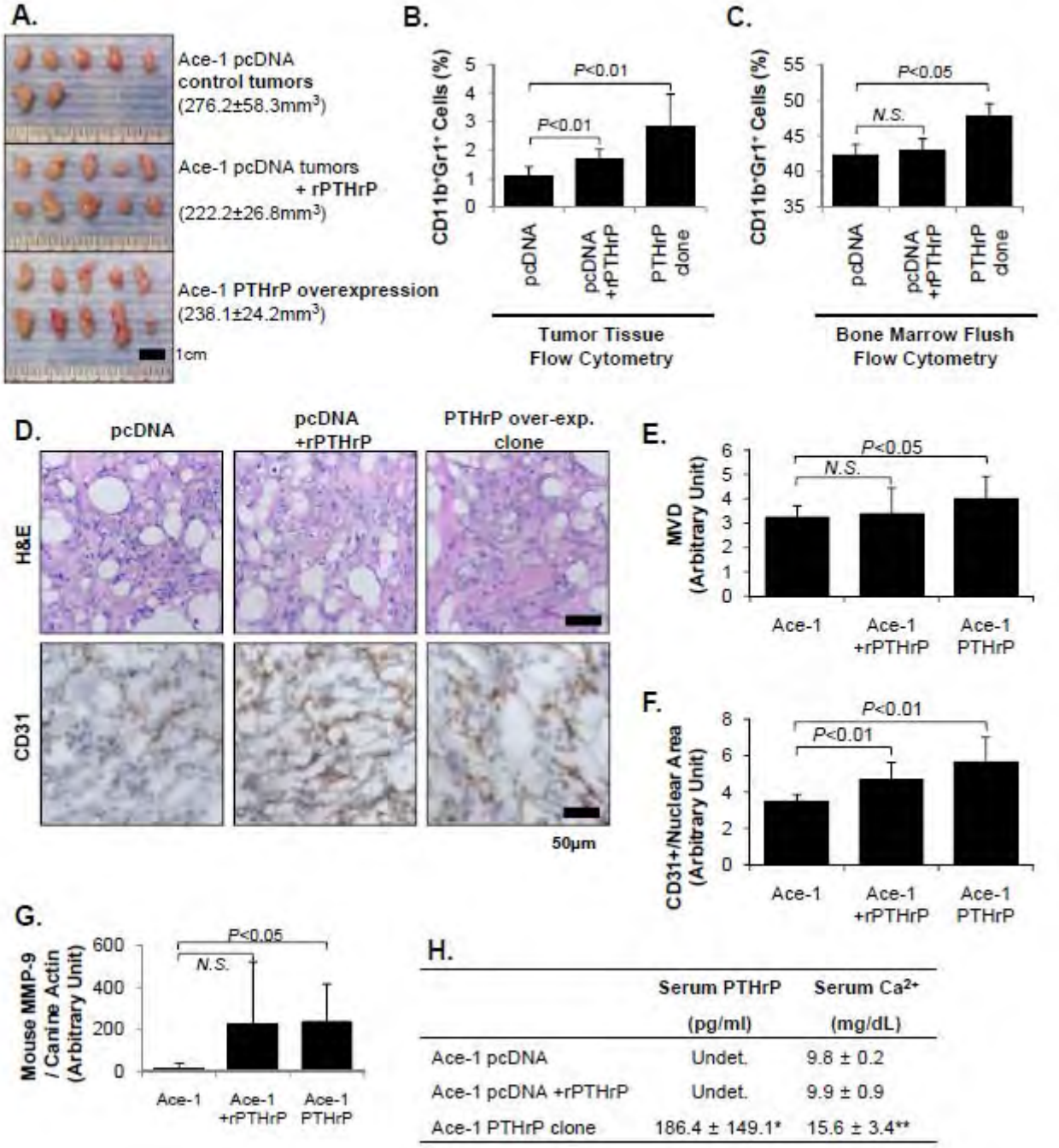

	Serum PTHrP (pg/ml)	Serum Ca^{2+} (mg/dL)
Ace-1 pcDNA	Undet.	9.8 ± 0.2
Ace-1 pcDNA +rPTHrP	Undet.	9.9 ± 0.9
Ace-1 PTHrP clone	186.4 ± 149.1*	15.6 ± 3.4**

Figure 2: Ectopic PTHrP increased $CD11b^+Gr1^+$ cells in prostate tumor tissues and the bone marrow. Ace-1 prostate cancer cells, expressing undetectable basal level of PTHrP, were engineered to overexpress PTHrP from pcDNA3.1 vectors (designated PTHrP OE). Vector-alone transfectant was used as a control (designated pcDNA). PTHrP expression was confirmed by an immuno-radiometric assay of tissue culture supernatants. Cells were injected subcutaneously into male athymic mice. **A**. PTHrP OE (*n*=10; right panel) were grown for a reduced period (i.e. 17 days) to produce similarly sized tumors as pcDNA control tumors (*n*=7; grown for 32 days; left panel). In addition, one group of mice carrying pcDNA tumors (*n*=10; middle panel) was administered with recombinant PTHrP (1-34) for 7 days (80μg/kg; once a day SQ injection) prior to euthanasia (designated rPTHrP). Mean tumor volume ± SEM (mm^3) for each group was indicated. No statistical significance (*P*>0.05 by Student's t-test) in any pair of groups. Scale bar: 1cm. **B**. Flow cytometric analyses of tumor tissues showed that both PTHrP OE and rPTHrP tumors had significantly increased percentage of $CD11b^+Gr1^+$ cells, compared with pcDNA controls (*n*=7~10 per group). **C**. Mice carrying

PTHrP OE tumors had increased percentage of $CD11b^{+}Gr1^{+}$ cells in the femoral bone marrow, compared with the pcDNA control group (n=7~10 per group). However, there was no difference between the pcDNA control and rPTHrP groups (N.S. stands for 'not significant' by Student's t-test). **D**. Tumor tissues were sectioned for H&E staining and murine CD31/PECAM immunohistochemical staining. Original magnification, ×20. Scale bars: 50μm. **E, F.** Microscopic images were obtained (3~4 randomly selected fields per tissue) for quantification of CD31-positive vessel area (brown stain) with normalization to total nuclear area (n=7~10 per group). Both PTHrP OE and rPTHrP tumors had significantly increased vascularity and CD31+ cells compared with the pcDNA control group (P<0.01, Student's t-test; n=7~10 per group). **G.**. *MMP-9* mRNA levels in PTHrP OE tumors, but not in rPTHrP tumors, were significantly higher than pcDNA control tumors (P<0.05, Student's t-test; n=7~10 per group). Data in all graphs are mean ± SEM. **H**. Serum PTHrP and Ca^{2+} levels were measured by immuno-radiometric assay and colorimetric assay, respectively. Mice with PTHrP OE tumors had significantly higher serum PTHrP and Ca^{2+} levels, compared with control mice carrying pcDNA tumors. * P<0.01, Mann-Whitney U test (PTHrP) or Student's t-test (Ca^{2+}).

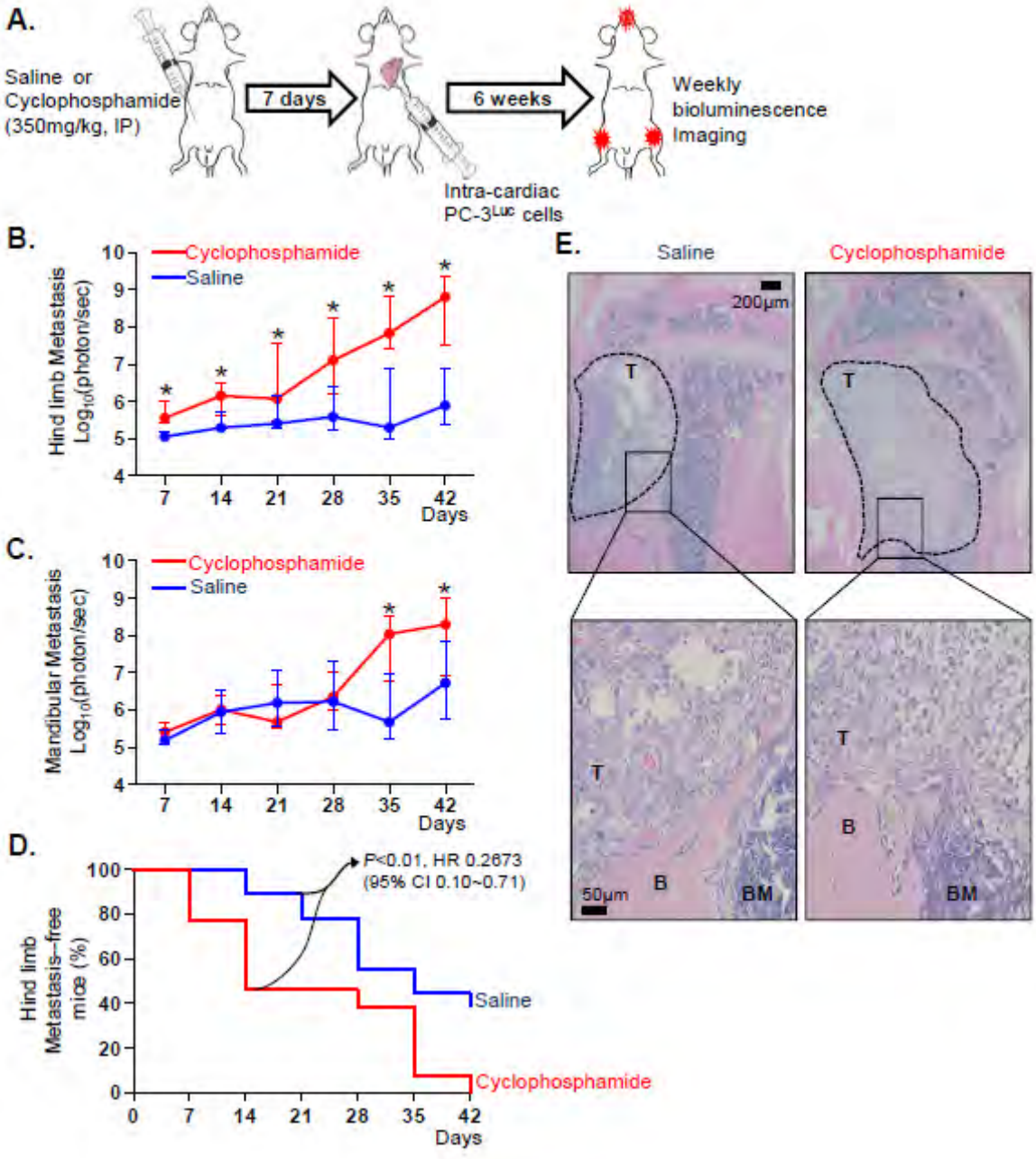

Figure 3: Cyclophosphamide (CY) enhances prostate cancer skeletal metastasis. A. Schematic

representation of the experimental design. Male athymic mice were divided into two groups and treated with saline or CY (350 mg/kg, i.p.). Following 7 days of recovery, PC-3^{Luc} cells were injected into the left heart ventricle (n=18 for saline control and n=13 for CY group). Development and subsequent growth of metastatic tumors were monitored by weekly *in vivo* bioluminescence imaging for 6 weeks. **B.** Hind limb metastatic tumor size was measured by weekly *in vivo* bioluminescence imaging. CY-treated mice had significantly increased photon emission from the hind limbs, compared to the saline-treated mice after day 28. Data are medians with interquartile range (i.e. 25th and 75th percentiles). Asterisks represent model-contrast P<0.01**. C.** Mandibular metastatic tumor size was measured, and median photon emission per second from the mandibular lesions in each group was plotted. The CY-treated group had increased photon emission compared to the saline-treated group after 35 days. Data are median ± interquartile range. Asterisks represent model-contrast P<0.01. **D**. Percentage of hind limb metastasis-free mice was plotted in a Kaplan-Meier curve. Lesions emitting more than 1×10^5 photon/second were considered as metastases. The CY group had significantly higher incidence of hind limb metastases than the saline control group (P<0.01 by logrank test). HR and CI stand for hazard ratio and confidence interval, respectively. **E**. Representative histological images of metastatic bone tumors. Tumor-bearing hind limb tibiae were dissected, followed by fixation, decalcification, sectioning and H&E staining. The presence of metastatic tumor cells was confirmed microscopically. Tumor perimeter is indicated by dotted lines in lower magnification images (×4 objective lens; upper panel). Higher magnification images (× 20 objective lens; lower panel) show tumor (designated "T"), bone (designated "B") and bone marrow (designated "BM").

Task 3: Aim 1: Altered hematopoietic microenvironment and tumor localization (macrophage depleted mice)
These experiments proved initially to be more challenging than anticipated with an extensive amount of characterization of the timing and dosing of the compound that regulates macrophage depletion in these mice requiring great detail. We are still generating and analyzing study data sets and presented initial findings as an invited speaker at the Cancer Induced Bone Disease meeting in Chicago (abstract appended). There was a statistically significant difference supporting that macrophage depletion results in smaller tumors (Figure 4). One difficulty in the interpretation of this data that we are currently trying to sort out is whether the phenotype is affected more by an ablation of osteoclasts or macrophages. But at this point it seems that the macrophage lineage cells are key mediators and has led us to examine macrophage function in greater detail in a submitted project currently under review by the DOD. This aspect of the project has early data; yet, final verification is still underway.

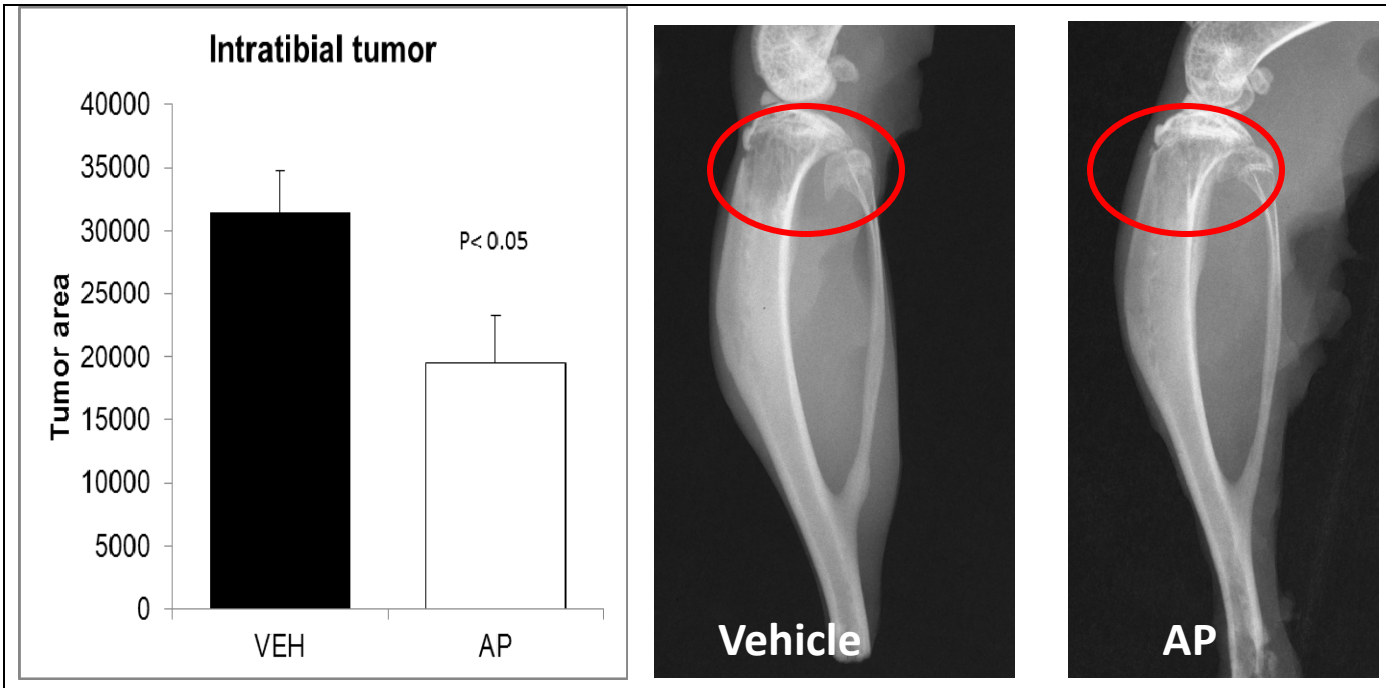

Figure 4: Myeloid lineage cells and tumor localization in bone. Mafia mice have a c-fms promoter driving a fas

apoptosis gene that is regulated by the administration of the AP compound. Mice were administered AP compound for 3 days prior to tumor injection into the tibiae. Reductions in myeloid lineage cells were confirmed by flow cytometric analyses (not shown). Tumor areas were significantly reduced when myeloid cells were reduced with administration of the AP compound (n=8/gp).

Task 4: Aim 2: PCa-derived PTHrP and angiogenesis via endothelial progenitor cells (EPCs)
We have tried several attempts to delineate the effects of PTHrP (both tumor derived and exogenous injection) on endothelial progenitor cells. Unfortunately the markers for EPCs are ill defined and our results have not yielded meaningful data. We have elected to move forward with other proposed approaches. This aspect of the project was not fruitful but is finished.

Task 5: PCa-derived PTHrP and angiogenesis via micro-vessel staining
Prostate cancer derived PTHrP results in increased microvessel density as measured using CD31 positive staining and demonstrated with PC-3 as well as ACE-1 prostate cancer cells (Figures 1D,E,F, 2D,E,F). Results have been found in repeated experiments and with more than one prostate cancer cell line. This aspect of the project is complete.

Task 6: PCa-derived PTHrP impact on angiogenesis and dependence for the osteoanabolic phenotype
With our studies to date it is clear that prostate cancer-derived PTHrP contributes to overall tumor growth as well as angiogenesis. However, we have not definitively been able to link PTHrP derived from prostate cancer with the osteoblastic phenotype. Studies using exogenously administered PTHrP were not able to increase the vascular volume in the bone microenvironment (only in the tumor) suggesting the bone microenvironment and hence the osteoblasts are not essential for the PTHrP impact on angiogenesis (data not shown, but summarized in part in appended abstract). For these studies, PTH or PTHrP was administered for varying time periods and at sacrifice mice were perfused with a microfil material composed of lead chromate. This allowed for micro-CT analysis of the three dimensional architecture of the vasculature. There was no alteration in vascular volume or vascular number with PTH/PTHrP. Instead, and via other studies we have developed a new hypothesis that suggests that PTHrP drives CD11b+Gr-1+ cells in the tumor and that this may lead to the development of phagocytic cells that remove apoptotic tumor cells and in the process produce bone anabolic factors such as TGFβ. Future studies will focus on this. This task has been completed.

Task 7: Identification of cell populations and mediators of PCa-derived PTHrP action
Several key mediators have been identified. CCL2 and IL6 were identified via analysis of serum from tumor inoculated mice (Figure 5) and CCL2 validated via the administration of anti-CCL2 with demonstration of inhibition of tumor localization in the skeleton (Figure 6). This work has also been linked to the CD11b+Gr-1+ cell population *in vivo* and *in vitro* (Figure 7). Mice were treated with PTHrP and their bone marrow CD11b+Gr-1+ cells isolated and evaluated for phosphorylation of Src kinase as a measure of biologic activity. PTHrP increased Src kinase phosphorylation in vivo. As CD11b+Gr-1+ cells do not have receptors for PTHrP we identified downstream mediators of PTHrP action by isolating CD11b+Gr-1+ cells and treating them in vitro with IL-6, CCL2, VEGF-A, RANKL and PTHrP. Il-6 and VEGF-A were capable of increasing Src phosphorylation and hence the candidate cell population CD11b+Gr-1+ cells and mediators (IL-6 and VEGF-A) have been identified. This task is complete.

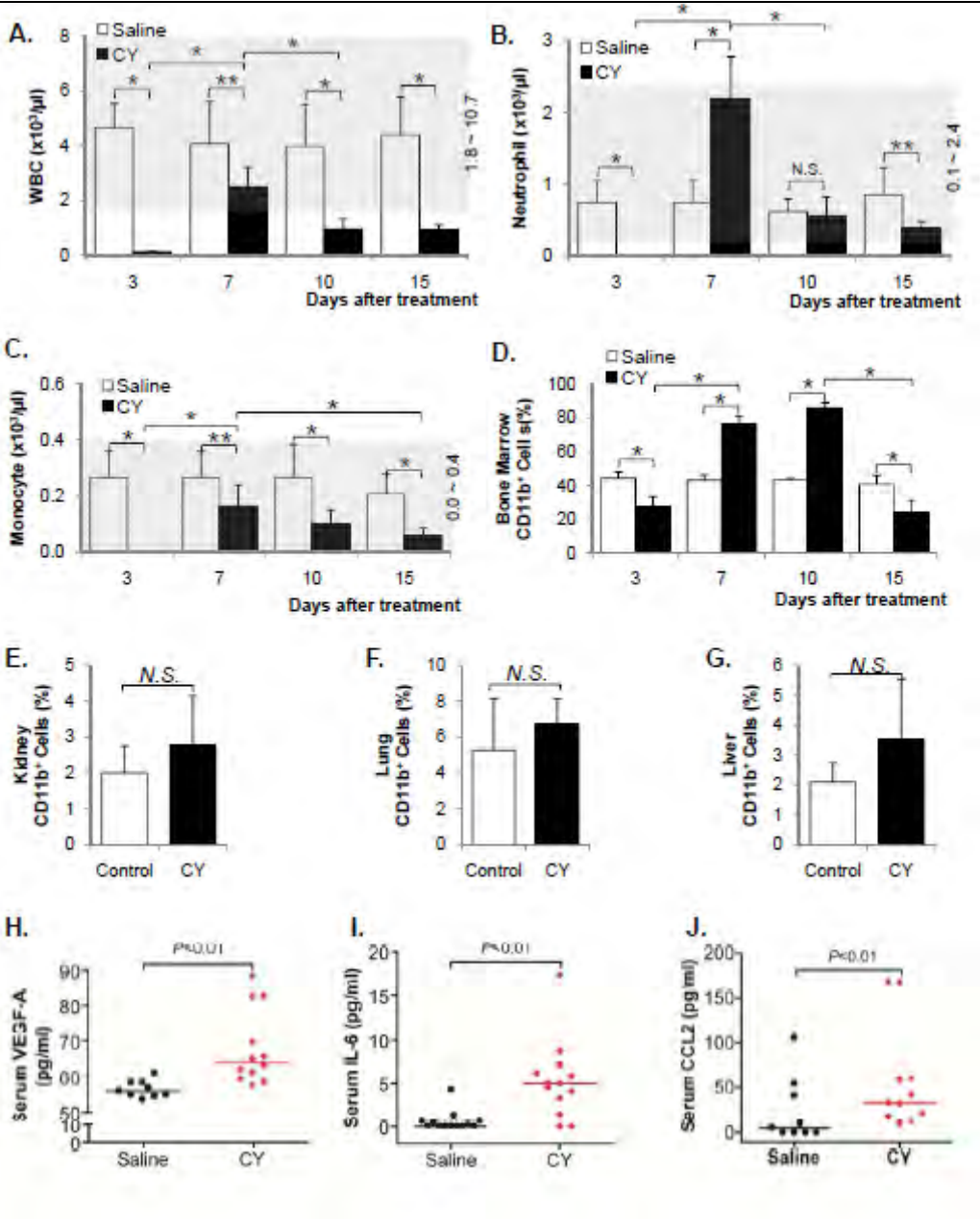

Figure 5: Cyclophosphamide effects on peripheral blood, and myeloid lineage cells in the bone marrow, and serum mediators. A–C. Male C57BL6/J mice (n=8 per group at each time point) were treated with saline (control) or CY followed by complete blood counting (CBC) with white blood cell (WBC) differential counting on 3, 7, 10 and 15 days after treatment. Data are mean ± standard deviation. Asterisks indicate statistical significance (* indicates P<0.01 and ** indicates P<0.05 by Student's t-test). Shade indicates standard range. **A**. CY-treated mice had significantly reduced WBC counts at all time points, compared to saline-treated groups. However, at day 7, a spike of total WBC count was observed. **B.** The increase of total WBC count on day 7 was associated with an expansion of neutrophils. The neutrophil number was below detection 3 days after CY treatment, but increased on day 7 post-CY treatment, followed by normalization (at day 10) and suppression (at day 15). **C.** Monocyte counts were lower than control groups at all time points. However, similar to neutrophil counts, the monocyte count in day 7 CY group was significantly increased, compared to day 3 CY group. **D.** Myeloid lineage cells in the bone marrow were expanded at day 7 post-CY. Male C57BL/6J mice (n=8 per group at each time point) were treated with saline (control) or CY followed by flushing bone marrow cells for flow cytometric analysis of myeloid lineage cell populations (expressing CD11b marker) on 3, 7, 10 and 15 days after treatment. Parallel to the changes of monocyte and neutrophil counts in the peripheral blood, the $CD11b^+$ population was suppressed at day 3, followed by increases at day 7 and 10. Data are mean ± standard deviation, and asterisks represent statistical significance (* indicates P<0.01 and ** indicates P<0.05 by

Student's t-test). **D– G.** CY treatment did not increase $CD11b^+$ myeloid cells in the solid organs. Male C57BL/6J mice (*n*=6/group) were treated with saline (control) or CY. After 7 days, kidney (**E**), lung (**F**) and liver (**G**) were surgically removed and digested for flow cytometric analyses of $CD11b^+$ myeloid cells. Data are mean ± standard deviation. N.S. indicates not significant by Student's t-test. **H.– J.** CY treatment increased myeloid-associated cytokines in serum. Male C57BL/6J mice (*n*=12 each) were treated with saline (control) or CY. After 7 days, whole blood was collected by cardiac puncture and serum cytokines including vascular endothelial growth factor (VEGF)-A (**H)**, IL-6 (**I**) and CCL2 (**J**) were measured by ELISA. Each dot represents an individual serum cytokine level, and bars represent median. CY treatment significantly increased VEGF-A, IL-6 and CCL2 levels, compared to saline-treated control groups (all $P<0.01$ by Mann Whitney *U* test).

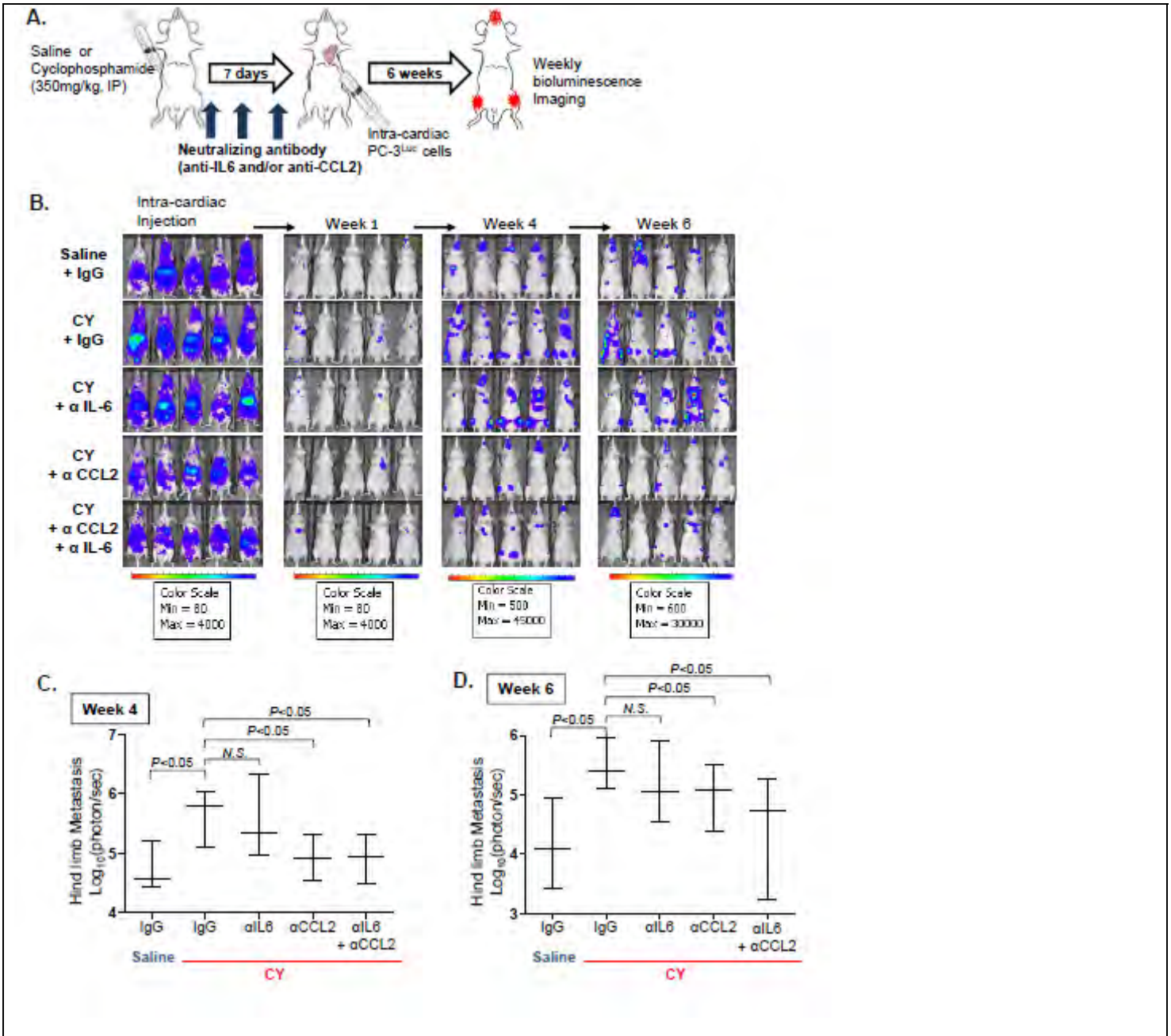

Figure 6: Neutralizing CCL2, but not IL-6, reverted cyclophosphamide-induced prostate cancer bone metastasis. A. Schematic representation of the experiment. Male athymic mice were treated with saline (*n*=10) or CY in combination with control IgG (*n*=14; 10 mg/kg, i.p.), anti-mouse IL-6 (*n*=11; 20 mg/kg, i.p.), anti-mouse CCL2 (*n*=12; 10 mg/kg, i.p.), or a combination of anti-IL-6 and CCL2 antibodies (*n*=12). Three doses

were given one day before CY treatment, and 3 and 6 days after CY treatment. On day 7 post-CY injection, PC-3^{Luc} cells were injected into the left heart ventricle. Development and subsequent growth of metastatic tumors were monitored by weekly *in vivo* bioluminescence imaging for 6 weeks. **B.** Serial images from five representative mice from each group are shown. CY treatment alone significantly increased skeletal metastasis (second row) compared to the saline treatment group (first row). Neutralizing CCL2 in the CY-treated mice prior to tumor inoculation significantly reduced skeletal metastasis (fourth row), while neutralizing IL-6 had no significant effects (third row). Treatment with a combination of anti-CCL2 and IL-6 antibodies (fifth row) had similar effects as anti-CCL2 antibody alone. **C.–D.** Week 4 (**C**) and Week 6 (**D**) bioluminescence data were quantified and plotted. Tumor size was measured by photon emission per second from the hind limb lesions in each group. Data are median ± interquartile range.

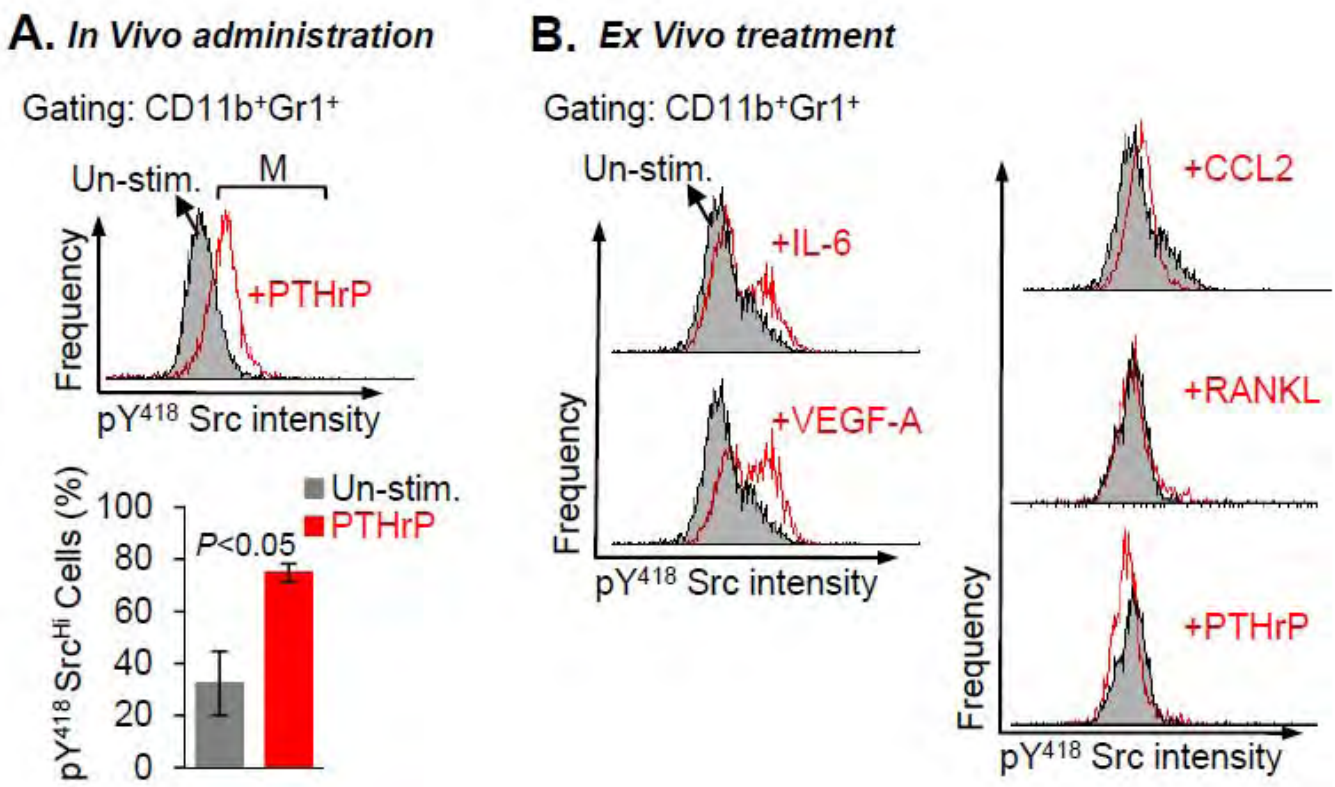

Figure 7: PTHrP phosphorylated [Y^{418}] Src family kinases in MDSCs A. Male athymic mice (*n*=3 per group) were stimulated with a single administration of recombinant PTHrP (1-34; 80μg/kg, SQ injection) or saline control (denoted 'Un-stim') , 8 hours prior to flow cytometric analyses of phospho-[Y^{418}] Src family kinase expression levels in CD11b^{+}Gr1^{+} bone marrow cells. Representative histograms from the control group (shaded) and the PTHrP-stimulated group (red) were overlapped to show. Quantification of CD11b^{+}Gr1^{+} cells expressing high levels of phospho-[Y^{418}] Src family kinases (indicated by a bracket 'M') showed that recombinant PTHrP treatment increased activating phosphorylation of Src family kinases. P<0.01, Student's t-test. **B**. CD11b/Gr1 double positive cells were sorted from the femoral bone marrow of male athymic mice, followed by treatment with saline, IL-6, VEGF-A, CCL-2, RANKL or PTHrP (100ng/ml for 0.5×10^{6} cells) for 1 hour at 37°C (*n*=3 per group). Representative histograms (red) were overlapped onto un-stimulated controls (shade) to show. Experiments were repeated more than 3 times.

Task 8: Data analysis, review, repetition as needed

Experiments have been analyzed as they developed, some aspects involved alternate strategies, experiments were repeated as needed and all have been completed. This task is complete.

KEY RESEARCH ACCOMPLISHMENTS: The key research accomplishments emanating from this research are summarized in the figure below as well as the **bulleted list** (on left).

Key Accomplishments

- Prostate cancer was found to produce PTHrP that circulates to the bone marrow
- PTHrP was found to interact with receptors on osteoblastic cells in bone
- PTHrP via targeting its receptor in osteoblasts was found to produce cytokines/mediators including IL-6, VEGF, CCL2
- The project identified these mediators to cause an expansion of hematopoietic cells termed myeloid derived suppressor cells (MDSCs)
- MDSCs were found to circulate and support tumor growth through mechanisms that are still under investigation but may include the promotion of angiogenesis as well as the process of efferocytosis and release of tumor supporting growth factors.

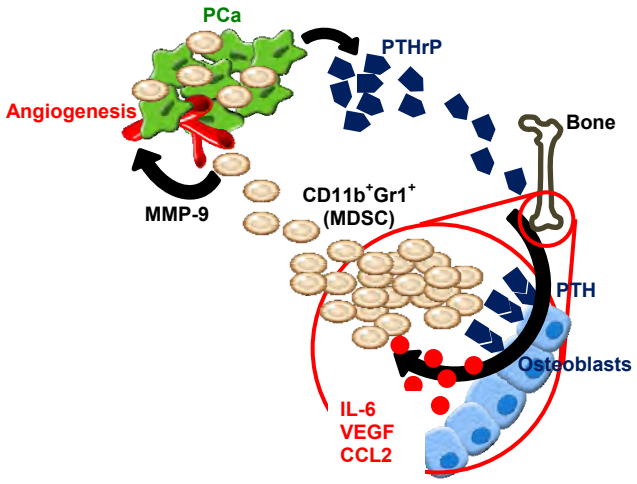

REPORTABLE OUTCOMES:

Publications

Li X, Loberg R, Liao J, Ying C, Snyder L, Pienta KJ, **McCauley LK**. A Destructive Cascade Mediated by CCL2 Facilitates Prostate Cancer Growth in Bone. Cancer Research, 69:1685-92, 2009. PMID: 19176388

Park S, **McCauley LK**, Gallick GE. Pre-Clinical Mouse Models of Prostate Cancer, in: Current Protocols in Pharmacology and Drug Discovery, 51:14.15-14.15.27., 2010. PMID: 21483646

Li X, Koh AJ, Soki F, Park S, Pienta K, **McCauley LK**. Inhibitory effects of megakaryocytes in prostate cancer skeletal metastasis. Journal of Bone and Mineral Research: 26:125-134, 2011 PMID: 20684002.

Li X, Liao J, Park SI, Koh AJ, Sadler WD, Pienta KJ, Rosol TJ, **McCauley LK**. Drugs Which Inhibit Osteoclast Function Suppress Tumor Growth through Calcium Reduction in Bone. Bone: 48(6):1354-61 2011. PMID: 21419883

Park SI, Soki FN, **McCauley LK**. Roles of bone marrow cells in skeletal metastases : No longer bystanders. Cancer Microenvironment, In press, on-line, 2011. PMID: 21809058

Weilbaecher KN, Guise TA, **McCauley LK**. Cancer to bone: a fatal attraction (Invited review): Nature Reviews Cancer: 11:411-25. PMID: 21593787

Park SI, Liao J, Berry J, Li X, Koh A, Michalski M, Eber M, Soki F, Sadler W, Sud S, Tisdelle S, Nemeth J, Snyder L, Wronski T, Pienta K, **McCauley LK**. Cyclophosphamide Creates a Receptive Microenvironment for Prostate Cancer Skeletal Metastasis. Conditionally accepted, Cancer Research 2011.

Park SI, **McCauley LK.** Nuclear Localization of Parathyroid Hormone-related Peptide Confers Resistance to Anoikis in Prostate Cancer Cells. Conditionally accepted, Endocrine Related Cancer 2011.

Abstracts: Numerous abstracts have been presented including two at the DOD Impact meeting in 2011. All abstracts have gone on to formulate publications with the exception of the four appended abstracts.

CONCLUSION:
In summary, this DOD project was very fruitful as a new paradigm of tumor/bone interaction was elucidated. In particular, new information that implicates cells of the myeloid lineage (MDSCs) in promoting tumor growth was found. PTHrP produced by prostate tumors circulates either in an endocrine or paracrine manner to interact with its receptor on cells of the osteoblast lineage. Through well characterized intracellular signaling, the PTHrP receptor activation leads to downstream gene transcriptional events that result in the production of a variety of cytokines/mediators. In particular, this project identified CCL2, VEGF, and IL-6 as contributing factors to the expansion of MDSCs in the marrow as well as their trafficking to primary tumors. Specifically, PTHrP administration *in vivo* resulted in Src phosphorylation that was attributed to IL-6 and VEGF activity. MDSCs were found to be 'informed' by prostate cancer derived PTHrP and to support tumor growth. A potential mechanism for this support is via increased angiogenesis due to MMP-9 upregulation which is an ongoing and future direction. Another potential mechanism is via the MDSC infiltation of tumors, phagocytosis/efferyocytosis of apoptotic tumor cells and production of TGFβ. These are future directions for this work. Clinical implications of the work include the identification of potential targets for therapeutic approaches including PTHrP, IL-6, CCL2, VEGF, and MMP-9 in addition to myeloid cells themselves.

REFERENCES: N/A

APPENDICES:

Submitted manuscripts

Two recent submitted abstracts

Cyclophosphamide Creates a Responsive Microenvironment for Prostate Cancer Skeletal Metastasis

Serk In Park,[1] Jinhui Liao,[1] Janice E. Berry,[1] Xin Li,[1] Amy J. Koh,[1] Megan N. Michalski,[1] Matthew R. Eber,[1] Fabiana N. Soki,[1] W. David Sadler,[1] Sudha Sud,[2] Sandra M. Tisdelle,[3] Stephanie D. Daignault,[4] Jeffrey A. Nemeth,[5] Linda A. Snyder,[5] Thomas J. Wronski,[3] Kenneth J. Pienta,[2] and Laurie K. McCauley[1, 6]

Affiliations:

[1] Department of Periodontics and Oral Medicine, the University of Michigan School of Dentistry, Ann Arbor, MI;

[2] Departments of Internal Medicine and Urology, the University of Michigan Medical School, Ann Arbor, MI;

[3] Department of Physiological Sciences, the University of Florida, Gainesville, FL;

[4] Comprehensive Cancer Center Biostatistics Core, the University of Michigan Medical School, Ann Arbor, MI;

[5] Ortho Biotech Oncology Research and Development, Centocor Inc., Radnor, PA; and

[6] Department of Pathology, the University of Michigan Medical School, Ann Arbor, MI

Running Title: Cyclophosphamide-induced prostate cancer bone metastasis

Keywords: Cyclophosphamide, prostate cancer, bone metastasis, myeloid cells, CCL2

Financial supports: This work was financially supported by the Department of Defense Prostate Cancer Research Program W81XWH-10-1-0546 (Serk In Park) and W81XWH-08-1-0037 (Laurie K. McCauley); the National Cancer Institute Program Project Grant P01CA093900 (Kenneth J. Pienta and Laurie K. McCauley); Specialized Program of Research Excellence (SPORE) 2 P50 CA69568 and American Cancer Society Clinical Research Professorship (Kenneth J. Pienta); and Centocor Inc. (Laurie K. McCauley).

Requests for reprints: Laurie K. McCauley, DDS, PhD, Professor and Chair, Department of Periodontics and Oral Medicine, University of Michigan School of Dentistry, 1011 N. University Avenue, Ann Arbor, MI 48109; E-mail: mccauley@umich.edu; Phone: +1-734-647-3206; Fax: +1-734-763-5503

Conflicts of interest: Linda A. Snyder and Jeffery A. Nemeth are employed by Centocor Inc. All other authors declare no financial conflict of interest.

Body text word count: 4774

Total Number of figures: 7

Total Number of Tables: 0

ABSTRACT

Bone, the most congenial soil for prostate and breast cancer metastasis, exhibits a complex microenvironment due to multiple types of constitutive cells. Prostate cancer has been shown to localize preferentially to bones with higher marrow cellularity. In this study, the effects of cyclophosphamide, a bone marrow-suppressive chemotherapeutic drug, were investigated on the development and growth of metastatic tumors in bone using an experimental prostate cancer metastasis model. Priming the murine host with cyclophosphamide prior to intra-cardiac tumor cell inoculation was found to significantly promote tumor localization and subsequent growth in bone. Abrupt expansion of myeloid lineage cells in the bone marrow and the peripheral blood was observed shortly after cyclophosphamide treatment, associated with increases in cytokines with myelogenic potentials such as C-C chemokine ligand (CCL) 2, interleukin (IL)-6 and vascular endothelial growth factor (VEGF)-A. More importantly, neutralizing host-derived murine CCL2, but not IL-6, in the pre-metastatic murine host significantly reduced the pro-metastatic effects of cyclophosphamide. These data suggest that bone marrow perturbation by cytotoxic chemotherapy contributes to bone metastasis, mediated by a transient increase of bone marrow myeloid cells and myelogenic cytokines that can be clinically intervened by blocking CCL2.

INTRODUCTION

Despite the recent advances in diagnosis and therapeutic modalities for prostate cancer, skeletal metastasis still accounts for the vast majority of prostate cancer-related morbidity and mortality (1). Bone is the predominant site of prostate cancer metastasis, and advanced-stage prostate cancer patients commonly develop metastatic bone lesions (2, 3). Unfortunately, the pathophysiology of skeletal metastasis is not yet completely understood, and there is no effective cure for patients with bone metastases. One major obstacle to better understanding bone metastasis is the unusual complexity of the tumor microenvironment in bone (4, 5). Bone provides a unique microenvironment, not only because of the calcified matrix, but also because of the presence of multiple cell types, including osteocytes, osteoclasts, osteoblasts, hematopoietic cells, stem cells, immune cells, fibroblasts and endothelial cells. Emerging evidence supports that cells in the bone marrow microenvironment are actively involved in prostate cancer metastasis (6, 7).

Bone marrow-derived myeloid lineage cells are critical regulators of tumor progression and metastasis (8-13). Yang *et al.* demonstrated that expansion of $Gr\text{-}1^{+}CD11b^{+}$ myeloid cells directly promotes tumor angiogenesis (9). Ahn and Brown further demonstrated that matrix metalloproteinase (MMP)-9 produced by bone marrow-derived myeloid cells contributes to tumor vasculogenesis, and that inhibition of myeloid cells suppressed tumor re-growth after irradiation (10, 11). More recently, Kozin *et al.* demonstrated that recruitment of myeloid cells promotes tumor re-growth after radiation therapy (12). Myeloid cells (expressing myeloid-specific surface markers such as CD11b and/or Gr-1) are a major component of undifferentiated bone marrow cells, and ultimately differentiate into monocytes, macrophages and granulocytes (13). Parallel to the tumorigenic roles of myeloid cells, monocyte-macrophages (i.e. fully

differentiated myeloid cells) also have been shown to participate in tumor metastasis. Recently, Mizutani and colleagues demonstrated that prostate cancer-derived factors, including C-C chemokine ligand 2 (CCL2, also known as monocyte chemoattractant protein-1 [MCP-1]), interleukin-6 (IL-6) and IL-8, promote $CD11b^+$ cell differentiation and macrophage recruitment, contributing to osteoclastogenesis, prostate cancer growth, and bone metastasis (14-16). Furthermore, monocyte-macrophage recruitment in the tumor site mediated by CCL2 promoted prostate cancer cell proliferation (17), survival (18), migration (19), and metastasis (16, 20). All of these data collectively support the critical roles of bone marrow-derived myeloid lineage cells in prostate cancer progression and bone metastasis. However, it is not clearly understood how the alterations in the bone marrow occur, which could provide clues for a therapeutic approach.

In clinical settings, chemotherapeutic drugs and/or irradiation perturb the bone marrow microenvironment, leading to alterations in marrow cellular composition. Although chemotherapy and irradiation are both bone marrow-suppressive, the subsequent recovery process may lead to temporary spikes of certain cell types, including monocytes and neutrophils (21, 22). Therefore, the net effects of the bone marrow-suppressive agents could have pro- or anti-tumorigenic effects. Interestingly, priming the murine host with cyclophosphamide, a bone marrow-suppressive chemotherapeutic drug, promoted subcutaneous tumor growth and metastasis in several mouse models, including an intravenous syngeneic lung metastasis model and an orthotopic colon-to-liver metastasis model. (23-26) Cyclophosphamide is a DNA-alkylating drug commonly included in chemotherapeutic regimens against breast and lung cancers, and Non-Hodgkin's lymphoma. In addition, cyclophosphamide is used in the standard conditioning regimen for recipients of myeloablative bone marrow transplantation (BMT), to enhance engraftment and to suppress host immune reaction. However, intriguing data showing

opposite effects (i.e. pro-metastatic effects) of chemotherapeutic drugs remain poorly investigated. To our best knowledge, the effects of cyclophosphamide on prostate cancer bone metastasis have never been reported. Given that prostate cancer has been shown to utilize similar strategies as hematopoietic stem/progenitor cell homing, and that prostate cancer has long been known to home typically to bones enriched with red marrow (27), we hypothesized that alterations induced by cyclophosphamide in the bone marrow microenvironment might contribute to prostate cancer colonization in the bone and/or subsequent tumor growth.

In the current study, we investigated pro-metastatic effects of bone marrow suppression in an experimental prostate cancer skeletal metastasis model, and explored the underlying mechanism that could be used to design methods of therapeutic intervention. Priming the murine host with a single cyclophosphamide dose significantly promoted the development of skeletal metastases and resulted in larger tumors at the endpoint. We discovered that myeloid lineage cells ($CD11b^+$ cells in the bone marrow; and monocytes/neutrophils in the peripheral blood) were expanded in the recovery phase of cyclophosphamide-induced bone marrow suppression. Additionally, treatment with a neutralizing antibody to host-derived murine CCL2, a myeloid cytokine, prevented cyclophosphamide-induced prostate cancer bone metastases.

MATERIALS AND METHODS

Animals and *in vivo* skeletal metastasis model of prostate cancer

Male athymic mice (Hsd:Athymic Nude-*Foxn1*^{nu}; 4 to 8 weeks of age) were purchased from Harlan Laboratories. The experimental protocols were approved, and performed in accordance with current regulations and standards of the University of Michigan Institutional Animal Care and Use Committee guidelines.

For the *in vivo* experimental prostate cancer skeletal metastasis model, the procedure of Park *et al*. was followed (28). In brief, mice were anesthetized and 100µl of cell suspension containing 2×10^5 luciferase-labeled PC-3 cells (PC-3^{Luc}) were injected into the left heart ventricle. Systemic circulation of the tumor cells was confirmed by *in vivo* bioluminescence imaging within 24 hours post-inoculation. Mice carrying strong bioluminescence signals only in the chest indicative of a failure of the ventricular injection (i.e. leakage into the pericardium or injection into the right ventricle) were removed from the study. Development and subsequent growth of metastatic tumors were examined by *in vivo* bioluminescence imaging (Xenogen® IVIS-200, Caliper Life Sciences) for 6 weeks, as described elsewhere (27, 28). Tumor-bearing hind limbs were harvested at euthanasia, fixed in 10% buffered formaldehyde and decalcified in 10% EDTA for 2 weeks. Metastatic tumor cells were microscopically confirmed by H&E staining.

Orthotopic bone tumor model of metastatic prostate cancer

To establish bone metastatic prostate tumors, PC-3^{Luc} cells (1×10^3 cells suspended in 20 µl Hank's Balanced Salt Solution) were injected in the proximal tibiae by a modification of the previously described method (28). Briefly, male athymic mice were anesthetized with

ketamine/xylazine mixture and a 27-gauge needle attached to a 1 ml syringe was used to bore the proximal tuberosity of tibia percutaneously, followed by injection of cell suspension into the proximal bone marrow space. Tumor cells were intentionally injected into the marrow cavity, instead of the bony tibia, to recapitulate tumor growth in the saline- or cyclophosphamide-treated bone marrow microenvironment.

Cyclophosphamide and Docetaxel

Cyclophosphamide (Sigma-Aldrich) or docetaxel (Sanofi-Aventis) was dissolved in sterile Dulbecco's PBS and filtered to produce a 35 mg/ml (Cyclophosphamide) or 20mg/ml (docetaxel) stock solutions. Mice were individually weighed prior to injection, and administered 350 mg/kg body weight (cyclophosphamide) or 40 mg/kg body weight (docetaxel) by intra-peritoneal injection.

***Ex vivo* murine bone marrow microvascular angiography**

Murine bone marrow vasculature was visualized by a modified method of Guldberg *et al*. (29, 30) Briefly, four- to five-week old male C57BL6/J mice were injected intra-peritoneally with cyclophosphamide (350 mg/kg) or an equal volume of saline (n=13 each group). After seven days, mice were anesthetized with ketamine/xylazine mixture and immobilized on an absorbent pad. Incisions were made to open the thoracic and peritoneal cavities. The femoral artery and vein on both hind limbs were exposed for visual inspection of perfusion. Immediately, heparin-supplemented Ringer's lactate solution was infused into the left heart ventricle using a scalp intravenous butterfly needle (23G × ¾ inch) for 9 minutes, and perfusate was flushed through the incised inferior vena cava. Mice were additionally perfused with 10%

buffered formalin for 9 minutes. Mice were then perfused with freshly diluted Microfil® (Flow Tech) solution for 7 minutes, using a 10 ml syringe attached to an electric syringe pump at the rate of 6 ml/minute. Mice were kept at 4°C overnight for curing, and femurs were dissected and decalcified in Cal-ExII decalcifier solution (Fisher) for 24 hours. Microfil®-filled microvascular structures were visualized by micro-computed tomography (μCT) scanning, and further analyzed for vascular volume changes.

ELISA of Serum Proteins

Mouse serum was collected by centrifugation of whole blood drawn by cardiac puncture at euthanasia. Mouse VEGF-A, mouse IL-6 and mouse CCL2 ELISA assays (R&D Systems) were performed. Sera were diluted (1:5 dilution for VEGF-A; 1:2 for IL-6 and CCL2), and assays were performed in duplicate according to the manufacturer's instructions.

Neutralizing Antibodies against CCL2 and IL-6

Anti-mouse CCL2 antibody (C1142, Centocor) and anti-mouse IL-6 antibody (Mab406, R&D Systems) were provided by Centocor Ortho Biotech Inc. C1142 is a rat/mouse chimeric antibody specific for mouse CCL2/MCP-1 and does not cross-react with human CCL2 or mouse MCP-5 (20, 31, 32). Non-specific IgG from mouse serum (Sigma-Aldrich) was used as a control antibody. Antibodies were diluted in sterile Dulbecco's PBS and administered by i.p. injection 24 hours before the cyclophosphamide treatment (20 mg/kg for Mab406; 10mg/kg for C1142 and control IgG), followed by two additional dosages (day 4 and day 1) prior to tumor cell inoculation (experimental prostate cancer metastasis) or euthanasia (for histology and serum cytokine analyses).

Flow Cytometry

Changes of $CD11b^+$ cells in response to cyclophosphamide were quantified by flow cytometric analysis. Bone marrow cells were collected by flushing femurs and tibiae. For analysis of $CD11b^+$ cell recruitment in solid organs, lungs, liver and kidney were surgically removed, homogenized and digested overnight at 37°C in DMEM supplemented with 10% FBS, 0.5 mg/ml collagenase (Sigma-Aldrich) and 1×penicillin/streptomycin antibiotics (Invitrogen). One million cells were used for antibody reaction (FITC conjugated-rat anti-mouse CD11b antibody; BD Bioscience) and flow cytometry (BD FACS Calibur or FACS Vantage SE).

Complete blood counting with white blood cell differentials

Whole blood was collected by cardiac puncture with a 25G × 5/8 inch needle attached to a 1ml syringe. Immediately, 50-100 μl of blood was transferred to EDTA-coated micro-tubes (BD Biosciences). Blood cell counting was performed in the University of Michigan Unit for Laboratory Animal Medicine (Pathology and Animal Diagnostics Core Laboratory), using a Forcyte™ automatic hematology analyzer (Oxford Science) The reference values of individual counts were provided by the manufacturer.

Quantitative PCR

Femurs and tibiae were surgically dissected and flushed with 3 ml TRIzol Reagent® (Invitrogen). Total RNA was prepared according to the manufacturer's specifications. Samples were reverse transcribed to synthesize cDNA (Applied Biosystems), followed by quantitative

PCR (TaqMan PCR master mix kit and ABI 7500 Thermal Cycler) for *CD31* (Applied Biosystems). Mouse *GAPDH* (Applied Biosystems) was used for normalization.

Statistical Analyses

Experimental skeletal metastasis experiments (intra-cardiac tumor injection followed by bioluminescence imaging) were analyzed using linear mixed models. The primary outcome was the natural log transformed bioluminescence measurement. Fixed covariates in the model included the groups in the experiment and time as measured in weeks and the interaction between group and time. The repeated measures aspect of the model, due to multiple measurements over time within each mouse (e.g. left and right hind limbs), was adjusted for in the model using a single order autoregressive correlation structure. Contrasts from the model were used to test the pair-wise comparisons of interest. Analyses were completed using SAS (SAS institute) with a type I error of 5%.

All other statistical analyses, including Kaplan-Meier analyses of metastasis-free mice, Student's t-tests comparing two groups, Mann-Whitney *U* tests of samples failing to distribute normally (as determined $P<0.01$ by Shapiro-Wilk test), were performed with GraphPad Prism for Windows Version 5.04 (GraphPad) or Microsoft Excel 2003 (Microsoft). Statistical tests and significance are indicated in figure legends.

RESULTS

Cyclophosphamide enhanced experimental prostate cancer skeletal metastasis in vivo

Cyclophosphamide (CY), a common chemotherapeutic agent, has been shown to promote subcutaneous tumor growth and experimental metastasis in various animal tumor models (23, 25, 26, 33). As a first stage of this study, we investigated the effects of cyclophosphamide on prostate cancer skeletal metastasis. The experimental design is schematically shown in **Figure 1A**. Male athymic mice were treated with saline or cyclophosphamide, followed 7 days later by intra-cardiac PC-3^{Luc} cell inoculation. The serum half-life of cyclophosphamide is less than 17 minutes (in mice) and 6.5 hours (in human), but mice were allowed 7 days of recovery to insure that the drug was completely cleared, in order to avoid any direct anti-tumor-effects of cyclophosphamide (34, 35). Interestingly, mice primed with cyclophosphamide developed significantly larger tumors in the hind limb long bones (**Figure 1B**) after 7 days, as indicated by increased average photon emission per second from the lesions. Cyclophosphamide-treated mice exhibited increased tumor bioluminescence in the mandible tumors also, but the effects were variable and not statistically significant until day-35 (**Figure 1C**). In addition, cyclophosphamide-primed mice developed hind limb metastases at an earlier time point (i.e. increased incidence of metastases on day-7, 14 and 21; **Figure 1D**), compared to the saline-treated group that developed detectable hind limb metastatic lesions only after 14 days. These data suggest that the larger tumor size on day 42 in the hind limbs of cyclophosphamide-treated mice (representative images shown in **Figure 1E**) is attributable to the early events following tumor cell inoculation.

A single dose of cyclophosphamide significantly disrupted bone marrow vascular integrity

Cyclophosphamide has been found to cause damage to endothelial cells, potentially promoting tumor cell seeding in the metastatic target organs (36). These data are consistent with our observation in **Figure 1** showing outgrowth of metastatic tumors at earlier time points in the cyclophosphamide-treated hosts. Consequently, an experiment was designed to test whether a single dose of cyclophosphamide could perturb endothelial integrity in the bone marrow, which might in turn lead to increased extravasation of tumor cells immediately after inoculation (**Figure 2A**). Because immunohistochemistry can only provide 2-dimensional images of selected cross-sections, we modified a technique of Guldberg *et al.* to reconstruct 3-dimensional vascular structures enclosed in calcified tissues (29, 30) (methods schematically represented in **Figure 2A**). In **Figure 2B**, this technique clearly demonstrated 3-dimensional structures of microvessels in the epiphyses and the central sinusoidal vessels in the diaphyses of saline controls. In sharp contrast, a single dose of cyclophosphamide very obviously disrupted vascular integrity and continuity (**Figure 2C**). Quantification of the images in **Figure 2B** and **C** demonstrated that bone marrow vascular volume was significantly reduced by cyclophosphamide treatment (**Figure 2D**). In addition, *CD31* gene expression, an endothelial-specific marker, was significantly suppressed with cyclophosphamide administration (**Figure 2E**), suggesting that cyclophosphamide-induced vascular disruption led to altered endothelial cells in the bone marrow.

Cyclophosphamide treatment did not cause systemic inflammation

We next ruled out the possibility that cyclophosphamide promoted metastasis by systemic inflammation secondary to the bone marrow suppression. Cyclophosphamide-treated

mice had significantly reduced body weight, compared to the saline control groups, and the effects lasted more than 2 weeks (**Supplemental Figure 1A**). However, cyclophosphamide-treated mice regained body weight with a similar trend to the saline-treated controls. In addition, cyclophosphamide-treated mice did not show any significant lethargy or signs of systemic inflammation, determined by serum levels of C-reactive protein (**Supplemental Figure 1B**).

Cyclophosphamide pre-treatment promoted orthotopic prostate tumor growth in bone

We next tested whether disruption of bone marrow vascular integrity secondary to cyclophosphamide treatment was causal to increased metastatic tumor growth in the bone. For this aim, we implanted PC-3^{Luc} cells directly into the tibiae of mice, 7 days after treatment with saline or cyclophosphamide (experimental scheme shown in **Figure 3A**). This approach was designed to circumvent the effects of vascular disruption that could contribute to initial tumor cell seeding. PC-3 tumors grew larger after 6 weeks in the cyclophosphamide-treated bone marrow, compared to saline treatment (**Figure 3B** and **C**), suggesting that alterations in the cyclophosphamide-treated murine host were responsible for promoting tumor growth and/or metastasis.

Cyclophosphamide transiently expanded myeloid lineage cells

Based on the observation that cyclophosphamide-induced skeletal metastasis was not solely mediated by vascular disruption (**Figures 2** and **3**), we next investigated the alterations induced by cyclophosphamide potentially contributing to tumor growth and/or metastasis. In analyses of complete blood counts (CBC) of mice treated with cyclophosphamide, neutrophil counts were significantly increased 7 days after cyclophosphamide. To analyze further, the

changes of white blood cell (WBC) differential counts were determined serially after cyclophosphamide administration. Total WBC counts were significantly reduced 3 to 15 days after cyclophosphamide, indicating that cyclophosphamide suppressed bone marrow, and that the effects lasted more than 2 weeks (**Figure 4A**). However, the WBC count was increased on day 7 compared to the day 3 cyclophosphamide group (**Figure 4A**). Furthermore, neutrophil number was below detection on day 3 but significantly spiked on day 7, immediately followed by suppression (**Figure 4B**). Additionally, monocyte counts showed a similar pattern to neutrophils (i.e. suppression followed by spike on day 7) (**Figure 4C**). Collectively, these data revealed that differentiated myeloid cells in the peripheral blood (i.e. monocytes and neutrophils) transiently increased during recovery from a single cyclophosphamide dose.

Because both monocytes and neutrophils are differentiated from myeloid lineage cells in the bone marrow, we sought to determine the nature of the changes of myeloid lineage cells in the bone marrow. Flow cytometric analyses of bone marrow cells from the mice treated with cyclophosphamide after 3, 7, 10 and 15 days revealed that myeloid lineage cells (expressing CD11b surface markers) were significantly expanded 7 and 10 days after cyclophosphamide administration with suppression on days 3 and 15 (**Figure 4D**). In contrast, there was no change in the numbers of $CD11b^+$ myeloid cells in other organs such as kidney, lung and liver (**Figures 4E**, **F** and **G**). As shown by Kopp *et al.*, increased angiogenic gene expression after irradiation or chemotherapy was attributed to recovery of the bone marrow sinusoidal endothelium (37). Hence, we next determined the serum protein levels of VEGF-A, IL-6 and CCL2. All three molecules have angiogenic properties and also promote myeloid cell proliferation and differentiation (38-40). All three serum cytokines were significantly increased by cyclophosphamide treatment (**Figure 4H**, **I** and **J**).

Cyclophosphamide-induced skeletal metastases temporally overlap with bone marrow myeloid cell expansion

Subsequently, we tested whether tumor injection time points post treatment with cyclophosphamide affect the development of skeletal metastasis. PC-3^{Luc} tumor cells were inoculated into the systemic circulation 3, 7 and 15 days after cyclophosphamide treatment (**Figure 5A**). The 7-day group had significantly more metastases, compared to the saline-treated control group, as observed previously. When tumor cells were injected at a later time point (i.e. 15 days after cyclophosphamide treatment), significantly fewer mice developed hind limb metastatic lesions, suggesting that levels of bone marrow myeloid cell populations correlate with hind limb metastases (**Figure 5B** and **C**). However, the 3-day group had similar metastatic pattern as the 7-day group (**Figure 5B**) and increased tumor size compared to the 7-day group (**Figure 5C**), potentially because of prolonged survival of tumor cells in the systemic circulation overriding the expansion of bone marrow myeloid cells.

Neutralizing host-derived murine CCL2, but not murine IL-6, inhibited cyclophosphamide-induced prostate cancer bone metastasis

The data described above collectively demonstrated that cyclophosphamide provided an environment conducive to experimental prostate cancer skeletal metastasis, potentially mediated by increase of serum cytokines and/or expansion of myeloid cells. We next determined the causal relationship of alterations induced by cyclophosphamide and tumor metastasis, using the intra-cardiac metastasis model in combination with neutralizing antibodies. Mice were treated with neutralizing antibodies targeting mouse IL-6 or mouse CCL2 during the 7 day recovery

phase after cyclophosphamide treatment (**Figure 6A**). Consistent with the observation in **Figure 1B**, cyclophosphamide treatment significantly enhanced the development and subsequent growth of experimental bone metastasis in this model (**Figure 6B; first and second rows**). Neutralizing IL-6 did not prevent development of metastasis in cyclophosphamide-treated mice (**Figure 6B; third row**). However, neutralizing CCL2 significantly inhibited the cyclophosphamide-induced prostate cancer metastasis *in vivo* (**Figure 6B; fourth row**; statistical comparison shown in **Figures 6C** and **D**), indicating that the upregulation of CCL2 in response to cyclophosphamide contributed to the development and progression of metastasis in this model. Moreover, administration of both antibodies against IL-6 and CCL2 had similar effects to the anti-CCL2 antibody alone group (**Figures 6B-D**). It should be well noted that neutralizing antibodies were administered *before* the tumor cell inoculation, in order to exclude the possibility of direct effects of the drug on the tumor cells. Therefore, the effects of neutralizing antibody were mainly due to the changes exerted on the host microenvironment. However, pre-clinical pharmacokinetic studies demonstrated that anti-CCL2 antibody can remain detectable in serum up to 10 days after administration, thus the possibility of direct effects may not be completely excluded (personal communications).

An alternative chemotherapeutic drug, docetaxel, did not promote skeletal metastases

To further determine the causal role of cyclophosphamide-induced myeloid cell expansion to the development of skeletal metastasis, the effects of docetaxel, a chemotherapeutic agent commonly included in prostate cancer treatment regimen, was tested. Docetaxel is known to be less bone marrow-suppressive, thus a different hematologic recovery pattern was expected. In contrast to CY-mediated pro-metastatic effects, pre-treatment of mice with docetaxel

decreased hind limb skeletal metastasis (**Figure 7B**). In addition, $CD11b^+$ myeloid cell enumeration in the docetaxel-treated bone marrow revealed similar but significantly blunted alterations in $CD11b^+$ cells in athymic mice (**Figure 7C**) as well as in C57BL6 mice (data not shown). Docetaxel-induced myeloid cell expansion (59.1 ± 12.1%) at day-7 was not sufficient enough to increase myeloid cells (neutrophils and monocytes) in the peripheral blood (**Figure 7D-F**).

DISCUSSION

Bone is the preferred site of metastasis for a number of human cancers in organs such as prostate, breast and lung. Multiple mechanisms have been proposed to explain why bone provides a congenial metastatic microenvironment. For example, bone is enriched with cytokines and growth factors that promote tumor cell proliferation, migration, and survival (for a detailed review, see (41)). In addition, bone houses the primary hematopoietic organ (i.e. bone marrow), containing multiple types of progenitor cells (such as endothelial progenitor cells) and hematopoietic cells of various tumorigenic potential. Previously, Schneider *et al.* demonstrated that expansion of bone marrow cellularity (by administration of parathyroid hormone) before inoculation of prostate tumor cells significantly promoted skeletal metastasis (27), suggesting bones with increased cellularity and active remodeling constitute a more congenial microenvironment for metastasis. In this context, it is reasonable to expect that cytotoxic chemotherapy and/or irradiation may impact skeletal metastasis by perturbing the bone marrow microenvironment.

This study demonstrated for the first time that alterations induced by cyclophosphamide, one of the most widely used chemotherapeutic drugs, enhanced bone metastasis in a prostate cancer animal model. Furthermore, we showed that the pro-metastatic effects of cyclophosphamide were significantly reversed by suppression of CCL2, which suggests the causal role of bone marrow myeloid lineage cell expansion in promoting metastasis in the mouse model used in this study. We demonstrated that a single dose of cyclophosphamide administration increased myelogenic cytokines, and correspondingly expanded the myeloid cell population in the bone marrow, as well as the numbers of monocytes and neutrophils transiently in the peripheral blood.

The unexpected "opposite" effect (i.e. pro-tumorigenic) of such a chemotherapeutic drug is not a novel observation in extra-skeletal sites. There have been several reports of chemotherapy-induced metastasis and/or tumor growth (25, 26, 33, 42). Most notably, Carmel and Brown demonstrated that pre-treatment of the host with cyclophosphamide, among many other chemotherapeutic drugs including actinomycin D, vinblastine, bleomycin, methotrexate and 5-fluorouracil, resulted in the most prominent pro-metastatic effects in a syngeneic sarcoma lung metastasis model (23). While most of the previous studies focused on an experimental pulmonary metastasis model, our data expanded the earlier observations by demonstrating the pro-metastatic effects of chemotherapy in a skeletal metastasis model. In addition, we demonstrated that docetaxel, which is less bone marrow-suppressive, accordingly resulted in no pro-metastatic effects. The data suggest that chemotherapeutic drugs with strong bone marrow suppression may have the adverse effect of promoting bone metastasis, a finding which has not been extensively investigated. Cyclophosphamide is not a standard chemotherapeutic drug for prostate cancer patients, but recently low-dose metronomic administration of cyclophosphamide is in clinical trials as an anti-angiogenic therapy in prostate cancer (43, 44). In addition, cyclophosphamide is widely used for treatment of breast cancer, which also has a strong propensity for skeletal metastasis. Consequently, the effects of varying dosages and administration scheduling of cyclophosphamide on bone metastasis warrant extensive further studies using pre-clinical mouse models and ultimately patient cohorts.

Our findings concerning the mechanisms involved in chemotherapy-enhanced metastasis have clinically therapeutic implications. We demonstrated that the numbers of bone marrow myeloid cells (as determined by $CD11b^+$ cells) and myelomonocytic cells in the peripheral blood (as determined by counting neutrophils and monocytes) are significantly increased after

cyclophosphamide administration, but not after docetaxel administration, potentially mediated by the increase of myelogenic cytokines including VEGF-A, IL-6 and/or CCL2. During the recovery phase after bone marrow suppression, spikes of monocytes and neutrophils are frequently observed in patients, and clinically considered a favorable prognostic sign (45). Monocytes and neutrophils arise from common progenitors, and the process is regulated by factors such as IL-3 and GM-CSF. Subsequent monocyte differentiation requires M-CSF, produced by activated monocytes, macrophages and endothelial cells in response to stimuli that also can promote neutrophil production. Our data in **Figure 4** confirmed in our animal model the abrupt increase of neutrophils and monocytes shortly after the cyclophosphamide administration. Moreover, significant increases in CCL2, IL-6 and VEGF-A, all of which are potent myelogenic factors, were observed simultaneously or before the expansion of myelomonocytic cells, supporting the roles of these factors in the expansion of $CD11b^+$ myeloid cells in the bone marrow. Increasing lines of evidence have established the tumorigenic roles of bone marrow-derived myeloid cells (for a detailed review, see (46)). Recently, Dai *et al.* observed that GM-CSF, a strong myelogenic cytokine, rescued chemotherapy-induced leucopenia of mice, but promoted bone metastasis of prostate tumor cells (47). Therefore, we reasoned that suppression of myelogenic cytokine(s) may reverse the adverse pro-metastatic effects of cyclophosphamide. Results here confirmed that neutralizing CCL2, but not IL-6, significantly inhibited the pro-metastatic effects of cyclophosphamide in our model. It should be well noted that anti-CCL2 antibody is specific to the murine host-derived CCL2, and does not cross-reacting with prostate cancer-derived human CCL2, and that the neutralizing antibody was administered in only three dosages *before* tumor cell inoculation. Collectively, our data in **Figures 4** and **6** suggest that neutralizing CCL2 reconditions the pre-metastatic host

microenvironment induced by chemotherapy. Moreover, a CCL2 antibody is currently in clinical trials for prostate cancer (clinical trial No. NCT00992186; clinicaltrials.gov) (48, 49), and thus we believe our observation has potential clinical significance for patients on bone marrow-suppressive chemotherapy.

Although our data demonstrates the efficacy of anti-CCL2 antibody in the cyclophosphamide-induced prostate cancer bone metastasis model, increased expression of CCL2 (and subsequent expansion of myeloid cells) may not be the only mechanism of promoting metastasis after cyclophosphamide treatment. The first alternative explanation for the pro-metastatic effects of cyclophosphamide is that it could be mediated by the effects on bone cells. Given that inhibition of osteoclasts reversed the effects of GM-CSF on metastasis in a mouse model (47), it is possible that the effects of CCL2 neutralizing antibody in our results were, in part, mediated by inhibition of osteoclastogenesis. In addition, we observed that the osteoblast-covered trabecular bone surface and total trabecular bone perimeter were significantly reduced by 1 week after a single cyclophosphamide administration and that serum TRAP5b, a marker for osteoclastic activity, was significantly increased by cyclophosphamide treatment (data not shown). Therefore, the pro-metastatic effects of cyclophosphamide in a model used in this study may be partly mediated by suppression of the osteoblast population and/or an increase in osteoclastic activity. However, histomorphometric analyses of the cyclophosphamide-treated femurs demonstrated no significant changes in the osteoclast surface or trabecular bone volume, after a single cyclophosphamide administration. The observed trend for decreased bone volume suggests that additional cyclophosphamide treatment of longer duration would induce trabecular bone loss. Secondly, while our results failed to confirm the causal role of cyclophosphamide-induced endothelial damages in metastasis (**Figures 2** and **3**), the possibility still remains for

further investigation. Cyclophosphamide is currently being tested for efficacy as anti-angiogenic therapy, and disruption of endothelial barrier function can promote extravasation of tumor cells in the metastatic microenvironment. The primary vasculature of bone marrow is a large central sinusoidal vessel that lacks smooth muscle cells (pericytes) (50), suggesting the bone marrow endothelium may be more prone to chemotherapeutic damage. A single dose of cyclophosphamide treatment significantly suppressed endothelial cells in the bone marrow (**Figure 2E)**, but not in lungs, liver and kidney (**Supplemental Figure 2**), all of which have sinusoidal endothelium. Previously, Shirota and Tavassoli demonstrated that cyclophosphamide induces endothelial damage detectable by electron microscopy, and destroys the integrity of bone marrow sinus endothelium (indicated by red blood cells in the extra-vascular space), leading to enhanced engraftment of bone marrow transplantation (36). Therefore, cyclophosphamide effects on metastasis may be varied in different dosing schedules (i.e. metronomic low-dose) or different tumor models.

In conclusion, this study demonstrated that priming the murine host with a single dose of cyclophosphamide significantly altered the bone microenvironment, leading to promotion of prostate cancer bone metastasis. In addition, suppression of host CCL2 by antibody treatment significantly reduced the adverse effects of cyclophosphamide.

ACKNOWLEDGEMENTS

The authors thank Rashesh Kapadia for assistance in micro-CT scanning and Drs. Evan T. Keller and Russell S. Taichman for scientific discussions.

REFERENCES

1. Weilbaecher KN, Guise TA, McCauley LK. Cancer to bone: a fatal attraction. *Nat Rev Cancer* 2011; 11: 411-25.

2. Bubendorf L, Schopfer A, Wagner U, Sauter G, Moch H, Willi N, et al. Metastatic patterns of prostate cancer: an autopsy study of 1,589 patients. *Hum Pathol* 2000; 31: 578-83.

3. Hess KR, Varadhachary GR, Taylor SH, Wei W, Raber MN, Lenzi R, et al. Metastatic patterns in adenocarcinoma. *Cancer* 2006; 106: 1624-33.

4. Casimiro S, Guise TA, Chirgwin J. The critical role of the bone microenvironment in cancer metastases. *Mol Cell Endocrinol* 2009; 310: 71-81.

5. Roodman GD. Mechanisms of bone metastasis. *N Engl J Med* 2004; 350: 1655-64.

6. Shiozawa Y, Pedersen EA, Havens AM, Jung Y, Mishra A, Joseph J, et al. Human prostate cancer metastases target the hematopoietic stem cell niche to establish footholds in mouse bone marrow. *J Clin Invest* 2011.

7. Li X, Koh AJ, Wang Z, Soki FN, Park SI, Pienta KJ, et al. Inhibitory effects of megakaryocytic cells in prostate cancer skeletal metastasis. *J Bone Miner Res* 2011; 26: 125-34.

8. Seandel M, Butler J, Lyden D, Rafii S. A catalytic role for proangiogenic marrow-derived cells in tumor neovascularization. *Cancer Cell* 2008; 13: 181-3.

9. Yang L, DeBusk LM, Fukuda K, Fingleton B, Green-Jarvis B, Shyr Y, et al. Expansion of myeloid immune suppressor Gr+CD11b+ cells in tumor-bearing host directly promotes tumor angiogenesis. *Cancer Cell* 2004; 6: 409-21.

10. Ahn GO, Brown JM. Matrix metalloproteinase-9 is required for tumor vasculogenesis but not for angiogenesis: role of bone marrow-derived myelomonocytic cells. *Cancer Cell* 2008; 13: 193-205.

11. Ahn GO, Tseng D, Liao CH, Dorie MJ, Czechowicz A, Brown JM. Inhibition of Mac-1 (CD11b/CD18) enhances tumor response to radiation by reducing myeloid cell recruitment. *Proc Natl Acad Sci U S A*; 107: 8363-8.

12. Kozin SV, Kamoun WS, Huang Y, Dawson MR, Jain RK, Duda DG. Recruitment of Myeloid but not Endothelial Precursor Cells Facilitates Tumor Regrowth after Local Irradiation. *Cancer Res* 2010; 70: 5679-85.

13. Ahn GO, Brown JM. Influence of bone marrow-derived hematopoietic cells on the tumor response to radiotherapy: experimental models and clinical perspectives. *Cell Cycle* 2009; 8: 970-6.

14. Mizutani K, Sud S, McGregor NA, Martinovski G, Rice BT, Craig MJ, et al. The chemokine CCL2 increases prostate tumor growth and bone metastasis through macrophage and osteoclast recruitment. *Neoplasia* 2009; 11: 1235-42.

15. Mizutani K, Sud S, Pienta KJ. Prostate cancer promotes CD11b positive cells to differentiate into osteoclasts. *J Cell Biochem* 2009; 106: 563-9.

16. Zhang J, Lu Y, Pienta KJ. Multiple roles of chemokine (C-C motif) ligand 2 in promoting prostate cancer growth. *J Natl Cancer Inst*; 102: 522-8.

17. Loberg RD, Ying C, Craig M, Yan L, Snyder LA, Pienta KJ. CCL2 as an important mediator of prostate cancer growth in vivo through the regulation of macrophage infiltration. *Neoplasia* 2007; 9: 556-62.

18. Roca H, Varsos ZS, Pienta KJ. CCL2 is a negative regulator of AMP-activated protein kinase to sustain mTOR complex-1 activation, survivin expression, and cell survival in human prostate cancer PC3 cells. *Neoplasia* 2009; 11: 1309-17.

19. van Golen KL, Ying C, Sequeira L, Dubyk CW, Reisenberger T, Chinnaiyan AM, et al. CCL2 induces prostate cancer transendothelial cell migration via activation of the small GTPase Rac. *J Cell Biochem* 2008; 104: 1587-97.

20. Li X, Loberg R, Liao J, Ying C, Snyder LA, Pienta KJ, et al. A destructive cascade mediated by CCL2 facilitates prostate cancer growth in bone. *Cancer Res* 2009; 69: 1685-92.

21. Richman CM, Weiner RS, Yankee RA. Increase in circulating stem cells following chemotherapy in man. *Blood* 1976; 47: 1031-9.

22. Abrams RA, Johnston-Early A, Kramer C, Minna JD, Cohen MH, Deisseroth AB. Amplification of circulating granulocyte-monocyte stem cell numbers following chemotherapy in patients with extensive small cell carcinoma of the lung. *Cancer Res* 1981; 41: 35-41.

23. Carmel RJ, Brown JM. The effect of cyclophosphamide and other drugs on the incidence of pulmonary metastases in mice. *Cancer Res* 1977; 37: 145-51.

24. Vollmer TL, Conley FK. Effect of cyclophosphamide on survival of mice and incidence of metastatic tumor following intravenous and intracardial inoculation of tumor cells. *Cancer Res* 1984; 44: 3902-6.

25. Yamauchi K, Yang M, Hayashi K, Jiang P, Yamamoto N, Tsuchiya H, et al. Induction of cancer metastasis by cyclophosphamide pretreatment of host mice: an opposite effect of chemotherapy. *Cancer Res* 2008; 68: 516-20.

26. Wu YJ, Muldoon LL, Dickey DT, Lewin SJ, Varallyay CG, Neuwelt EA. Cyclophosphamide enhances human tumor growth in nude rat xenografted tumor models. *Neoplasia* 2009; 11: 187-95.

27. Schneider A, Kalikin LM, Mattos AC, Keller ET, Allen MJ, Pienta KJ, et al. Bone turnover mediates preferential localization of prostate cancer in the skeleton. *Endocrinology* 2005; 146: 1727-36.

28. Park SI, Kim SJ, McCauley LK, Gallick GE. Pre-Clinical Mouse Models of Human Prostate Cancer and their Utility in Drug Discovery. *Curr Protoc Pharmacol* 2011; 51: 14 5- 5 27.

29. Butcher JT, Sedmera D, Guldberg RE, Markwald RR. Quantitative volumetric analysis of cardiac morphogenesis assessed through micro-computed tomography. *Dev Dyn* 2007; 236: 802-9.

30. Guldberg RE, Duvall CL, Peister A, Oest ME, Lin AS, Palmer AW, et al. 3D imaging of tissue integration with porous biomaterials. *Biomaterials* 2008; 29: 3757-61.

31. Loberg RD, Ying C, Craig M, Day LL, Sargent E, Neeley C, et al. Targeting CCL2 with systemic delivery of neutralizing antibodies induces prostate cancer tumor regression in vivo. *Cancer Res* 2007; 67: 9417-24.

32. Tsui P, Das A, Whitaker B, Tornetta M, Stowell N, Kesavan P, et al. Generation, characterization and biological activity of CCL2 (MCP-1/JE) and CCL12 (MCP-5) specific antibodies. *Hum Antibodies* 2007; 16: 117-25.

33. Man S, Zhang Y, Gao W, Yan L, Ma C. Cyclophosphamide promotes pulmonary metastasis on mouse lung adenocarcinoma. *Clin Exp Metastasis* 2008; 25: 855-64.

34. Bagley CM, Jr., Bostick FW, DeVita VT, Jr. Clinical pharmacology of cyclophosphamide. *Cancer Res* 1973; 33: 226-33.

35. Kline I, Gang M, Tyrer DD, Mantel N, Venditti JM, Goldin A. Duration of drug levels in mice as indicated by residual antileukemic efficacy. *Chemotherapy* 1968; 13: 28-41.

36. Shirota T, Tavassoli M. Cyclophosphamide-induced alterations of bone marrow endothelium: implications in homing of marrow cells after transplantation. *Exp Hematol* 1991; 19: 369-73.

37. Kopp HG, Avecilla ST, Hooper AT, Shmelkov SV, Ramos CA, Zhang F, et al. Tie2 activation contributes to hemangiogenic regeneration after myelosuppression. *Blood* 2005; 106: 505-13.

38. Ferrara N, Gerber HP, LeCouter J. The biology of VEGF and its receptors. *Nat Med* 2003; 9: 669-76.

39. Kim S, Takahashi H, Lin WW, Descargues P, Grivennikov S, Kim Y, et al. Carcinoma-produced factors activate myeloid cells through TLR2 to stimulate metastasis. *Nature* 2009; 457: 102-6.

40. Roca H, Varsos ZS, Sud S, Craig MJ, Ying C, Pienta KJ. CCL2 and interleukin-6 promote survival of human CD11b+ peripheral blood mononuclear cells and induce M2-type macrophage polarization. *J Biol Chem* 2009; 284: 34342-54.

41. Chantrain CF, Feron O, Marbaix E, Declerck YA. Bone marrow microenvironment and tumor progression. *Cancer Microenviron* 2008; 1: 23-35.

42. van Putten LM, Kram LK, van Dierendonck HH, Smink T, Fuzy M. Enhancement by drugs of metastatic lung nodule formation after intravenous tumour cell injection. *Int J Cancer* 1975; 15: 588-95.

43. Emmenegger U, Morton GC, Francia G, Shaked Y, Franco M, Weinerman A, et al. Low-dose metronomic daily cyclophosphamide and weekly tirapazamine: a well-tolerated combination regimen with enhanced efficacy that exploits tumor hypoxia. *Cancer Res* 2006; 66: 1664-74.

44. Lord R, Nair S, Schache A, Spicer J, Somaihah N, Khoo V, et al. Low dose metronomic oral cyclophosphamide for hormone resistant prostate cancer: a phase II study. *J Urol* 2007; 177: 2136-40.

45. McClatchey KD, ed. *Clinical Laboratory Medicine*. Philadelphia, Pennsylvania, USA: Lippincott Williams & Wilkins; 2001.

46. Chung AS, Lee J, Ferrara N. Targeting the tumour vasculature: insights from physiological angiogenesis. *Nat Rev Cancer*; 10: 505-14.

47. Dai J, Lu Y, Yu C, Keller JM, Mizokami A, Zhang J, et al. Reversal of Chemotherapy-Induced Leukopenia Using Granulocyte Macrophage Colony-Stimulating Factor Promotes Bone Metastasis That Can Be Blocked with Osteoclast Inhibitors. *Cancer Res* 2010; 70: 5014-23.

48. Forster MD, Patnaik A, Sandhu SK, Papadopoulos K, Tromp BJ, Messiou C, et al. Pre-final analysis of first-in-human, first-in-class, phase I clinical trial of CNTO 888, a human monoclonal antibody to the CC-chemokine ligand 2 (CCL2) in patients (pts) with advanced solid tumors. *J Clin Oncol (Meeting Abstracts)*; 28: 2548-.

49. Sandhu SK, Fong PC, Frentzas S, Patnaik A, Papadopoulos K, Tromp B, et al. First-in-human, first-in-class, phase I study of a human monoclonal antibody CNTO 888 to the CC-chemokine ligand 2 (CCL2/MCP-1) in patients with solid tumors. *J Clin Oncol (Meeting Abstracts)* 2009; 27: e13500-.

50. Travlos GS. Normal structure, function, and histology of the bone marrow. *Toxicol Pathol* 2006; 34: 548-65.

FIGURE LEGENDS

Figure 1 Priming mice with a single administration of cyclophosphamide (CY) enhanced experimental prostate cancer skeletal metastasis

A. Schematic representation of the experimental design. Male athymic mice were divided into two groups and treated with saline or CY (350 mg/kg, i.p.). Following 7 days of recovery, PC-3^{Luc} cells were injected into the left heart ventricle (n=18 for saline control and n=13 for CY group). Development and subsequent growth of metastatic tumors were monitored by weekly *in vivo* bioluminescence imaging for 6 weeks.

B. Hind limb metastatic tumor size was measured by weekly *in vivo* bioluminescence imaging. CY-treated mice had significantly increased photon emission from the hind limbs, compared to the saline-treated mice after day 28. Data are medians with interquartile range (i.e. 25th and 75th percentiles). Asterisks represent model-contrast P<0.01.

C. Mandibular metastatic tumor size was measured, and median photon emission per second from the mandibular lesions in each group was plotted. The CY-treated group had increased photon emission compared to the saline-treated group after 35 days. Data are median ± interquartile range. Asterisks represent model-contrast P<0.01.

D. Percentage of hind limb metastasis-free mice was plotted in a Kaplan-Meier curve. Lesions emitting more than 1×10^5 photon/second were considered as metastases. The CY group had significantly higher incidence of hind limb metastases than the saline control group (P<0.01 by logrank test). HR and CI stand for hazard ratio and confidence interval, respectively.

E. Representative histological images of metastatic bone tumors. Tumor-bearing hind limb tibiae were dissected, followed by fixation, decalcification, sectioning and H&E staining. The presence of metastatic tumor cells was confirmed microscopically. Tumor perimeter is indicated by dotted lines in lower magnification images (×4 objective lens; upper panel). Higher magnification images (× 20 objective lens; lower panel) show tumor (designated "T"), bone (designated "B") and bone marrow (designated "BM").

Figure 2 A single administration of cyclophosphamide significantly disrupted bone marrow vascular integrity

A. Schematic representation of *ex vivo* murine bone marrow microvascular angiography. Male C57BL6/J mice were divided into two groups (*n*=12 each) and treated with saline or CY. Following 7 days of recovery, mice were perfused sequentially with heparin-supplemented Ringer's lactate solution, 10% buffered formalin and liquid-phase radiopaque monomeric compound (Microfil®) via the intra-cardiac route. After overnight polymerization at 4°C, femurs were dissected, decalcified and scanned with micro-computerized tomography (μCT).

B. Five representative μCT images of *ex vivo* femoral angiography from the saline-treated group (*n*=12) are shown. Note microvessels in the epiphyses and the central sinusoid in the diaphysis.

C. Five representative μCT images of *ex vivo* femoral angiography from the CY-treated group (*n*=12) are shown, demonstrating disintegration of vascular structures.

D. µCT data were analyzed to quantify the total vascular volume (per bone). Data are mean ± standard error. The CY group had a significantly reduced vascular volume ($P<0.05$ by Mann Whitney *U* test).

E. Femurs of saline- or CY-treated C57B6/J mice ($n=10$/group; the same dosage and schedule as described in A-C) were dissected, and bone marrow was flushed with TRIzol reagent to harvest RNA. RNA samples were reverse-transcribed followed by quantitative PCR to measure the expression of *CD31/PECAM* endothelial cell marker. Data are mean ± standard deviation. Bone marrow from the CY group had significantly reduced *CD31/PECAM* expression levels ($P<0.01$ by Student's t-test).

Figure 3 Cyclophosphamide pre-treatment directly promoted orthotopic PC-3 tumor growth in bone

A. Schematic representation of the experiment. Male athymic mice were divided into two groups ($n=8$ each) and treated with saline or CY. Following 7 days of recovery, PC-3^{Luc} cells were injected into the bone marrow space of the right proximal tibiae. Tumor growth in bone was monitored by weekly *in vivo* bioluminescence imaging for 6 weeks.

B. CY pre-treated mice had significantly increased tumor size after 42 days ($P<0.05$ by Student's t-test). Data are mean ± standard error.

C. Representative images of *in vivo* bioluminescence on day 42 are shown.

Figure 4 Cyclophosphamide transiently expanded monocytes and neutrophils in the peripheral blood, and myeloid lineage cells in the bone marrow during the recovery phase after bone marrow suppression

A. – C. Male C57BL6/J mice (n=8 per group at each time point) were treated with saline (control) or CY followed by complete blood counting (CBC) with white blood cell (WBC) differential counting on 3, 7, 10 and 15 days after treatment. Data are mean ± standard deviation. Asterisks indicate statistical significance (* indicates P<0.01 and ** indicates P<0.05 by Student's t-test). Shade indicates standard range. **A**. CY-treated mice had significantly reduced WBC counts at all time points, compared to saline-treated groups. However, at day 7, a spike of total WBC count was observed. **B.** The increase of total WBC count on day 7 was associated with an expansion of neutrophils. The neutrophil number was below detection 3 days after CY treatment, but increased on day 7 post-CY treatment, followed by normalization (at day 10) and suppression (at day 15). **C.** Monocyte counts were lower than control groups at all time points. However, similar to neutrophil counts, the monocyte count in day 7 CY group was significantly increased, compared to day 3 CY group.

D. Myeloid lineage cells in the bone marrow were expanded at day 7 post-CY. Male C57BL/6J mice (n=8 per group at each time point) were treated with saline (control) or CY followed by flushing bone marrow cells for flow cytometric analysis of myeloid lineage cell populations (expressing CD11b marker) on 3, 7, 10 and 15 days after treatment. Parallel to the changes of monocyte and neutrophil counts in the peripheral blood, the $CD11b^+$ population was suppressed at day 3, followed by increases at day 7 and 10. Data are mean ± standard deviation, and asterisks represent statistical significance (* indicates P<0.01 and ** indicates P<0.05 by Student's t-test).

E. – G. CY treatment did not increase $CD11b^+$ myeloid cells in the solid organs. Male C57BL/6J mice (n=6/group) were treated with saline (control) or CY. After 7 days,

kidney (**E**), lung (**F**) and liver (**G**) were surgically removed and digested for flow cytometric analyses of $CD11b^+$ myeloid cells. Data are mean ± standard deviation. N.S. indicates not significant by Student's t-test.

H. – J. CY treatment increased myeloid-associated cytokines in serum. Male C57BL/6J mice (*n*=12 each) were treated with saline (control) or CY. After 7 days, whole blood was collected by cardiac puncture and serum cytokines including vascular endothelial growth factor (VEGF)-A (**H)**, IL-6 (**I**) and CCL2 (**J**) were measured by ELISA. Each dot represents an individual serum cytokine level, and bars represent median. CY treatment significantly increased VEGF-A, IL-6 and CCL2 levels, compared to saline-treated control groups (all $P<0.01$ by Mann Whitney *U* test).

Figure 5 Recovery time after cyclophosphamide administration affected development of skeletal metastases.

A. Schematic representation of the experiment. Male athymic mice were treated with saline or CY (350 mg/kg, i.p.). Following 3, 7 or 15 days of recovery respectively, $PC\text{-}3^{Luc}$ tumor cells were inoculated via intra-cardiac injection. Development and subsequent growth of metastatic tumors were monitored by weekly *in vivo* bioluminescence imaging for 5 weeks.

B. Percentage of metastasis-free mice was plotted in a Kaplan-Meier survival curve. The 7-day group had significantly increased hind limb metastases compared to the saline-treated control group ($P<0.01$ by logrank test, hazard ratio [HR]=0.07 with 95% confidence interval of ratio [CI]=0.02~0.25). The 3-day group was similar to the 7-day group ($P=0.67$ by logrank test, HR=0.78 with 95% CI =0.25~2.43), while the 15-day group had

significantly slower development of metastases compared to the 7-day group (P<0.05 by logrank test, HR =3.116 with 95% CI=1.1~8.9).

C. Hind limb metastatic tumor size was measured by weekly *in vivo* bioluminescence imaging. All CY-treated groups had significantly increased photon emission from the hind limbs compared to the saline-treated mice (model-contrast P<0.01 at all time points). The 3-Day group had significantly increased tumor burden compared to the 7-day group on week-5 imaging (model-contrast P<0.01), while the 15-day group had significantly reduced tumor burden compared to the 7-day group (model-contrast P<0.01). Data are median ± interquartile range.

Figure 6 Neutralizing CCL2, but not IL-6, reverted cyclophosphamide-induced prostate cancer bone metastasis.

A. Schematic representation of the experiment. Male athymic mice were treated with saline (n=10) or CY in combination with control IgG (n=14; 10 mg/kg, i.p.), anti-mouse IL-6 (n=11; 20 mg/kg, i.p.), anti-mouse CCL2 (n=12; 10 mg/kg, i.p.), or a combination of anti-IL-6 and CCL2 antibodies (n=12). Three doses were given one day before CY treatment, and 3 and 6 days after CY treatment. On day 7 post-CY injection, PC-3^{Luc} cells were injected into the left heart ventricle. Development and subsequent growth of metastatic tumors were monitored by weekly *in vivo* bioluminescence imaging for 6 weeks.

B. Serial images from five representative mice from each group are shown. CY treatment alone significantly increased skeletal metastasis (second row) compared to the saline treatment group (first row). Neutralizing CCL2 in the CY-treated mice prior to tumor

inoculation significantly reduced skeletal metastasis (fourth row), while neutralizing IL-6 had no significant effects (third row). Treatment with a combination of anti-CCL2 and IL-6 antibodies (fifth row) had similar effects as anti-CCL2 antibody alone.

C. –D. Week 4 (**C**) and Week 6 (**D**) bioluminescence data were quantified and plotted. Tumor size was measured by photon emission per second from the hind limb lesions in each group. Data are median ± interquartile range.

Figure 7 Docetaxel pre-treatment did not promote the development of hind limb skeletal metastasis

A. Schematic representation of the experiment. Male athymic mice were treated with saline or docetaxel (40 mg/kg, i.p.). Following 7 days of recovery, PC-3^{Luc} cells were injected into the left heart ventricle (n=10 for saline control and n=12 for docetaxel group). Development and subsequent growth of metastatic tumors were monitored by weekly *in vivo* bioluminescence imaging for 6 weeks.

B. Hind limb metastatic tumor size was measured by weekly *in vivo* bioluminescence imaging. Docetaxel-treated mice had significantly decreased photon emission from the hind limbs, compared to the saline-treated mice after day 21. Data are medians with interquartile range. Asterisks represent model-contrast P<0.01.

C. Docetaxel induced myeloid cell expansion similarly, but to a lesser extent than CY. Male athymic mice were treated with saline, CY (350mg/kg, i.p.) or docetaxel (40mg/kg, i.p.), followed by flushing bone marrow cells for flow cytometric analysis of myeloid lineage cell populations (expressing CD11b marker) on 3, 7 and 15 days after treatment (n=8 per

group at each time point). Data are mean ± standard deviation, and asterisks represent statistical significance (* indicates $P<0.01$ and ** indicates $P<0.05$ by Student's t-test).

D. –F. The numbers of WBC (**D**), neutrophils (**E**) and monocytes (**F**) did not change after docetaxel treatment. Male C57BL6/J mice ($n=10$ per group) were treated with saline (control) or docetaxel (40 mg/kg, i.p.) followed by complete blood counting (CBC) with white blood cell (WBC) differential counting 7 days after treatment. Data are mean ± standard deviation. NS stands for not significant ($P>0.05$ by Student's t-test).

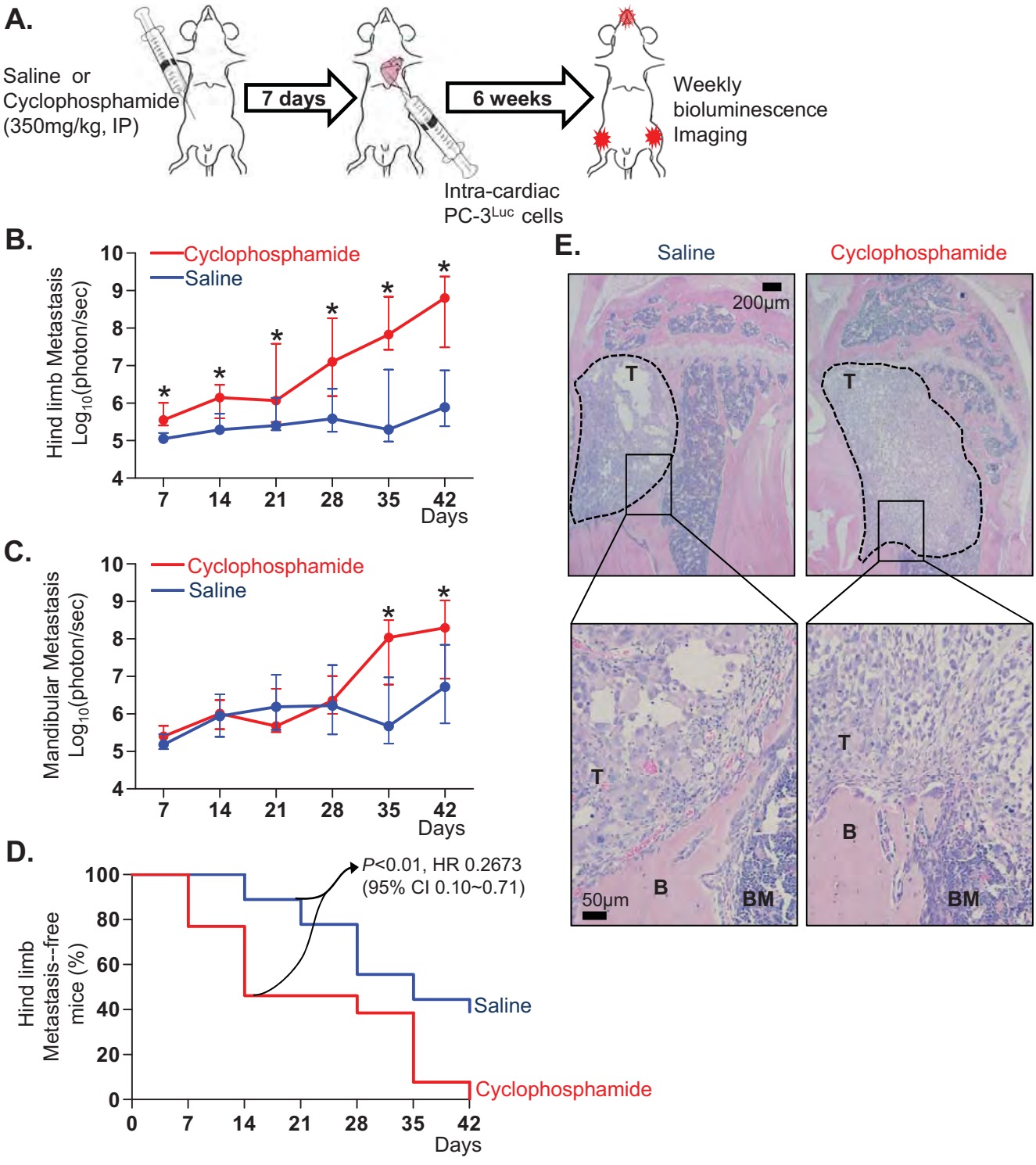
A.
Saline or
Cyclophosphamide
(350mg/kg, IP)
7 days
6 weeks
Weekly
bioluminescence
Imaging
Intra-cardiac
PC-3Luc cells
B.
Cyclophosphamide
Saline
Hind limb Metastasis
Log10(photon/sec)
Days
C.
Cyclophosphamide
Saline
Mandibular Metastasis
Log10(photon/sec)
Days
D.
P<0.01, HR 0.2673
(95% CI 0.10~0.71)
Hind limb
Metastasis--free
mice (%)
Saline
Cyclophosphamide
Days
E.
Saline
Cyclophosphamide
200μm
T
B
BM
50μm

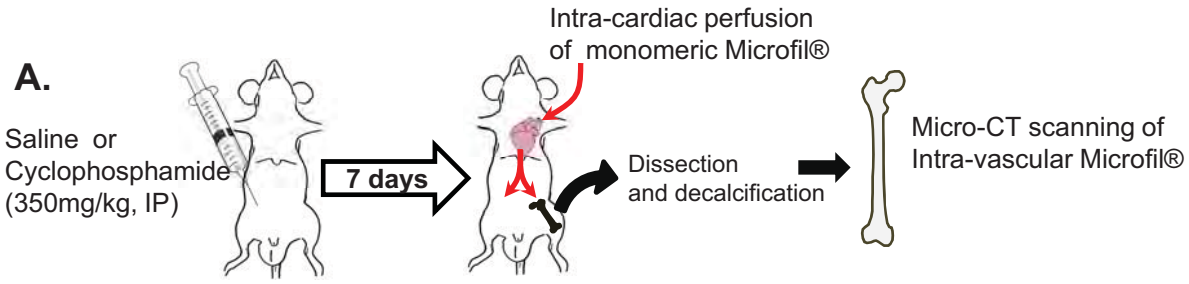
A.
Saline or
Cyclophosphamide
(350mg/kg, IP)
7 days
Intra-cardiac perfusion
of monomeric Microfil®
Dissection
and decalcification
Micro-CT scanning of
Intra-vascular Microfil®

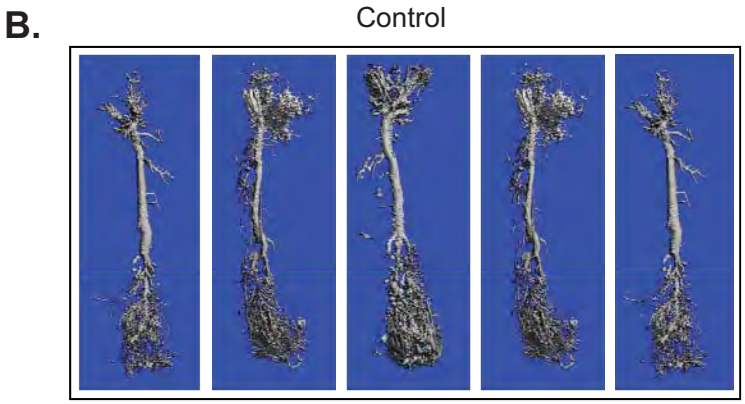
B.
Control

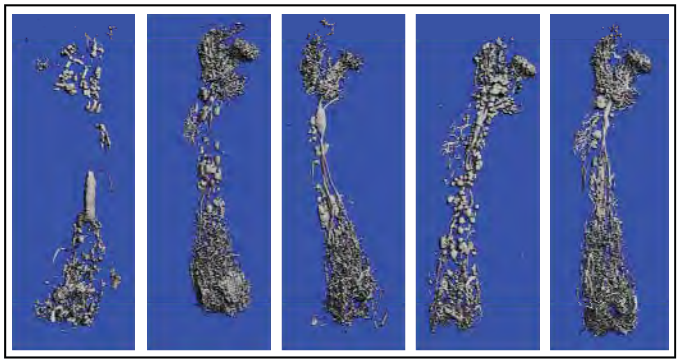
C.
Cyclophosphamide

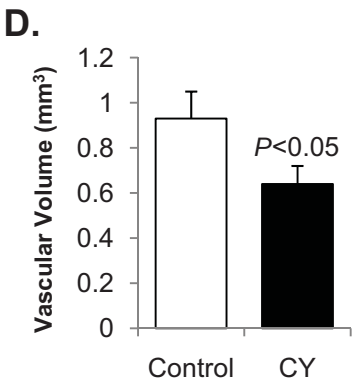
D.
Vascular Volume (mm³)
1.2
1
0.8
0.6
0.4
0.2
0
P<0.05
Control
CY

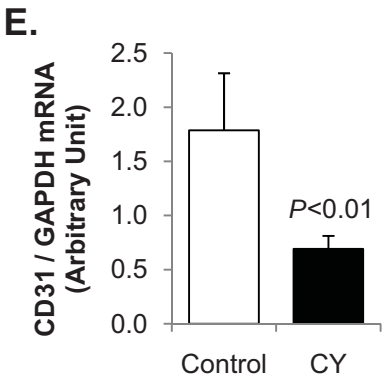
E.
CD31 / GAPDH mRNA
(Arbitrary Unit)
2.5
2.0
1.5
1.0
0.5
0.0
P<0.01
Control
CY

Figure 3

SI Park *et al.*

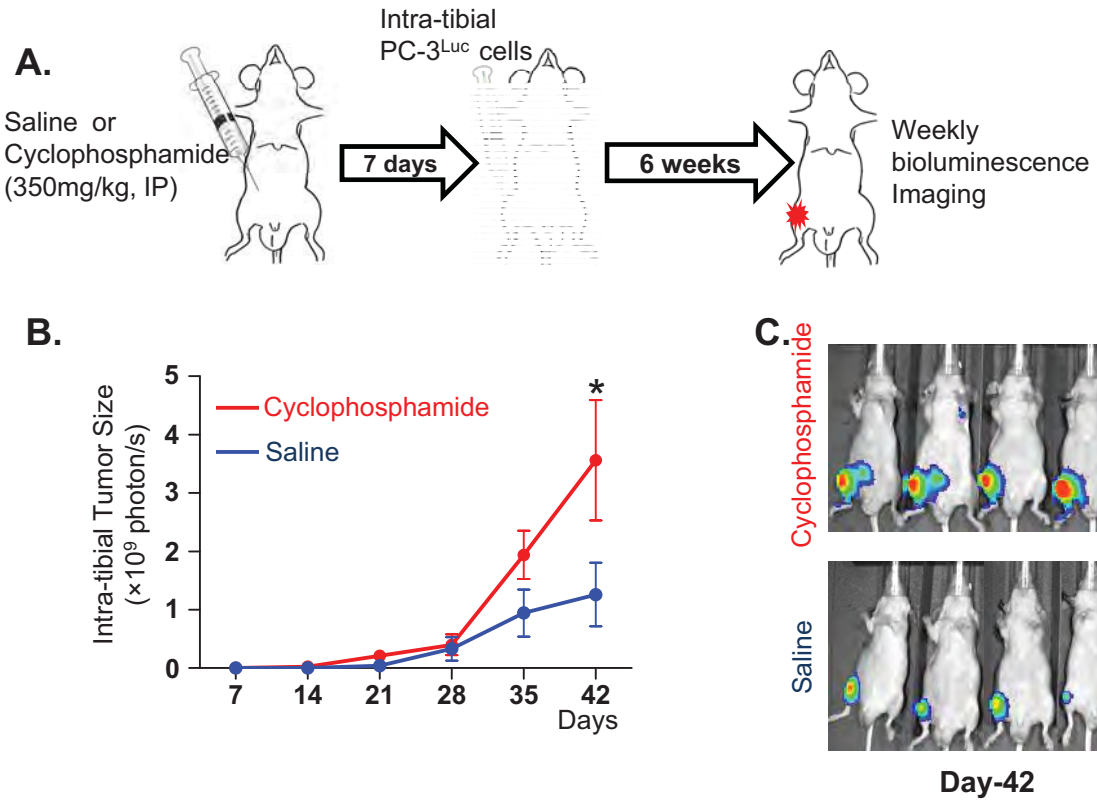

Figure 4

SI Park *et al.*

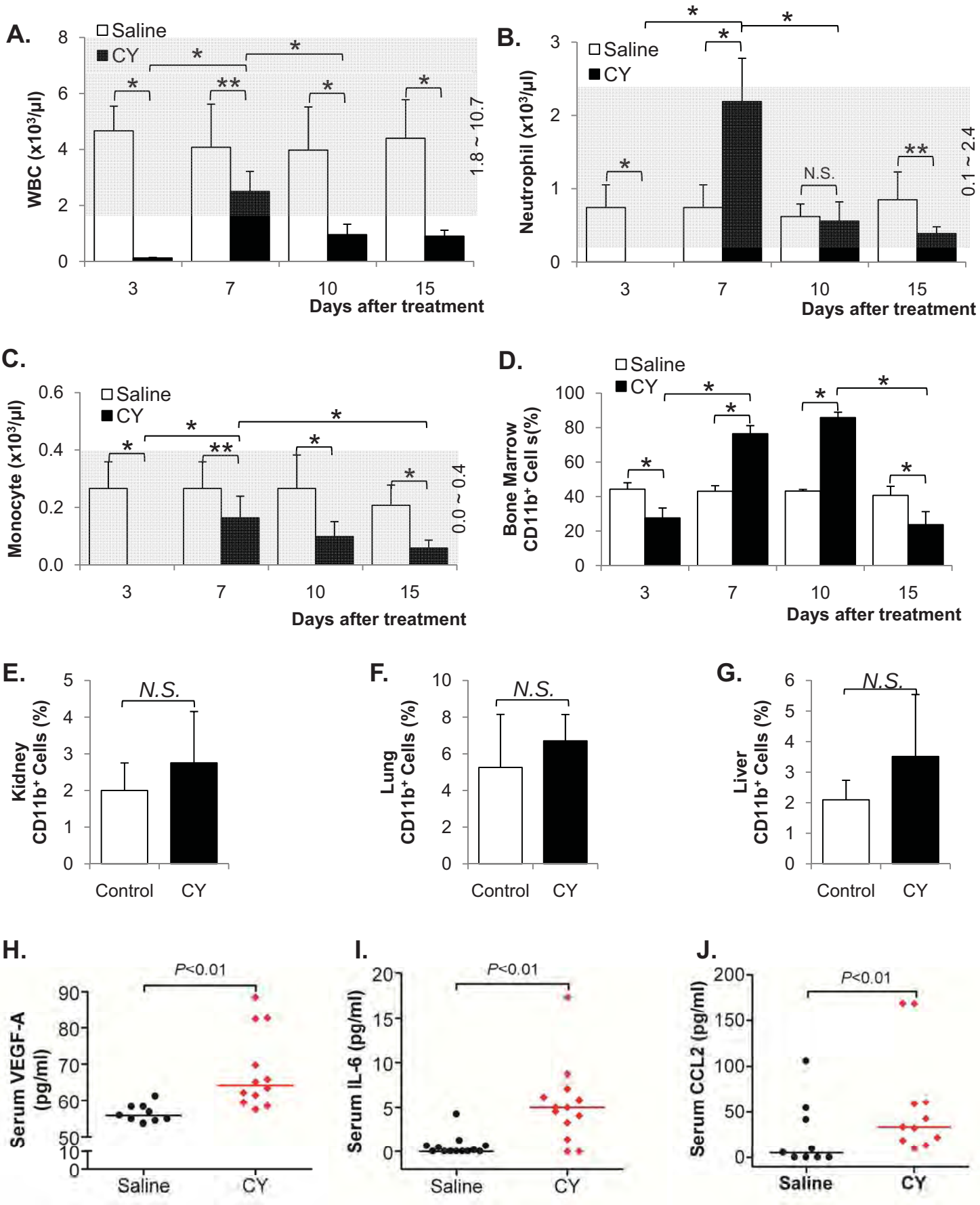

Figure 5 SI Park *et al.*

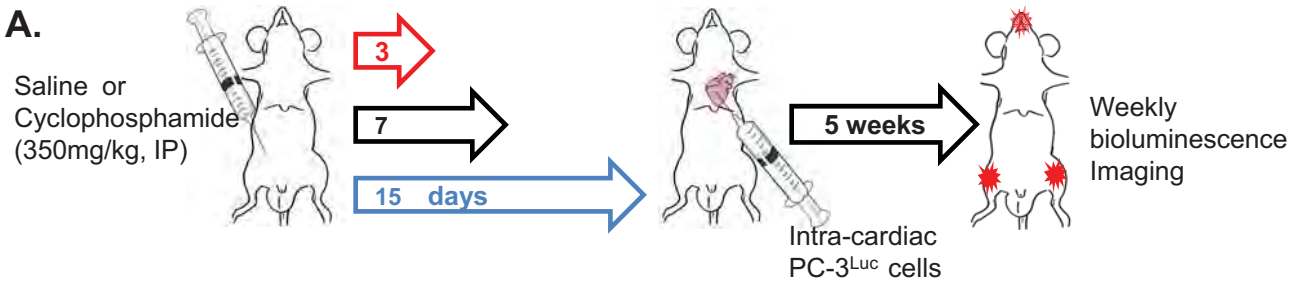

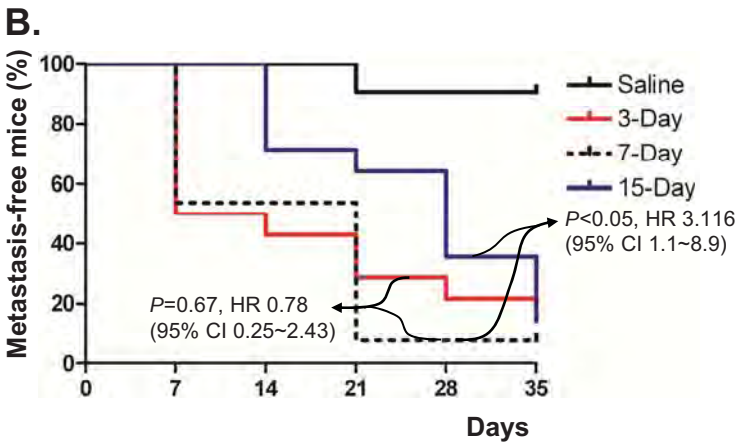

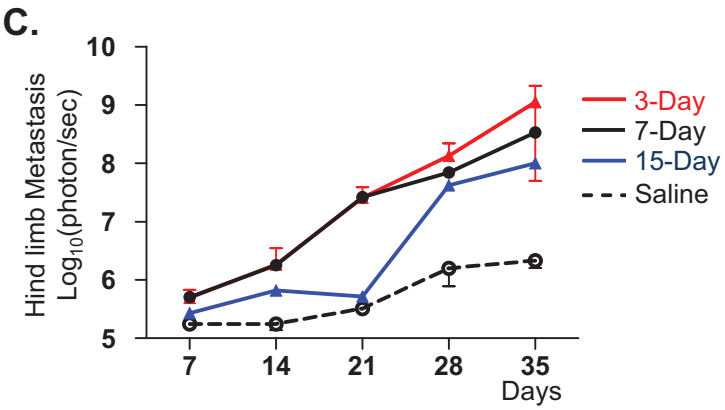

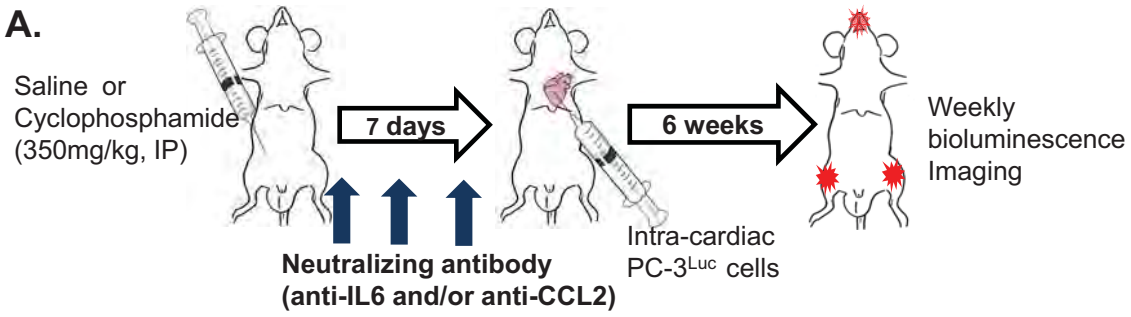
A.
Saline or
Cyclophosphamide
(350mg/kg, IP)
7 days
6 weeks
Weekly
bioluminescence
Imaging
Intra-cardiac
PC-3Luc cells
Neutralizing antibody
(anti-IL6 and/or anti-CCL2)

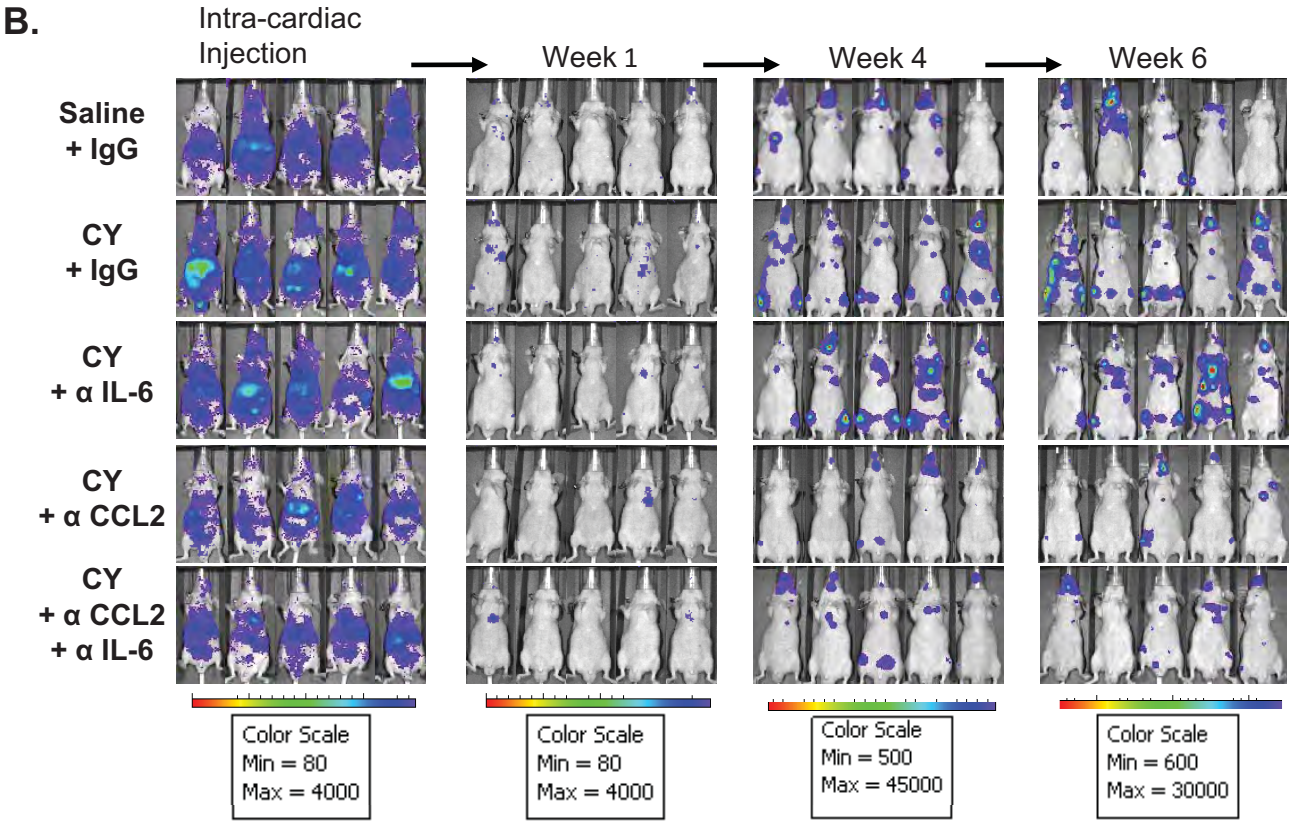
B.
Intra-cardiac
Injection
Week 1
Week 4
Week 6
Saline
+ IgG
CY
+ IgG
CY
+ α IL-6
CY
+ α CCL2
CY
+ α CCL2
+ α IL-6
Color Scale
Min = 80
Max = 4000
Color Scale
Min = 80
Max = 4000
Color Scale
Min = 500
Max = 45000
Color Scale
Min = 600
Max = 30000

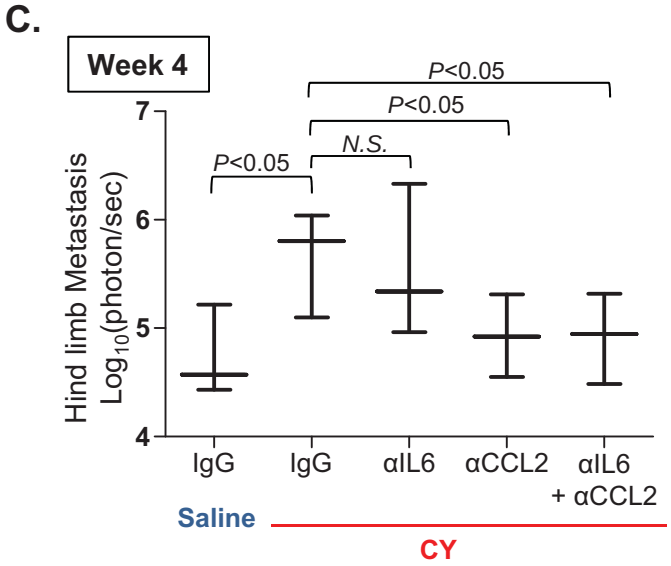
C.
Week 4
P<0.05
P<0.05
N.S.
P<0.05
Hind limb Metastasis
Log10(photon/sec)
7
6
5
4
IgG
IgG
αIL6
αCCL2
αIL6
+ αCCL2
Saline
CY

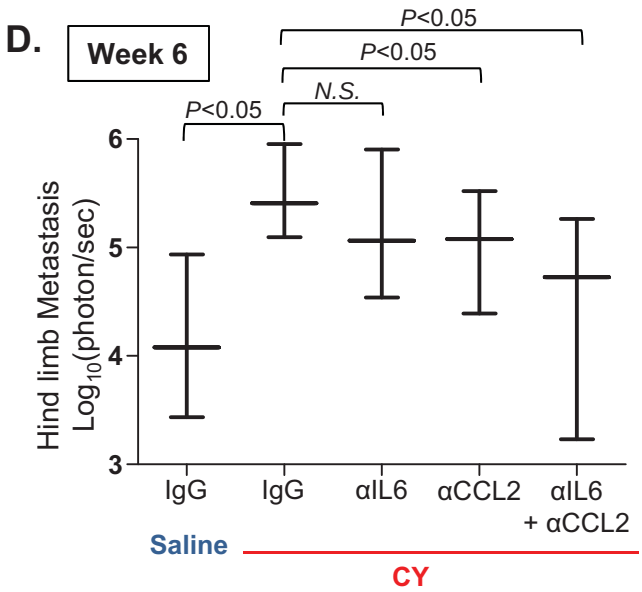
D.
Week 6
P<0.05
P<0.05
N.S.
P<0.05
Hind limb Metastasis
Log10(photon/sec)
6
5
4
3
IgG
IgG
αIL6
αCCL2
αIL6
+ αCCL2
Saline
CY

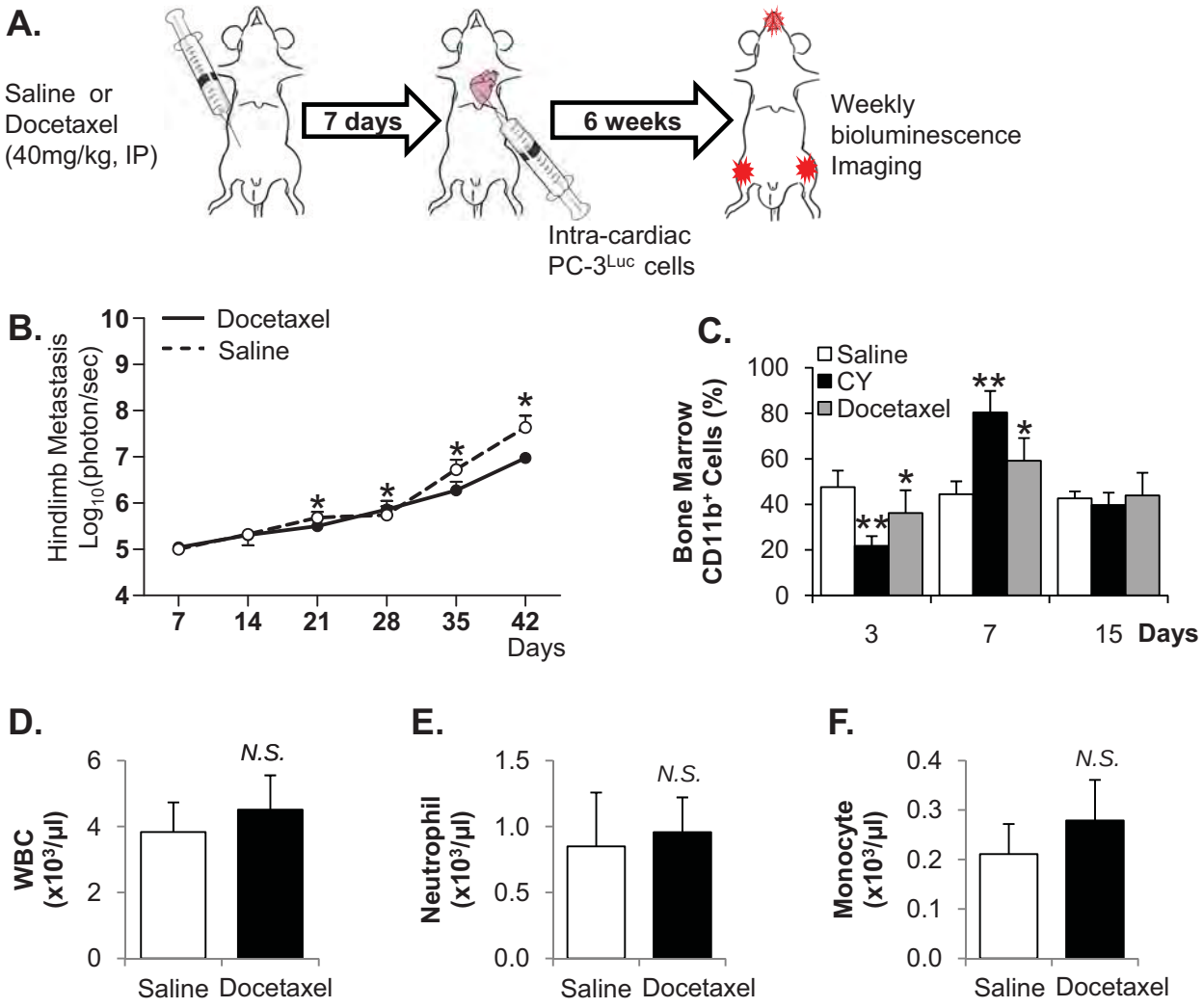
A.
Saline or
Docetaxel
(40mg/kg, IP)
7 days
6 weeks
Weekly
bioluminescence
Imaging
Intra-cardiac
PC-3Luc cells
B.
Docetaxel
Saline
Hindlimb Metastasis
Log10(photon/sec)
10
9
8
7
6
5
4
7
14
21
28
35
42
Days
C.
Saline
CY
Docetaxel
Bone Marrow
CD11b+ Cells (%)
100
80
60
40
20
0
3
7
15
Days
D.
WBC
(x10³/μl)
6
4
2
0
N.S.
Saline
Docetaxel
E.
Neutrophil
(x10³/μl)
1.5
1.0
0.5
0.0
N.S.
Saline
Docetaxel
F.
Monocyte
(x10³/μl)
0.4
0.3
0.2
0.1
0.0
N.S.
Saline
Docetaxel

Supplemental Figure 1

SI Park *et al.*

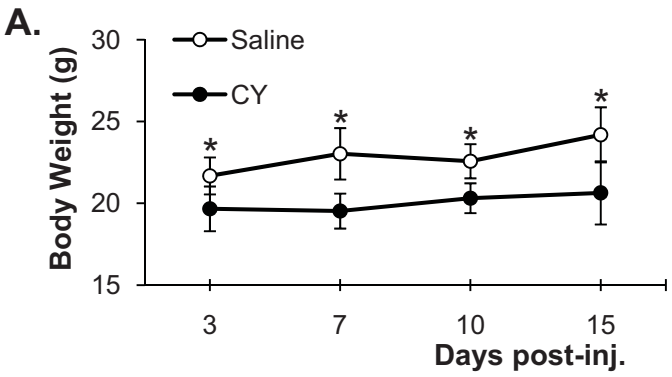

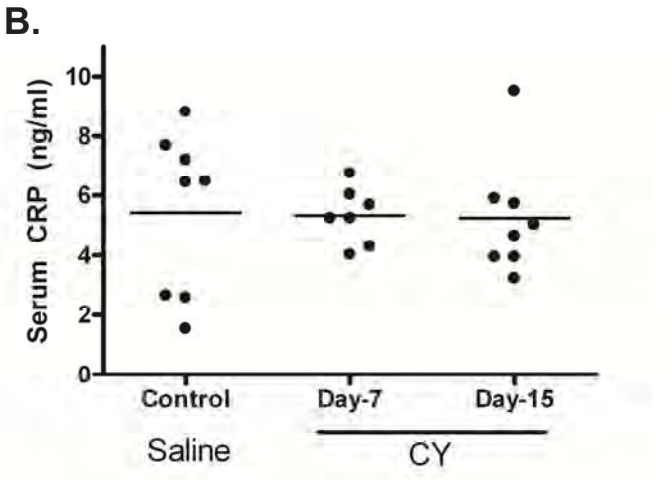

Supplemental Figure 2

SI Park *et al.*

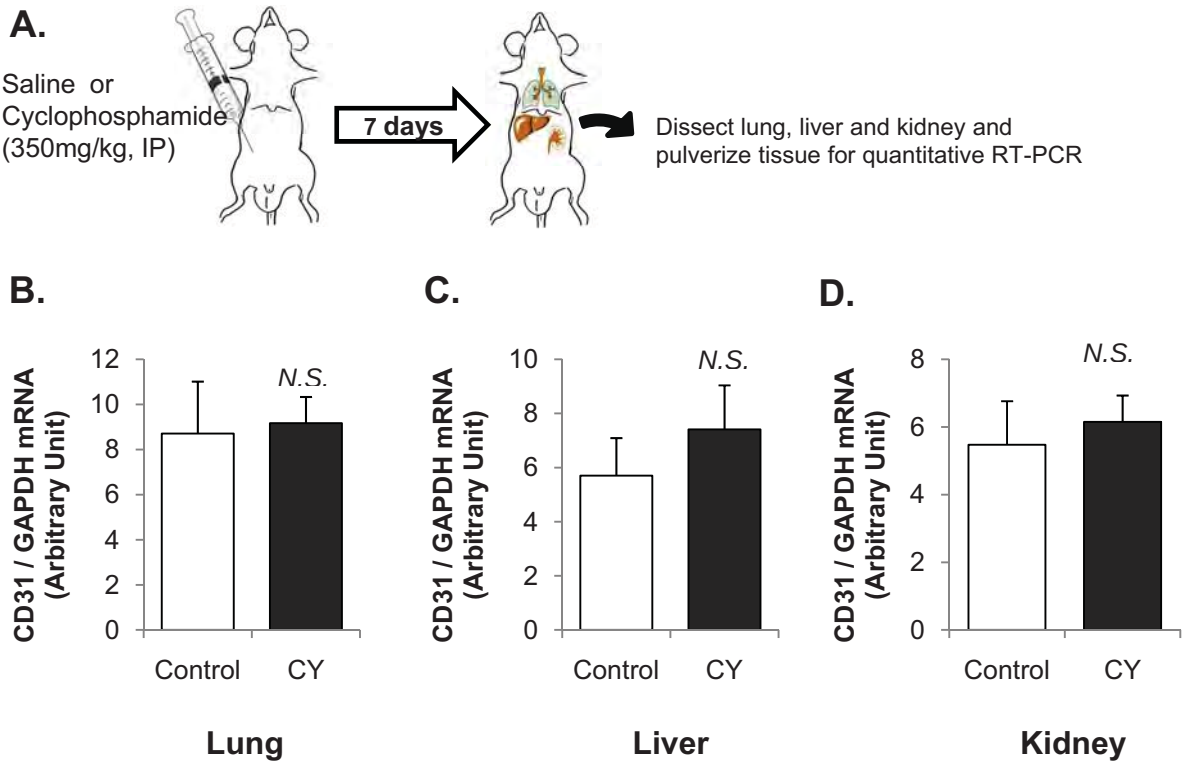

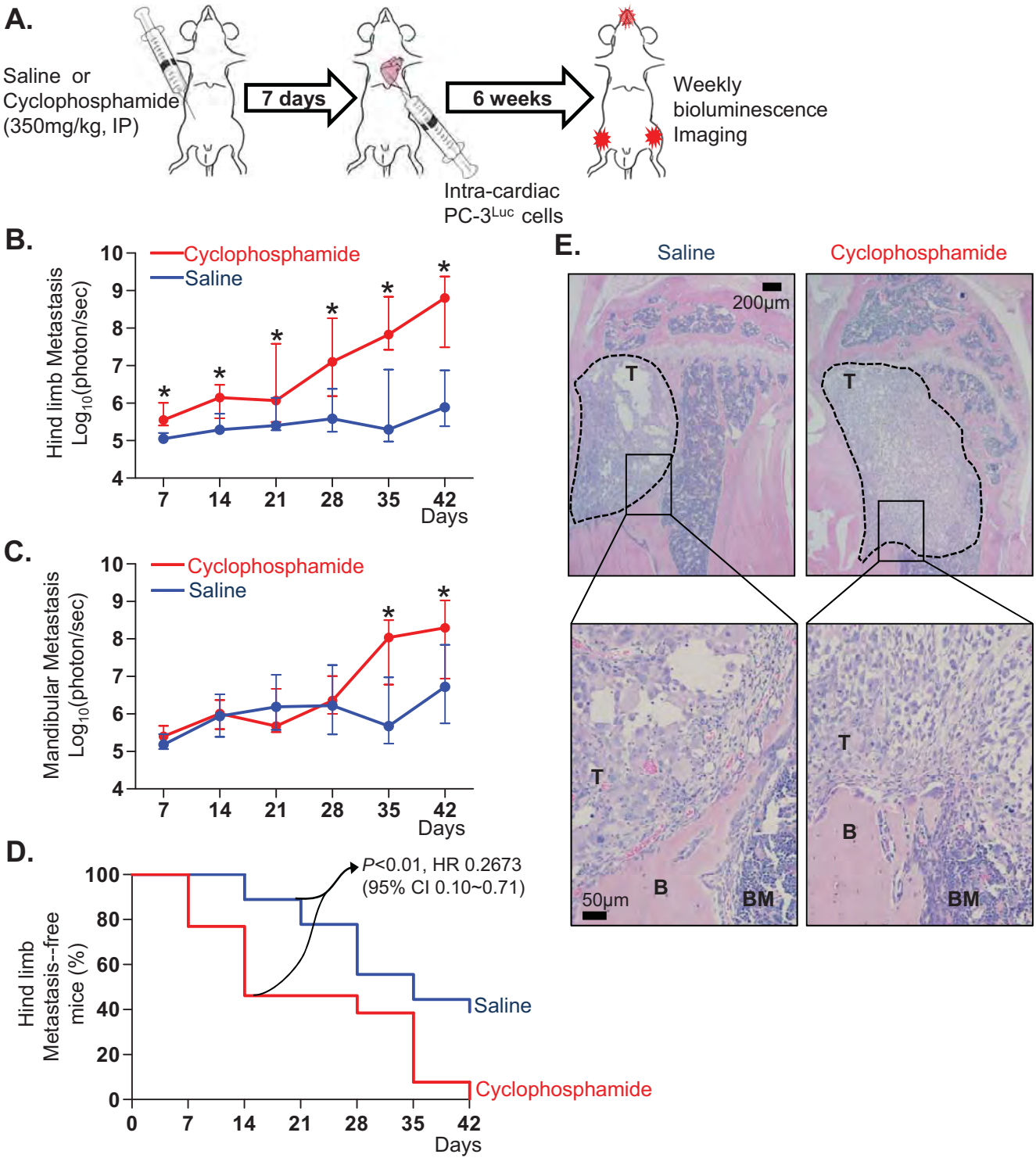
A.
Saline or
Cyclophosphamide
(350mg/kg, IP)
7 days
6 weeks
Weekly
bioluminescence
Imaging
Intra-cardiac
PC-3Luc cells
B.
Cyclophosphamide
Saline
Hind limb Metastasis
Log10(photon/sec)
Days
C.
Cyclophosphamide
Saline
Mandibular Metastasis
Log10(photon/sec)
Days
D.
P<0.01, HR 0.2673
(95% CI 0.10~0.71)
Hind limb
Metastasis--free
mice (%)
Saline
Cyclophosphamide
Days
E.
Saline
Cyclophosphamide
200μm
T
B
BM
50μm

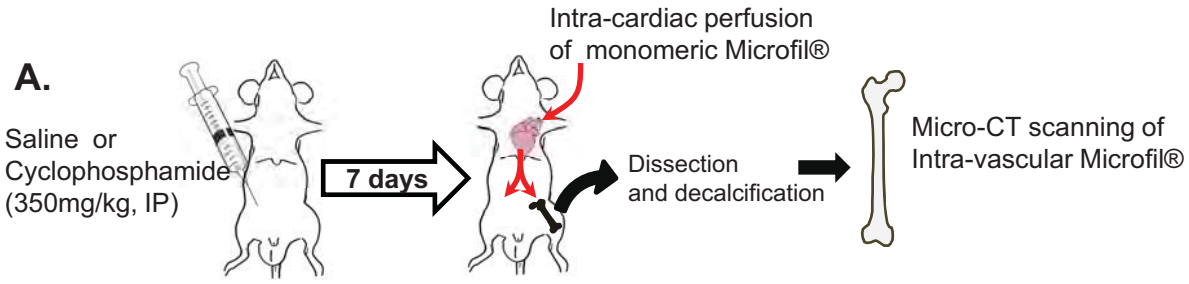
A.
Saline or
Cyclophosphamide
(350mg/kg, IP)
7 days
Intra-cardiac perfusion
of monomeric Microfil®
Dissection
and decalcification
Micro-CT scanning of
Intra-vascular Microfil®

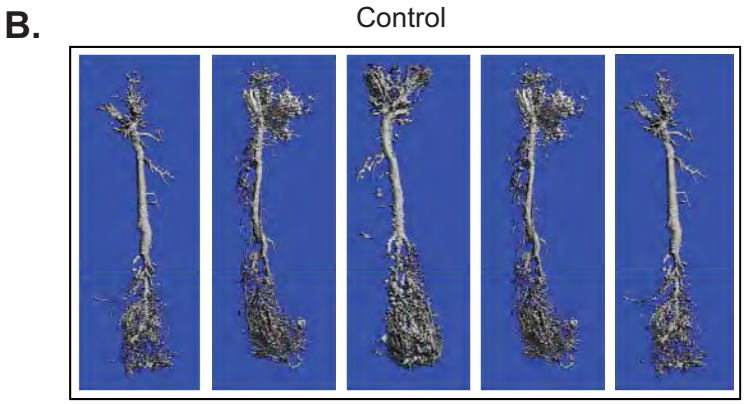
B.
Control

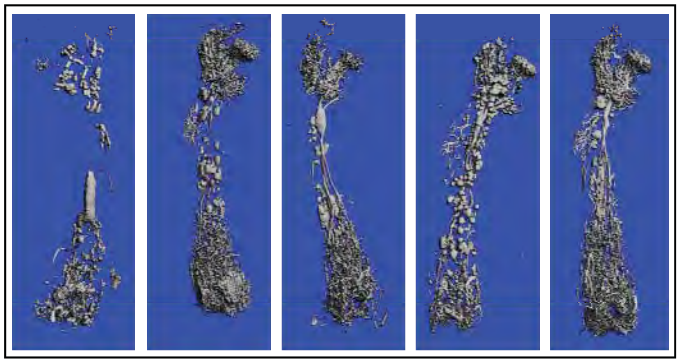
C.
Cyclophosphamide

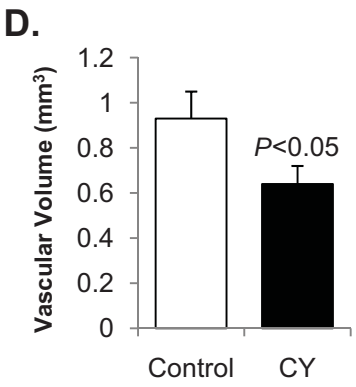
D.
Vascular Volume (mm³)
1.2
1
0.8
0.6
0.4
0.2
0
P<0.05
Control
CY

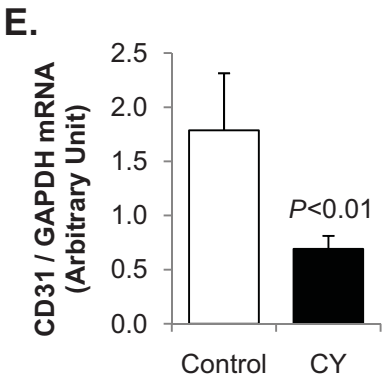
E.
CD31 / GAPDH mRNA
(Arbitrary Unit)
2.5
2.0
1.5
1.0
0.5
0.0
P<0.01
Control
CY

Figure 3

SI Park *et al.*

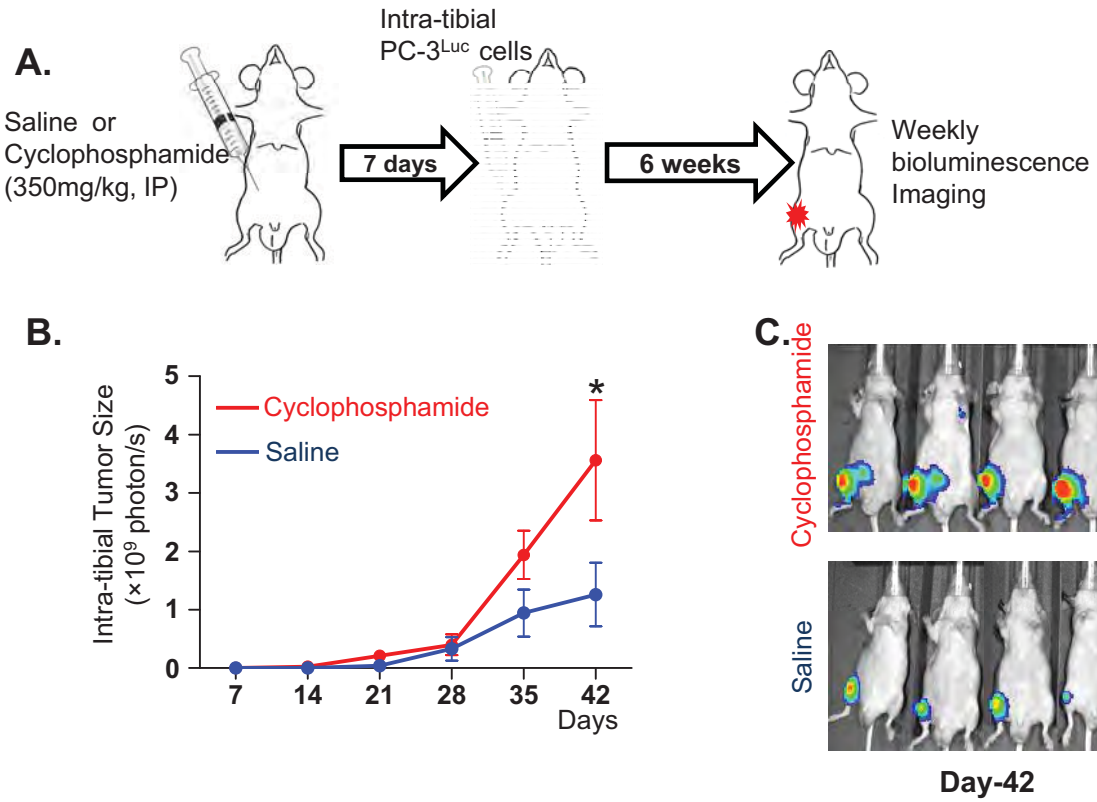

Figure 4

SI Park *et al.*

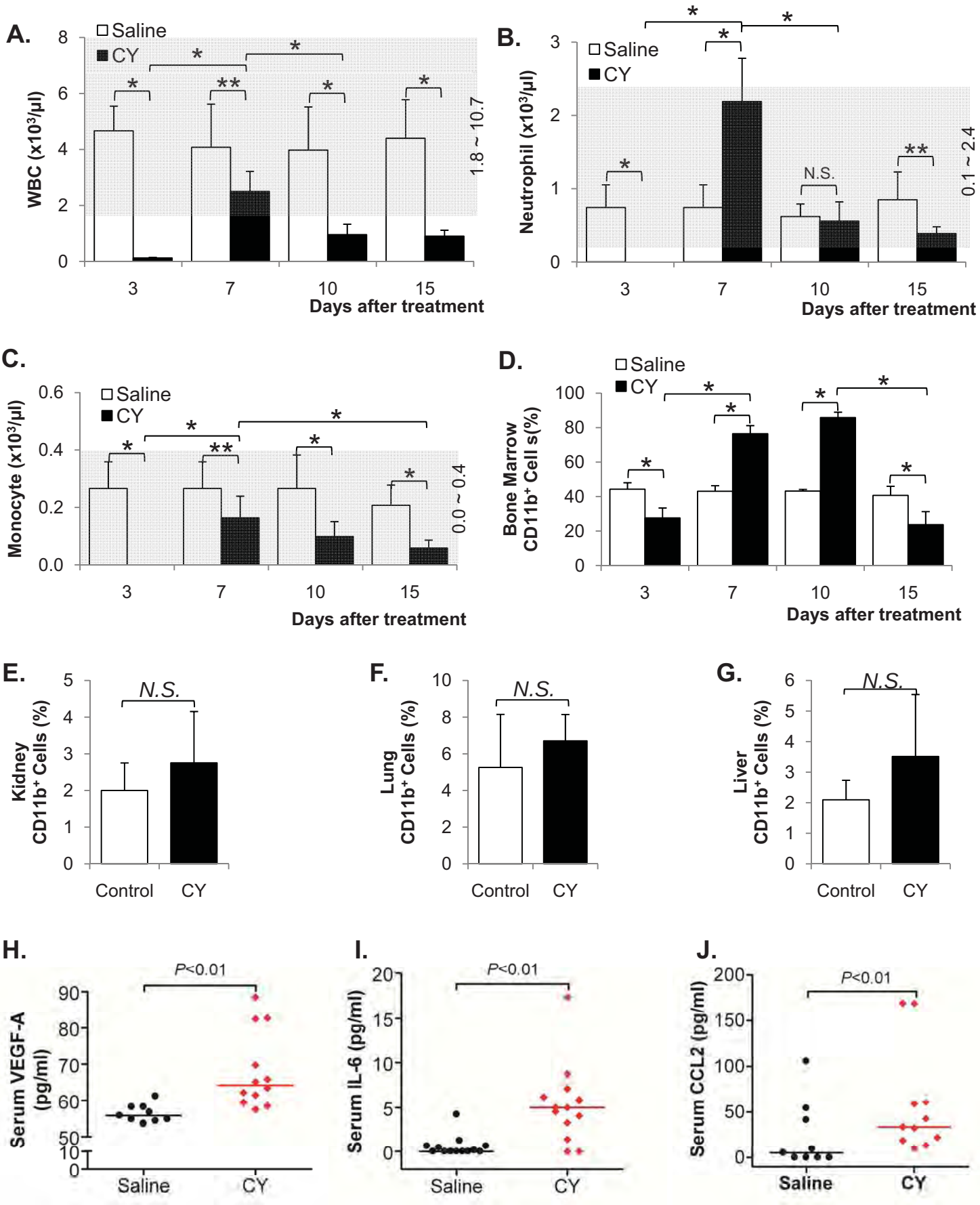

Figure 5 SI Park *et al.*

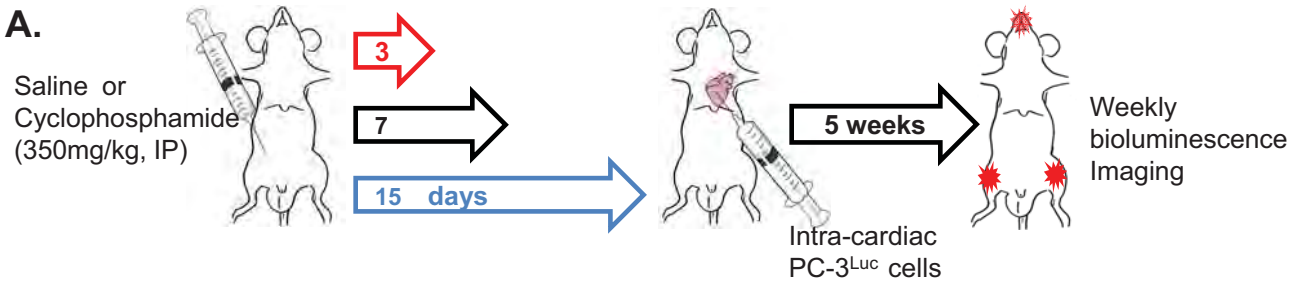

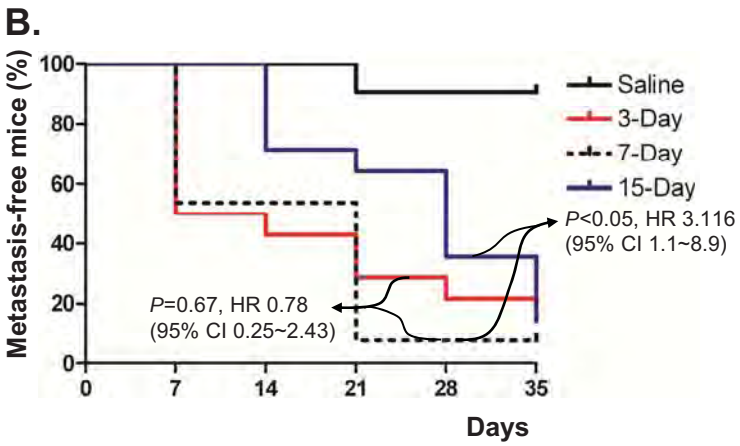

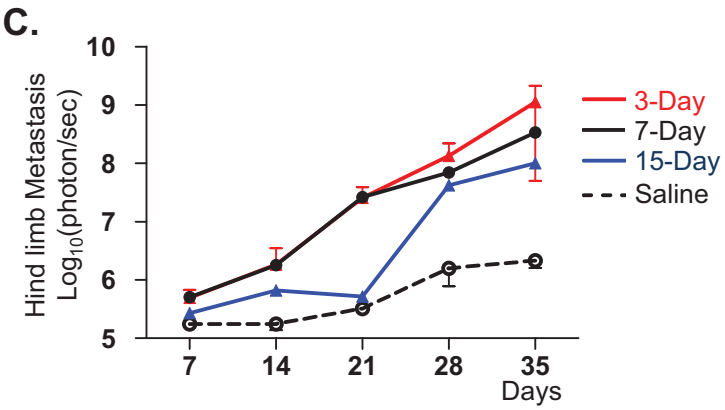

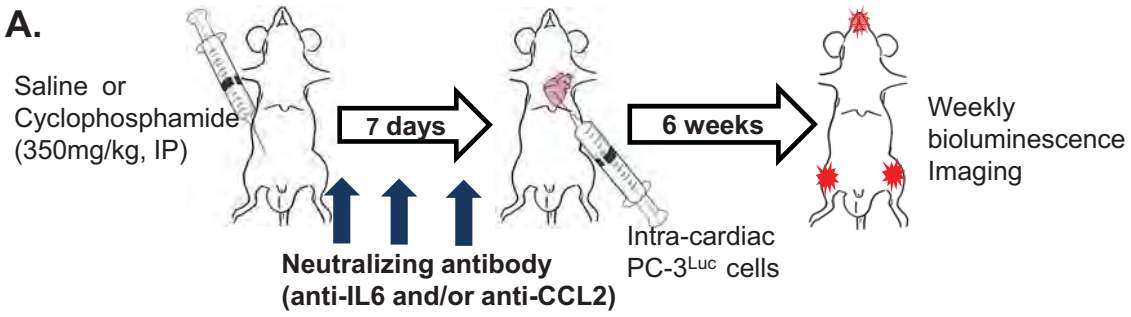
A.
Saline or
Cyclophosphamide
(350mg/kg, IP)
7 days
6 weeks
Weekly
bioluminescence
Imaging
Intra-cardiac
PC-3Luc cells
Neutralizing antibody
(anti-IL6 and/or anti-CCL2)

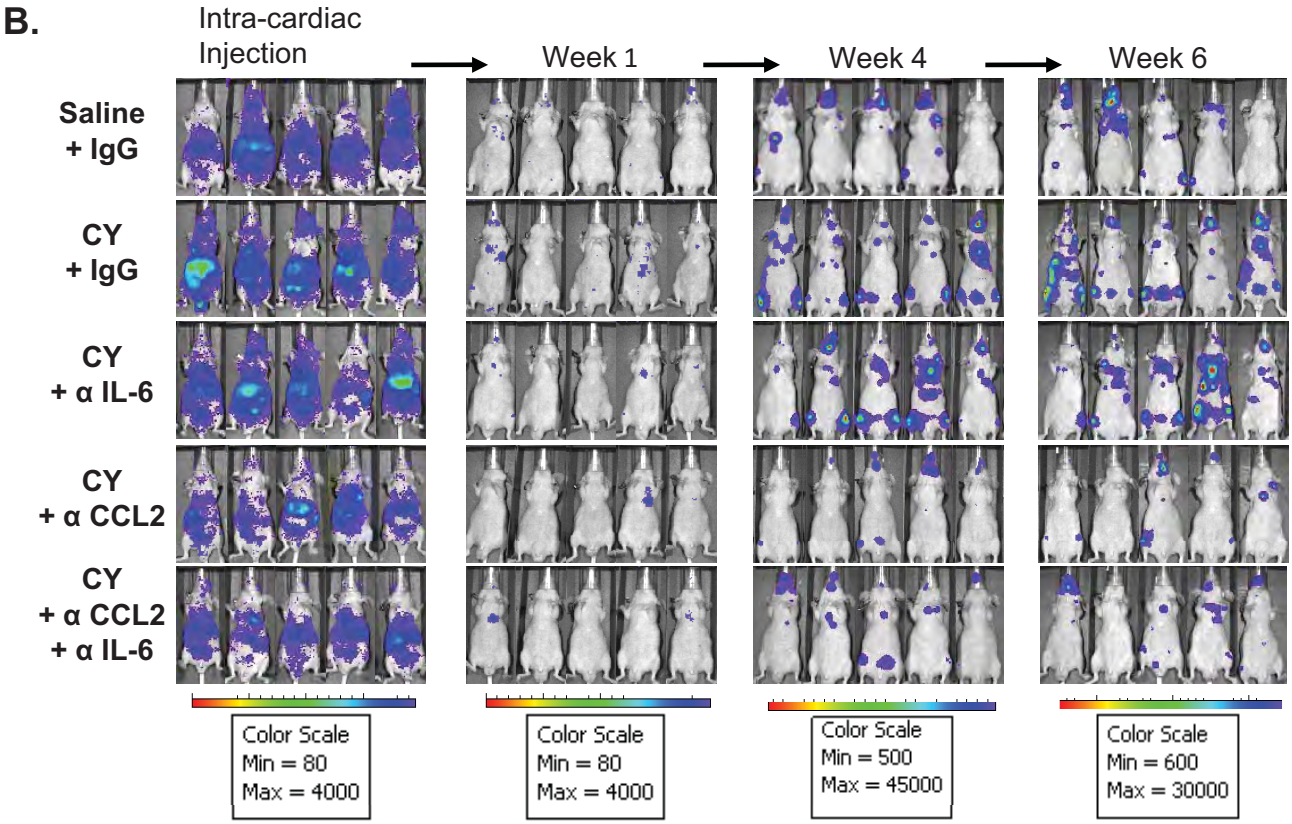
B.
Intra-cardiac
Injection
Week 1
Week 4
Week 6
Saline
+ IgG
CY
+ IgG
CY
+ α IL-6
CY
+ α CCL2
CY
+ α CCL2
+ α IL-6
Color Scale
Min = 80
Max = 4000
Color Scale
Min = 80
Max = 4000
Color Scale
Min = 500
Max = 45000
Color Scale
Min = 600
Max = 30000

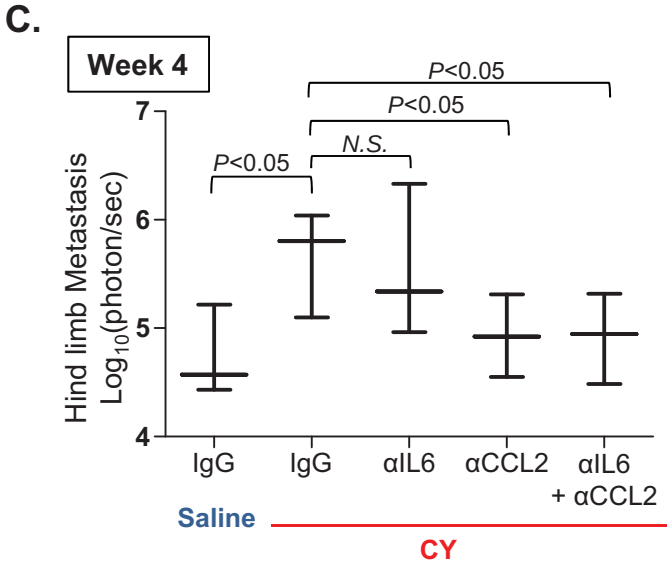
C.
Week 4
P<0.05
P<0.05
N.S.
P<0.05
Hind limb Metastasis
Log10(photon/sec)
7
6
5
4
IgG
IgG
αIL6
αCCL2
αIL6
+ αCCL2
Saline
CY

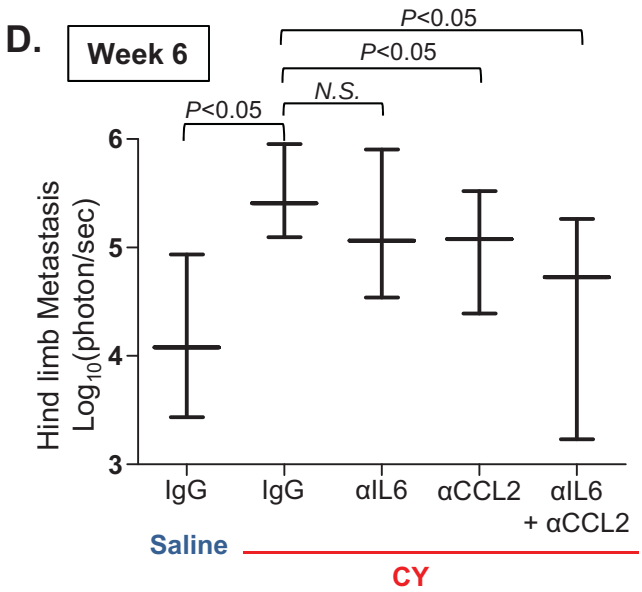
D.
Week 6
P<0.05
P<0.05
N.S.
P<0.05
Hind limb Metastasis
Log10(photon/sec)
6
5
4
3
IgG
IgG
αIL6
αCCL2
αIL6
+ αCCL2
Saline
CY

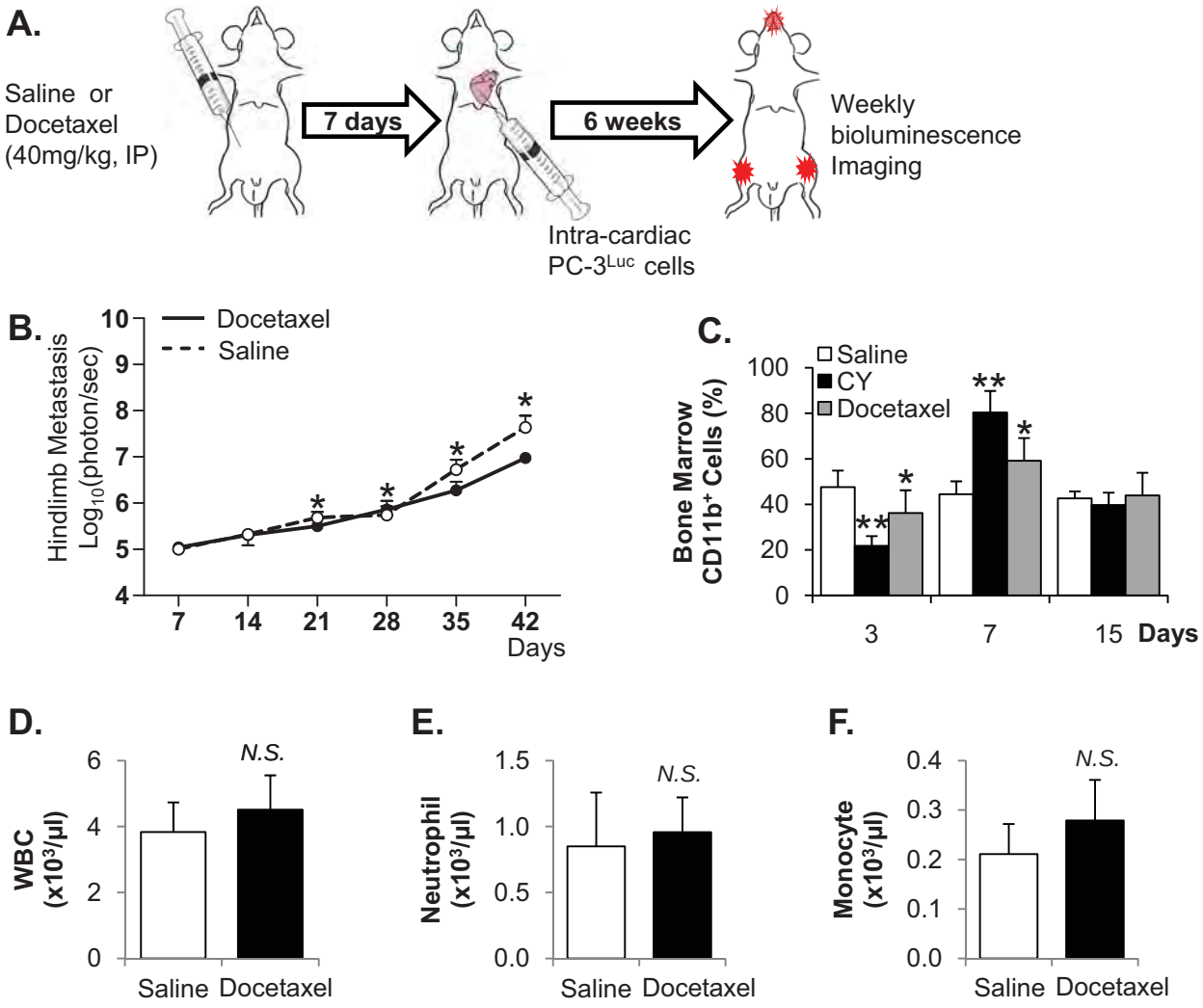
A.
Saline or
Docetaxel
(40mg/kg, IP)
7 days
6 weeks
Weekly
bioluminescence
Imaging
Intra-cardiac
PC-3Luc cells
B.
Docetaxel
Saline
Hindlimb Metastasis
Log10(photon/sec)
10
9
8
7
6
5
4
7
14
21
28
35
42
Days
C.
Saline
CY
Docetaxel
Bone Marrow
CD11b+ Cells (%)
100
80
60
40
20
0
3
7
15
Days
D.
WBC
(x10³/μl)
6
4
2
0
N.S.
Saline
Docetaxel
E.
Neutrophil
(x10³/μl)
1.5
1.0
0.5
0.0
N.S.
Saline
Docetaxel
F.
Monocyte
(x10³/μl)
0.4
0.3
0.2
0.1
0.0
N.S.
Saline
Docetaxel

Supplemental Figure 1

SI Park *et al.*

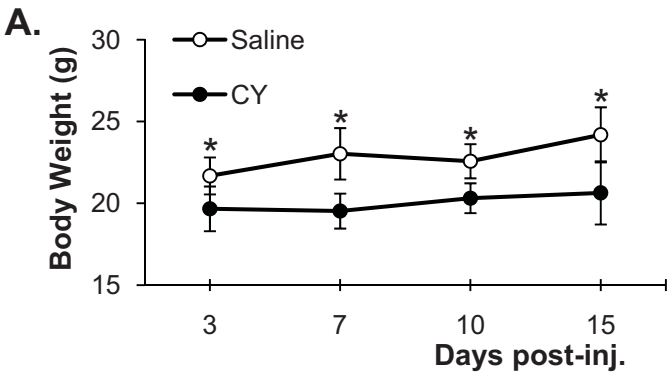

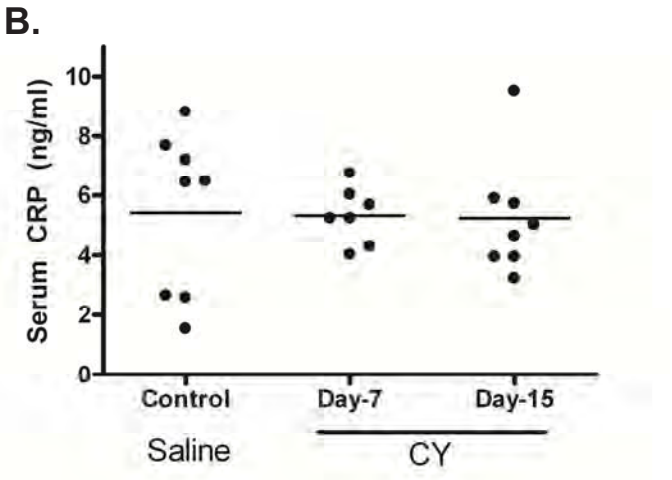

Supplemental Figure 2

SI Park *et al.*

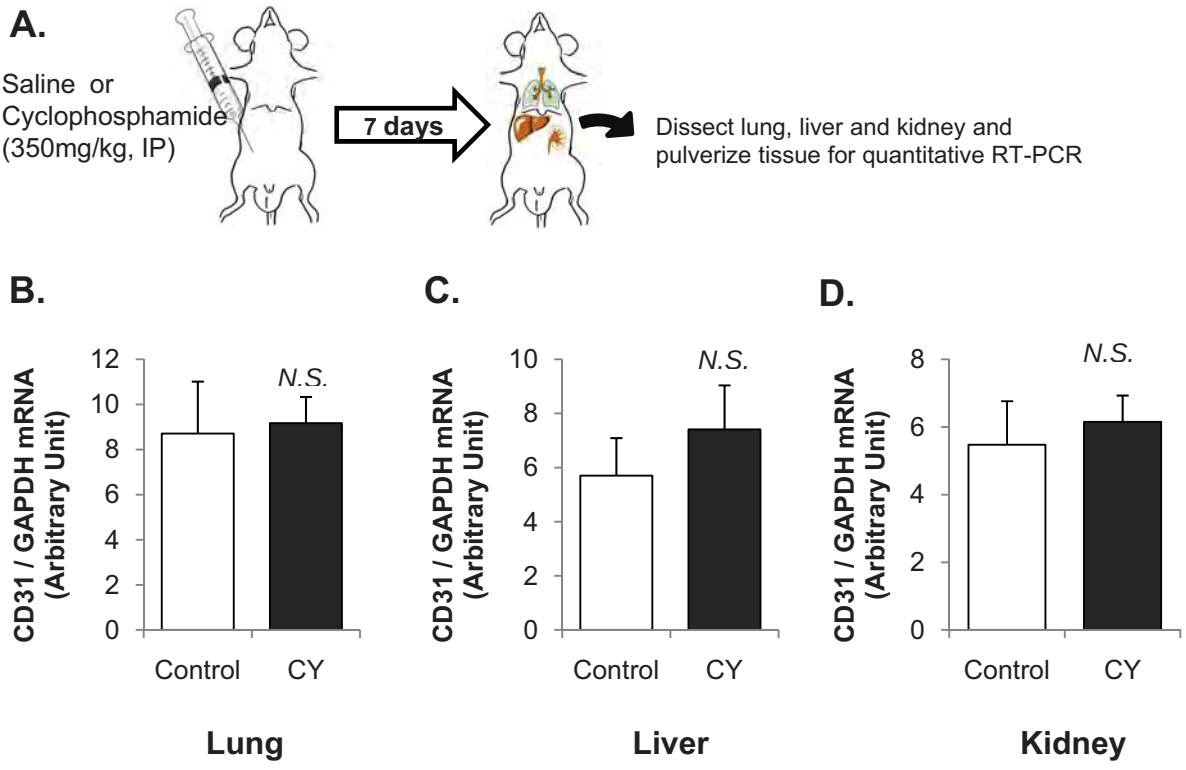

A. **Immunoradiometric Assay**

PTHrP (pg ml^{-1} 1×10^{6}cells^{-1} 48 hours^{-1})	Average	Std. Dev.
PC-3^{Luc} Parental	2349.4	38.0
Empty Vector Control	1453.94	29.4
PTHrP Knockdown Clone 5	961.8	12.8
PTHrP Knockdown Clone 10	457.8	4.1

B. **Doubling Time *in vitro***

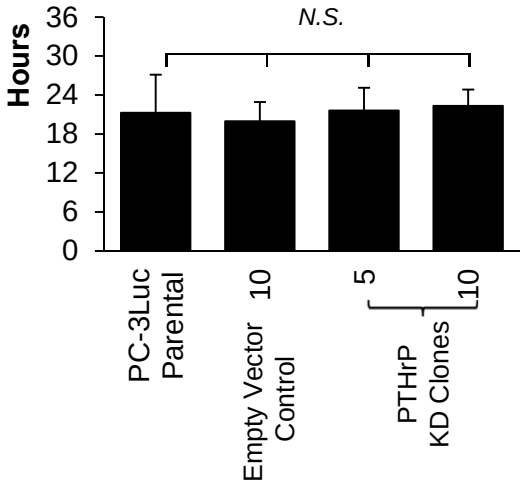

C.

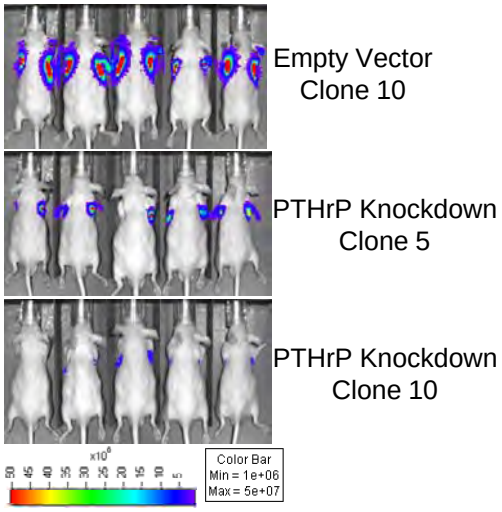

Figure 2

SI Park and LK McCauley

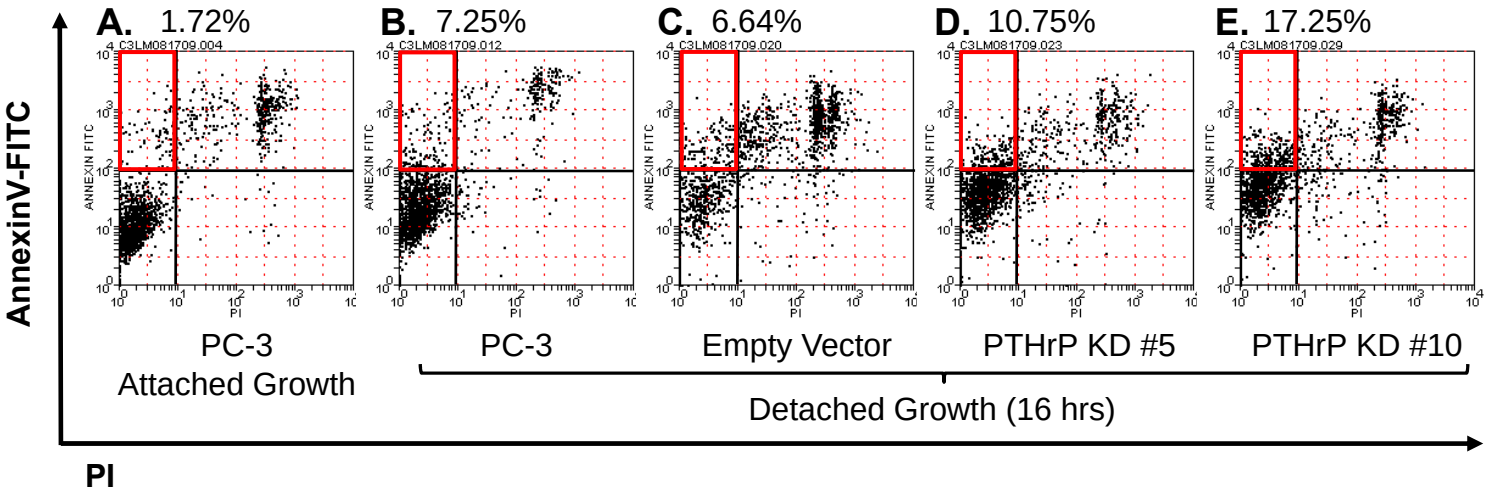

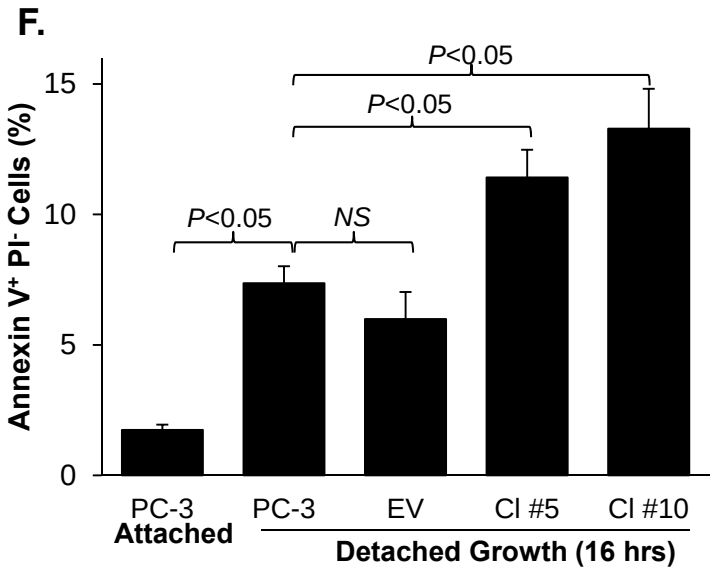

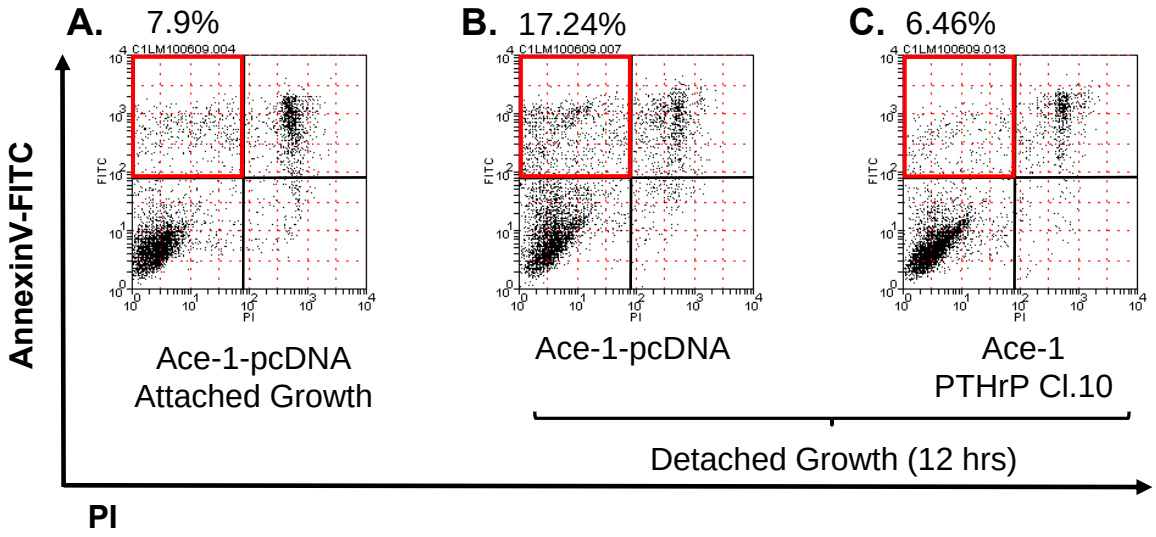
A. 7.9%
B. 17.24%
C. 6.46%
AnnexinV-FITC
PI
Ace-1-pcDNA
Attached Growth
Ace-1-pcDNA
Ace-1
PTHrP Cl.10
Detached Growth (12 hrs)

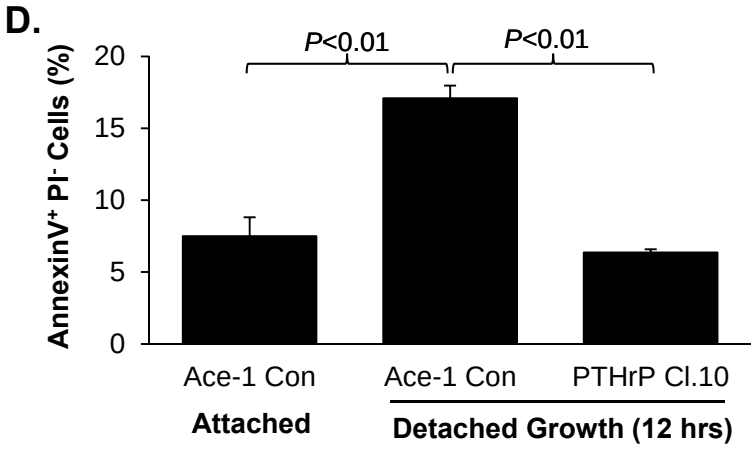
D.
P<0.01
P<0.01
AnnexinV+ PI- Cells (%)
20
15
10
5
0
Ace-1 Con
Ace-1 Con
PTHrP Cl.10
Attached
Detached Growth (12 hrs)

Figure 4

SI Park and LK McCauley

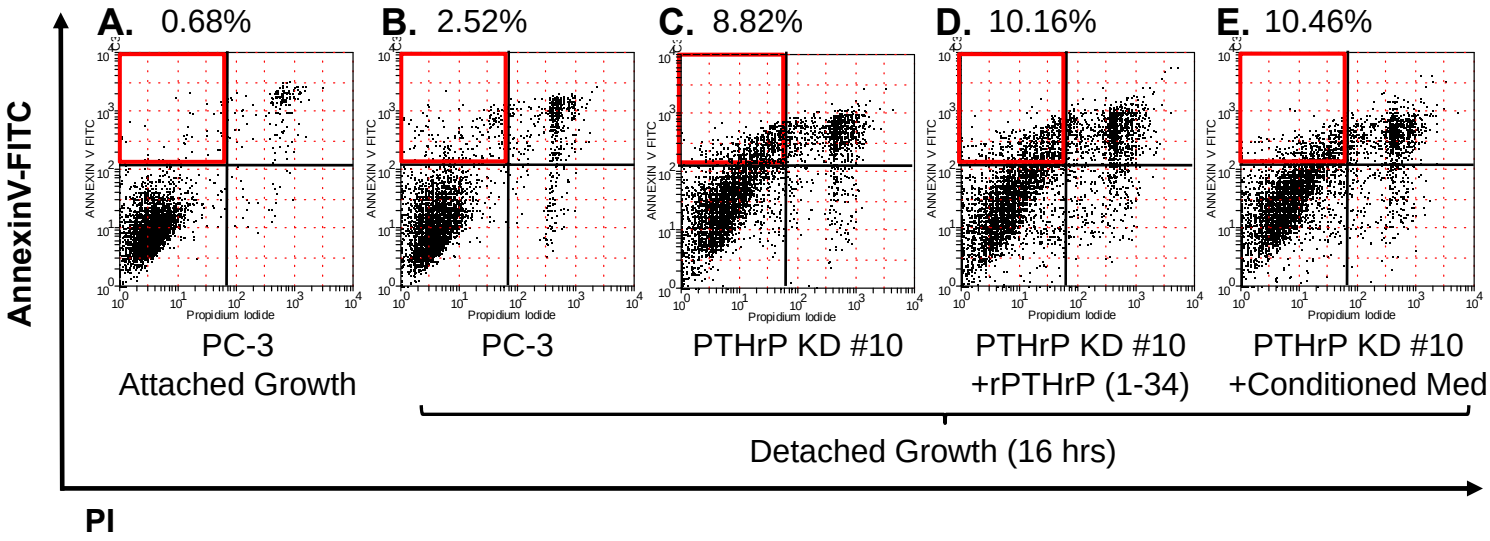

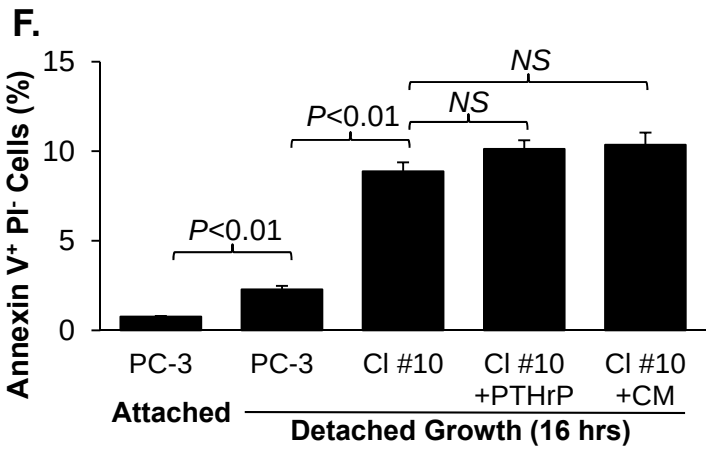

Figure 5

SI Park and LK McCauley

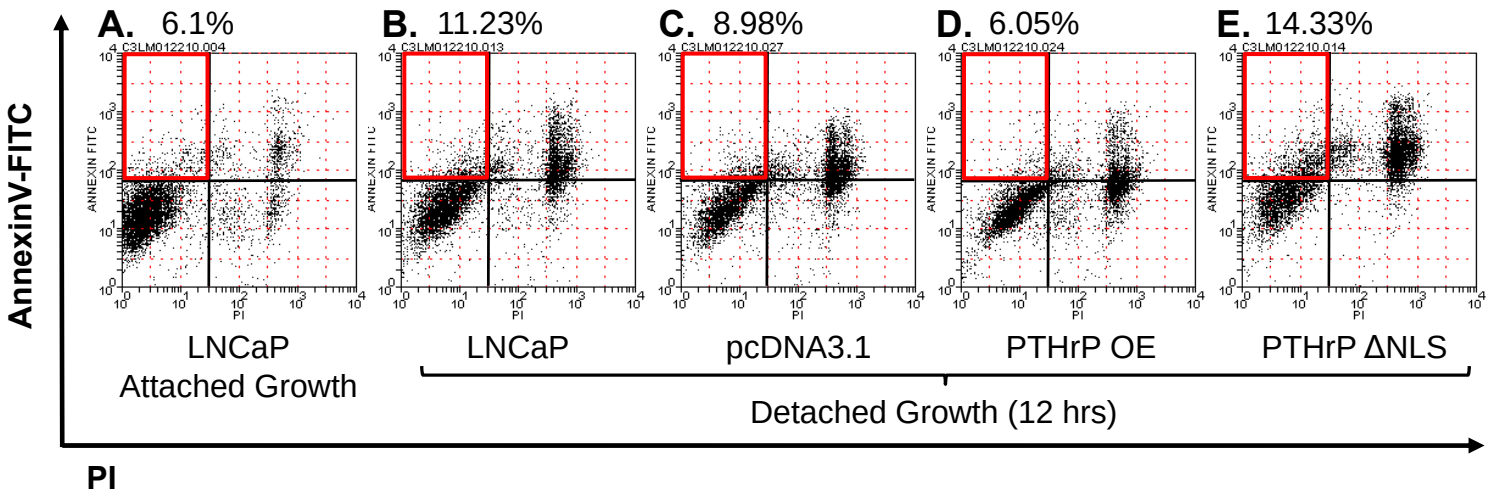

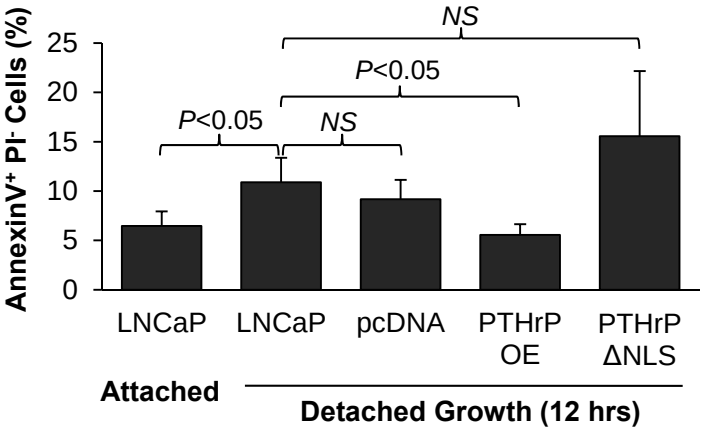

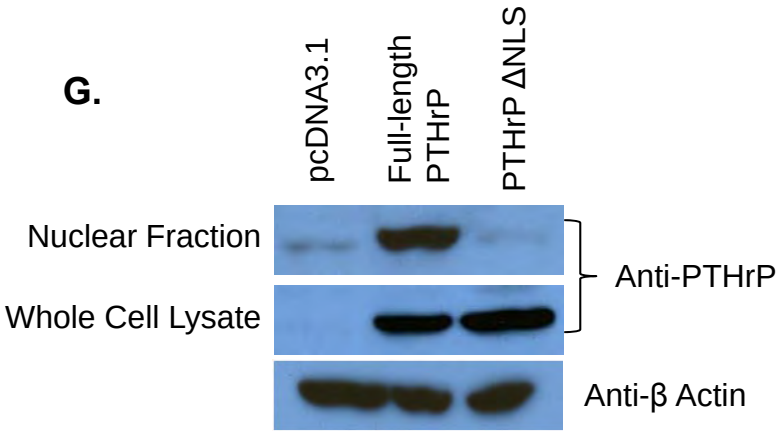

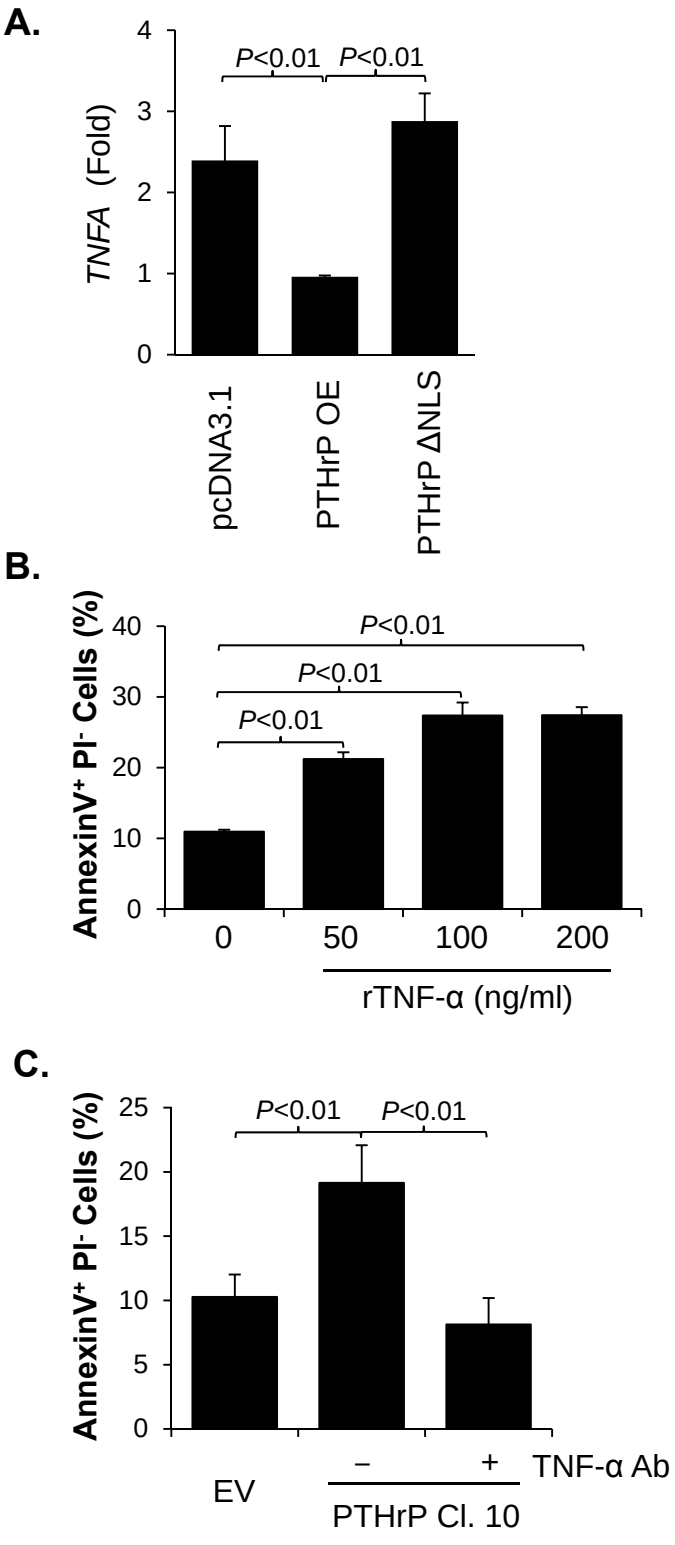
A.
P<0.01
P<0.01
TNFA (Fold)
0
1
2
3
4
pcDNA3.1
PTHrP OE
PTHrP ΔNLS
B.
AnnexinV+ PI- Cells (%)
P<0.01
P<0.01
P<0.01
0
10
20
30
40
0
50
100
200
rTNF-α (ng/ml)
C.
AnnexinV+ PI- Cells (%)
P<0.01
P<0.01
0
5
10
15
20
25
EV
–
+
TNF-α Ab
PTHrP Cl. 10

A.

Cells	Hind Limb Tumor Incidence	5 weeks after Intra-cardiac inoculation
PC-3^{Luc} Empty Vector	**14 / 14**	
PC-3^{Luc} PTHrP Cl.10	**3 / 11**	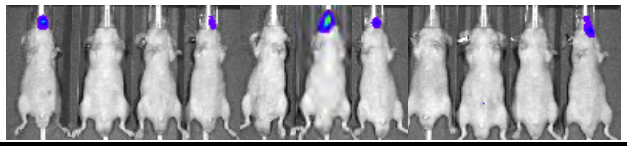

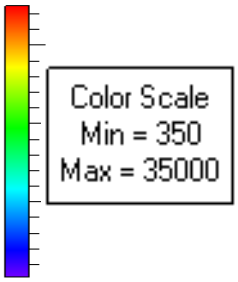

B.

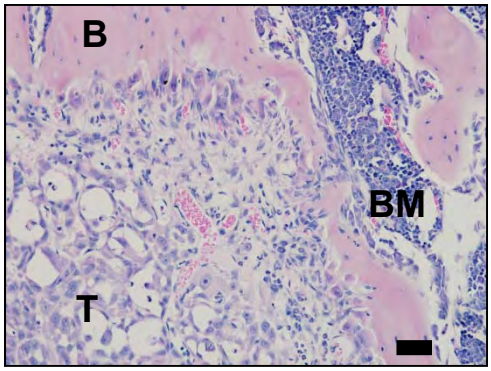

50µm

Nuclear Localization of Parathyroid Hormone-related Peptide Confers Resistance to Anoikis in Prostate Cancer Cells

Serk In Park[1] and Laurie K. McCauley[1, 2]

Affiliations:

[1]Department of Periodontics and Oral Medicine, University of Michigan School of Dentistry, 1011 N. University Ave. , Ann Arbor , Michigan 48109 U.S.A.; and

[2]Department of Pathology, University of Michigan Medical School, 1500 East Medical Center Drive, Ann Arbor, Michigan 48109 U.S.A.

Keywords: Parathyroid hormone-related peptide; prostate cancer; anoikis; metastasis

Short title: PTHrP regulates anoikis of prostate cancer cells

Requests for reprints: Laurie K. McCauley, DDS, PhD, Professor and Chair, Department of Periodontics and Oral Medicine, University of Michigan School of Dentistry, 1011 N. University Avenue, Ann Arbor, MI 48109; E-mail: mccauley@umich.edu; Phone: +1-734-647-3206; Fax: +1-734-763-5503

ABSTRACT

Prostate cancer remains a leading cause of cancer-related death in men, largely attributable to distant metastases, most frequently to bones. Despite intensive investigations, molecular mechanisms underlying metastasis are not completely understood. Among prostate cancer-derived factors, parathyroid hormone-related peptide (PTHrP), first discovered as an etiologic factor for malignancy-induced hypercalcemia, regulates many cellular functions critical to tumor growth, angiogenesis and metastasis. In this study, the role of PTHrP in tumor cell survival from detachment-induced apoptosis (i.e. anoikis) was investigated. Reduction of *PTHRP* gene expression in human prostate cancer cells (PC-3) increased the percentage of apoptotic cells when cultured in suspension. Conversely, overexpression of PTHrP protected prostate cancer cells (Ace-1 and LNCaP, both typically expressing low or undetectable basal PTHrP) from anoikis. Overexpression of nuclear localization signal (NLS)-defective PTHrP failed to protect cells from anoikis, suggesting that PTHrP-dependent protection from anoikis is an intracrine event. A PCR-based apoptosis-related gene array showed that detachment increased expression of the *TNFA* gene (encoding the pro-apoptotic protein tumor necrosis factor-α) 4-fold greater in *PTHRP*-knockdown PC-3 cells than in control PC-3 cells. In parallel, *TNFA* gene expression was significantly reduced in PTHrP-overexpressing LNCaP cells, but not in NLS-defective PTHrP overexpressing LNCaP cells, when compared with control LNCaP cells. Subsequently, in a prostate cancer skeletal metastasis mouse model, PTHrP-knockdown PC-3 cells resulted in significantly fewer metastatic lesions compared with control PC-3 cells, suggesting PTHrP mediated anti-anoikis events in the bloodstream. In conclusion, nuclear localization of PTHrP confers prostate cancer cell resistance to anoikis, potentially contributing to prostate cancer metastasis.

INTRODUCTION

Prostate cancer is the second most frequently diagnosed cancer and the sixth leading cause of cancer-related death in males worldwide, notwithstanding the improved early detection methods and therapeutic modalities (Jemal, et al. 2011). Advanced-stage prostate cancer patients commonly develop metastatic lesions, most frequently in the skeleton, which ultimately account for the high mortality rate as well as severe morbidities (Weilbaecher, et al. 2011). In sharp contrast, the molecular mechanism leading to metastasis is not yet completely understood. Metastatic colonization in distant organs requires disseminating tumor cells to have essential cellular functions, such as invasion of extracellular matrices, survival in the bloodstream, extravasation and adaptation in the new environment (Langley and Fidler 2011), which are mediated by numerous tumor-derived factors. Prostate cancer is uniquely positioned because of its strong propensity to interact with and metastasize to bone. In this regard, prostate cancer cells express numerous bone-modulating cytokines including parathyroid hormone-related peptide (PTHrP), osteoprotegerin (OPG), receptor activator of nuclear factor κ-B ligand (RANKL), and others (Deftos, et al. 2005). However, contributions of those bone-modulating factors to metastasis remain under-investigated.

PTHrP was first discovered as an etiologic factor for malignancy-induced hypercalcemia by increasing osteoclastogenesis (Suva, et al. 1987). Later, PTHrP expression was identified in carcinoma cells such as lung, breast and prostate cancer cells (Downey, et al. 1997; Iwamura, et al. 1993; Moseley, et al. 1987). Similar to its physiologic counterpart, parathyroid hormone (PTH), PTHrP binds to its cognate PTH/PTHrP receptor (PPR) expressed on osteoblasts and also found on some tumor cells (Downey et al. 1997; Iddon, et al. 2000), triggering the cyclic AMP/ protein kinase A (PKA) signal transduction pathway. In addition to autocrine/paracrine

effects mediated by receptor binding, PTHrP has been shown to localize to the nucleus, leading to inhibition of apoptosis in chondrocytes and prostate cancer cells (Dougherty, et al. 1999; Henderson, et al. 1995). Chondrocytes expressing PTHrP with a deletion of the nuclear localization signal (NLS) showed increased apoptosis (Henderson et al. 1995), indicating that PTHrP functions as an anti-apoptotic factor. However, the potential role of PTHrP in tumor cells, particularly in the context of metastatic cascades, is under-investigated. For example, tumor cells are triggered to undergo apoptosis when the cells lose attachment to their extracellular matrix, a cellular phenomena termed anoikis. Evasion of anoikis in the metastatic process (e.g. in the bloodstream) is essential to successful colonization of tumor cells in distant organs (Sakamoto and Kyprianou 2010).

In this study, the function of PTHrP in the context of prostate cancer was examined using an *in vitro* anoikis model as well as an *in vivo* experimental bone metastasis model. PTHrP protected prostate cancer cells from anoikis, effects of which were mediated by nuclear localization of PTHrP and reduced expression of tumor necrosis factor (TNF)-α. Prostate tumor cells expressing lower PTHrP resulted in significantly fewer metastatic lesions compared with cells expressing higher PTHrP, potentially mediated by increased anoikis due to loss of intracrine PTHrP activity.

MATERIALS AND METHODS

Cells

PC-3, LNCaP and Ace-1 prostate carcinoma cells were selected to study the function of PTHrP, because PC-3 cells express high levels of endogenous PTHrP while LNCaP and Ace-1 cells do not express detectable PTHrP. The canine prostate carcinoma cell line (Ace-1) was kindly provided by Dr. Thomas Rosol (Ohio State University, USA) (LeRoy, et al. 2006; Thudi, et al. 2011). Cells were maintained as monolayer cultures in RPMI-1640 media supplemented with 10% v/v fetal bovine serum and 1× penicillin/streptomycin and glutamate (all from Invitrogen, Carlsbad, California). For *in vivo* bioluminescence imaging, luciferase-labeled PC-3 cells (designated PC-3^{Luc}) were produced by stably transfecting a luciferase-expressing pLazarus retroviral construct as previously described (Schneider, et al. 2005). In addition, *PTHRP* (NCBI reference number NM_198966) gene expression was reduced in PC-3^{Luc} cells via a lentiviral vector (pLenti4/Block-iT™ DEST vector; Invitrogen, Carlsbad, California) expressing short-hairpin RNA targeting 5'-GGGCAGATACCTAACTCAGGA-3'. An empty vector was used as a control. Lentiviral supernatants were prepared using 293T packaging cells (the University of Michigan Viral Vector Core Laboratory, Ann Arbor, Michigan), followed by transduction of PC-3^{Luc} cells with polybrene (6μg ml^{-1}). Subsequently, transduced cells were grown in bleomycin selection media (Zeocin™ 200μg ml^{-1}; Invitrogen, Carlsbad, California), and stable clones were selected and expanded for further experiments.

LNCaP and Ace-1 cells, normally express undetectable basal levels of PTHrP. They were transfected with full-length PTHrP, nuclear localization signal- (i.e. amino acids 87-107) defective PTHrP (Henderson et al. 1995), or empty pcDNA3.1 vectors, as previously described (Dougherty et al. 1999; Liao, et al. 2008).

Measurement of PTHrP

PTHrP expression was measured from the culture supernatant using an immuno-radiometric assay kit (Diagnostic Systems Laboratories, Webster, Texas), detecting amino acids 1-87 (Ratcliffe, et al. 1991). Briefly, one million cells were seeded in a 6-well plate in complete RPMI-1640 media (in triplicate), followed by media change with serum-free RPMI-1640 24 hours later. Subsequently, cells were incubated for 48 hours and cell-free supernatants collected. The PTHrP assay was performed as suggested by the manufacturer.

Calculation of *in vitro* doubling time

PTHrP-knockdown and empty vector control PC-3^{Luc} cells were synchronized (by overnight serum starvation), followed by seeding (1×10^5cells/well, in triplicate) and enumeration 24, 48, 72 and 96 hours later with the aid of a hemacytometer and trypan blue dye. The doubling time (Td) was calculated using the formula: $Td=(T_2-T_1)\times(\log2/\log(Q_2/Q_1))$, where Q_1 and Q_2 are cell numbers at two time points (T_1 and T_2), respectively.

***In vivo* tumor growth**

All animal experimental protocols were approved and performed in accordance with current regulations and standards of the University of Michigan Institutional Animal Care and Use Committee guidelines.

For *in* vivo tumor growth, male athymic mice (Hsd: Athymic nude –*Foxn1*^{nu}; 4 weeks old; Harlan Laboratories, Indianapolis, Indiana) were anesthetized and 100µl of cell suspension containing 1×10^6 cells were mixed with 100µl of growth factor-reduced Matrigel™ (Invitrogen,

Carlsbad, California), and injected subcutaneously into both flanks (n=10 each group). After 3 weeks, bioluminescence imaging was performed to measure tumor size, followed by euthanasia and tumor tissue harvesting.

Anoikis assay and flow cytometry

To induce anoikis *in vitro*, prostate cancer cells were cultured in suspension as previously described (Minard, et al. 2006). Briefly, 6-well tissue culture plates were covered with 4% w/v endotoxin-free agarose. Prostate cancer cells were approximately 80% confluent at the initiation of overnight serum-starvation (for synchronization). Subsequently, cells were trypsinized and counted , followed by seeding 1×10^6 cells per well in RMPI-1640 media supplemented with 2% v/v fetal bovine serum on regular culture plates or agarose-covered plates (in sextuplicate). After 12-16 hours of incubation at 37°C, cells were harvested by pipetting (for cells in suspension) or trypsinization (for attached cells), followed by washing with ice-cold PBS and centrifugation.

For flow cytometric analyses, cells were re-suspended in Annexin V binding buffer (BD Biosciences, San Jose, California), followed by addition of fluorescein isothiocyanate (FITC)-conjugated anti-Annexin V and propidium iodide (BD Biosciences, San Jose, California). Subsequently, cells were washed once with ice-cold PBS and analyzed by flow cytometer (BD FACS Calibur) with Cell Quest analyses software (BD Biosciences, BD Biosciences, San Jose, California).

Apoptotic gene array

PTHRP-knockdown and empty vector control PC-3^{Luc} cells were grown on regular or 4% w/v agarose-covered 10cm tissue culture plates (in duplicate) for 16 hours. Subsequently, cells were lysed and total RNA prepared (Qiagen RNeasy Mini-kit; Qiagen, Valencia, California). RNA samples were reverse transcribed (RT^2 First Strand Kit; SA Biosciences, Frederick, Maryland), followed by quantitative PCR-based human apoptotic gene array (SA Biosciences, Frederick, Maryland) according to the manufacturer's suggested protocols (Li, et al. 2011). Analyses of data were performed using computer software provided by the manufacturer. A complete list of 84 apoptosis-related genes included in the analyses, detailed protocols and analysis method can be found at the manufacturer's web site (http://www.sabiosciences.com/rt_pcr_product/HTML/PAHS-012A.html).

In vivo metastasis model

To test the metastatic potentials of PC-3^{Luc} clones, cells were inoculated into the systemic circulation via an intra-cardiac route, as previously described (Park, et al. 2011a), followed by *in vivo* bioluminescence imaging. In brief, male athymic mice (Hsd: Athymic nude –*Foxn1*^{nu}; 6 weeks old; Harlan Laboratories, Indianapolis, Indiana) were anesthetized and 100µl of cell suspension containing 2×10^5 cells were injected into the left heart ventricle. Systemic circulation of the tumor cells were confirmed by *in vivo* bioluminescence imaging immediately after inoculation. Metastatic hindlimb tumors were detected and quantified also by bioluminescence imaging (Caliper Life Sciences, Alameda, California). Tumor-bearing hindlimb bones were harvested at euthanasia, fixed in 10% v/v buffered formaldehyde and decalcified in 10% w/v EDTA for 2 weeks. Metastatic tumor cells were microscopically confirmed.

Cytokines and antibodies

Recombinant human TNF-α and anti-human TNF-α neutralizing antibody were purchased from Peprotech, Inc. (Rocky Hill, New Jersey) For Western blotting, anti-PTHrP antibody (H-137; a rabbit polyclonal antibody against amino acids 41-177 of human PTHrP) was purchased from Santa Cruz Biotechnology (Santa Cruz, California).

Statistical analyses

All statistical tests were performed by Microsoft™ Excel or GraphPad™ Prism Version 5. Student's t-test was used to compare two groups and the $P<0.05$ level was considered significant. All statistical tests were two-sided and data expressed as a mean ± standard deviation.

RESULTS

PTHrP knockdown reduced *in vivo* tumor growth without affecting *in vitro* proliferation

As a first approach to investigate the function of PTHrP in prostate cancer cells, *PTHRP* gene expression was reduced in PC-3^{Luc} human prostate cancer cells using an shRNA technique. Stable clones were confirmed and selected according to level of PTHrP expression (**Figure 1A**) in the cell culture supernatants. Two knockdown clones (Clone No. 5 and 10) showed more than 50% reduction of PTHrP expression, compared to parental PC-3^{Luc} cells, while an empty vector control clone also showed mild reduction, but not to the extent of clones 5 and 10. PTHrP has been shown to regulate cellular proliferation (Dougherty et al. 1999). However, cell enumeration assays demonstrated that PTHrP knockdown did not affect *in vitro* cellular doubling time of PC-3^{Luc} cells (**Figure 1B)**, suggesting that the reduced level of PTHrP expression was sufficient to maintain cellular proliferation, at least in PC-3^{Luc} cells which express high basal levels of PTHrP. In contrast, PTHrP knockdown resulted in significantly reduced tumor growth *in vivo* (**Figure 1C**), suggesting that PTHrP regulates tumor cell proliferation and/or survival via a mechanism other than direct regulation of cell proliferation.

Reduction of PTHrP expression sensitized PC-3^{Luc} cells to detachment-induced apoptosis

In routine maintenance sub-culturing, differential plating efficiency among *PTHRP*-knockdown and control clones was noted, leading to a hypothesis that *PTHRP*-knockdown PC-3 cells are more prone to detachment-induced apoptosis. To test this, PC-3^{Luc} cells and *PTHRP*-knockdown clones were grown in suspension for an extended time, followed by flow cytometric analyses of apoptotic cells. Detachment increased the percentage of apoptotic Annexin V^+ PI^- PC-3^{Luc} cells (**Figure 2A** and **B**), and empty vector control cells (**Figure 2C**). Interestingly,

PTHRP-knockdown clones had a significantly increased percentage of Annexin V^+ PI^- apoptotic cells (**Figure 2D-F**), indicating that reduction of PTHrP expression inhibits survival of prostate tumor cells in suspension.

PTHrP overexpression rescued Ace-1 prostate cancer cells from anoikis

To further investigate the role of PTHrP in anoikis, an alternative approach (i.e. ectopic expression of PTHrP) was employed. An additional prostate cancer cell line, Ace-1, had been previously shown to express undetectable levels of PTHrP (Liao et al. 2008). A PTHrP overexpression vector or empty pcDNA3.1 vector (as a control) were transfected into Ace-1 cells, resulting in Ace-1 PTHrP clone 10 and Ace-1 pcDNA, respectively. PTHrP expression was measured and confirmed by immuno-radiometric assay of culture supernatants. The Ace-1 PTHrP clone 10 expressed 282.2 ± 9.83 (pg ml^{-1} $1\times10^6 cells^{-1}$ 48 $hours^{-1}$) while Ace-1 pcDNA control cells expressed undetectable levels of PTHrP. Cells were induced to undergo anoikis by culturing in suspension (**Figure 3**). PTHrP overexpressing Ace-1 cells had significantly fewer apoptotic cells, compared to Ace-1 pcDNA control cells (**Figure 3A-D**), indicating a causal role of PTHrP in protection from anoikis.

Recombinant PTHrP (1-34) failed to rescue PC-3 cells from anoikis

Data in **Figures 2** and **3** demonstrated prostate tumor cells expressing higher PTHrP have increased survival from detachment-induced apoptosis. Because PTHrP functions primarily via paracrine/autocrine manners through its cognate parathyroid hormone type 1 receptor (PPR), we next tested whether exogenous PTHrP would rescue the *PTHRP*-knockdown clones from anoikis. Recombinant PTHrP (amino acids 1 through 34, the functional PPR-binding fragment) or

conditioned media from the parental PC-3^{Luc} cell culture which contains full-length PTHrP was added to *PTHRP*-knockdown PC-3 clones in suspension. Neither recombinant PTHrP (1-34) nor the conditioned media rescued *PTHRP*-knockdown PC-3 cells from anoikis (**Figure 4**), suggesting PTHrP-dependent survival is not via N-terminus paracrine effects.

Overexpression of full-length PTHrP, but not nuclear localization signal-defective PTHrP, rescues prostate cancer cells from anoikis

PTHrP localizes to the nucleus and has been shown to protect colon tumor cells from drug-induced apoptosis (Bhatia, et al. 2009b; Shen, et al. 2007a). This mechanism was evaluated on PTHrP- or nuclear localization signal-defective PTHrP overexpressing prostate tumor cells. Human prostate cancer cells, LNCaP, expressing undetectable basal levels of PTHrP were engineered to express full-length PTHrP (designated PTHrP OE), nuclear localization signal (NLS)-defective PTHrP (designated PTHrP ΔNLS) or pcDNA3.1 (as a control) (**Figure 5G**). Cells were cultured in suspension to induce anoikis, followed by flow cytometric analyses. Interestingly, NLS-defective PTHrP failed to rescue LNCaP cells from anoikis while full-length PTHrP significantly supported LNCaP cell survival in suspension (**Figure 5 A-F**). Overall, **Figures 1-5** demonstrate that PTHrP promotes prostate tumor cell survival from detachment-induced apoptosis via an intracrine manner (nuclear localization) and not a paracrine manner, potentially contributing to tumor growth *in vivo*.

Detachment induced greater tumor necrosis factor-α expression in *PTHRP*-knockdown PC-3 cells than in empty-vector control cells

To investigate downstream mediators of PTHrP-dependent anoikis, a quantitative PCR-based gene array (detecting 84 human apoptosis-related genes) experiment was performed. Detachment-induced genes were identified by comparing mRNA from cells cultured in an agarose-covered plate with cells cultured on a regular plate (columns **A** and **B** in **Table 1**). Among 84 apoptosis-related genes tested, tumor necrosis factor-α (*TNFA*) gene expression was increased more than 4-fold in *PTHRP*-knockdown PC-3 cells compared with empty-vector control PC-3 cells, indicating an inverse correlation of PTHrP nuclear localization with a pro-apoptotic gene (*TNFA*).

Nuclear localization signal-defective PTHrP failed to decrease *TNFA* in response to detachment

To validate the observation in the gene array data (**Table 1**), detachment-induced *TNFA* expression was confirmed in an additional cell line (LNCaP) expressing full-length PTHrP or NLS-defective PTHrP. Overexpression of PTHrP in LNCaP cells significantly reduced *TNFA* gene expression, while NLS-defective PTHrP failed to do so, supporting a negative correlation between PTHrP expression and *TNFA* **(Figure 6A)**. Data from **Figure 1-6** and **Table 1** all together demonstrated that prostate tumor cells expressing higher PTHrP have increased resistance to anoikis by suppressing a pro-apoptotic gene (*TNFA*).

Recombinant TNF-α promotes anoikis and neutralizing TNF-α protects cells from anoikis

The causal role of TNF-α in PTHrP-dependent anoikis was further examined. Recombinant human TNF-α administration promoted anoikis in empty-vector control PC-3 cells (**Figure 6B**). More importantly, neutralizing TNF-α reduced the percentage of apoptotic PTHrP-

knockdown PC-3 cells in an *in vitro* anoikis experiment model (**Figure 6C**). These results establish the causal relationship between TNF-α and PTHrP-mediated anoikis in PC-3 cells.

Reduction of PTHrP expression decreased prostate cancer skeletal metastasis

The biological significance of PTHrP-dependent resistance to anoikis was examined using an experimental prostate cancer skeletal metastasis model. Prostate cancer cells expressing high PTHrP were anticipated to produce more metastatic lesions via increased survival in the bloodstream, compared to prostate cancer cells expressing low PTHrP (**Figure 7**). In our previous experiments, PC-3 cells develop metastatic lesions predominantly in bones (i.e. hind limbs and mandibles) in an intra-cardiac injection model (Park et al. 2011a; Schneider et al. 2005). Accordingly, *PTHRP*-knockdown or empty-vector PC-3^{Luc} cells were introduced into the systemic circulation and skeletal lesions were measured via *in vivo* bioluminescence imaging 5 weeks later. Because of differential *in vivo* growth rates (**Figure 1C**), instead of comparing hindlimb tumor size (quantified by photon emission from each lesion), incidence of hindlimb metastatic lesions was reasoned to be a more appropriate comparison. *PTHRP*-knockdown PC-3^{Luc} (clone No. 10) produced significantly fewer hind limb metastatic lesions, compared to empty-vector control PC-3^{Luc} cells, potentially due to decreased survival from anoikis in the bloodstream.

DISCUSSION

The current study demonstrated that tumor-derived PTHrP promotes prostate cancer metastasis, in part, by conferring resistance to anoikis, and that the PTHrP-dependent protection from anoikis is mediated by nuclear translocalization. Reduction of *PTHRP* gene expression in luciferase-labeled PC-3 human prostate cancer cells did not alter *in vitro* cellular proliferation but significantly decreased *in vivo* tumor growth, suggesting that PTHrP regulates cellular functions (such as evasion of apoptosis) in addition to previously known effects on proliferation. Indeed, PTHrP-knockdown cells had impaired ability to attach to the culture plates, leading to investigation of the mechanisms of PTHrP protection from anoikis. However, the discrepancy between *in vitro* proliferation and *in vivo* tumor growth might be attributable to other cellular functions. Firstly, as wild-type PC-3 cells express high basal levels of PTHrP, reduction of PTHrP expression to 20~40% (in PTHrP knockdown clones 5 and 10) may not be sufficient to affect cellular proliferation, but enough to sensitize the cells to apoptotic stimuli. In addition, as PTHrP has been shown to regulate tumor angiogenesis (Liao et al. 2008), effects on *in vivo* tumor growth could simply be secondary to reduced angiogenesis. Murine endothelial cell-specific CD31/PECAM immunohistochemistry of the tumor tissue confirmed that PTHrP knockdown tumors had significantly reduced mean vessel density (data not shown). Lastly, because PTHrP functions as a mediator in the crosstalk between the primary tumor and the bone/bone marrow, where a conducive environment presents, prostate tumors expressing low PTHrP may grow slower because of reduced recruitment of bone marrow-derived cells with tumorigenic functions (Park, et al. 2011b). On the other hand, subsequent data (**Figures 2-5**) clearly demonstrated that PTHrP nuclear translocalization protects prostate tumor cells from anoikis, partly contributing to suppression of *in vivo* tumor growth of PTHrP-knockdown cells.

Anti-apoptotic effects of PTHrP were first demonstrated in chondrocytes (Henderson et al. 1995), mediated by up-regulation of the anti-apoptotic protein Bcl-2 (Amling, et al. 1997). Later, PTHrP was shown to protect LoVo colon tumor cells from apoptosis by up-regulating the PI3K/AKT pathway (Shen, et al. 2007b). Additionally, PTHrP protected prostate tumor cells (C4-2 and PC-3) from chemotherapy-induced apoptosis in an intracrine manner (Bhatia, et al. 2009a), of which observations were expanded by our current study. Therefore, PTHrP-mediated protection from apoptosis can be generalized to multiple inducers of apoptosis (e.g. chemotherapy, detachment, etc), which can account for the correlation between PTHrP expression and metastatic potential of tumor cells (Hiraki, et al. 2002; Liao and McCauley 2006). Apoptosis induced by disrupted epithelial cell-matrix interactions was described by Frisch et al. (Frisch and Francis 1994), and termed "anoikis." Evasion of anoikis was reasoned, and later proved to be a critical function of metastatic tumor cells (Sakamoto, et al. 2010; Yawata, et al. 1998). Data from the present study expands the role of PTHrP in protecting prostate tumor cells from anoikis, leading to decreased skeletal metastasis in PTHrP-knockdown cells compared with control PC-3 cells.

Interestingly, the PCR-based gene array data demonstrated that PTHrP prevents anoikis by down-regulating the pro-apoptotic gene *TNFA*, which was confirmed in an additional human prostate cancer cell line. However, the mechanism of transcriptional down-regulation by nuclear translocalization of PTHrP is unclear and requires further investigation. One potential mechanism underlying PTHrP-regulated gene expression is interaction with RNA. Aarts *et al.* demonstrated that nuclear PTHrP interacts with messenger RNA, which may lead to degradation of transcripts (Aarts, et al. 1999). Recently, deletion of mid-region, nuclear localization and C-terminus of PTHrP (i.e. protein domains other than N-terminus which is recognized by the

cognate receptor) decreases expression of genes essential to skeletal development (such as Runx1, Runx 2 and Sox 9) while increasing expression of cell cycle inhibitors (such as p21 and p16), supporting a role for PTHrP in transcriptional regulation (Toribio, et al. 2010). Therefore, despite lack of definitive experimental evidence, nuclear localization of PTHrP may play critical roles in regulating gene expression, resulting in cellular phenotypes such as protection from apoptosis.

The current study has potential clinical significance by providing an additional molecular mechanism contributing to prostate cancer skeletal metastasis. Reduction of PTHrP resulted in decreased metastatic lesions in an experimental skeletal metastasis model. Incidence of skeletal metastatic lesions in hind limbs was significantly lower than the empty-vector control group, not to mention hind limb metastatic tumor size (as determined by average photon emission from metastatic lesions in each group). However, we reasoned that the comparison of tumor size between two groups may not be an adequate approach to analyze the data, because two clones (empty vector control clone and PTHrP knockdown clone) had significantly different growth potential *in vivo*, thus the hind limb tumor size quantification was not included in the data. Instead, as PTHrP-knockdown cells produced significantly fewer metastatic lesions in the hind limbs compared to 100% development of hind limb metastasis in the empty-vector control cells, this likely reflects the altered ability for cells to survive the trajectory from injection to tumor cell lodging and growth in bone.

In conclusion, the current study demonstrates a role for PTHrP in protecting prostate tumor cells from anoikis *in vitro*, down-regulating *TNFA* gene expression, and supporting metastatic potential of prostate tumor cells *in vivo*.

DECLARATION OF INTEREST

Neither author has a financial conflict of interest.

FUNDING

This work was financially supported by the U. S. Department of Defense Prostate Cancer Research Program Grants W81XWH-10-1-0546 (Serk In Park) and W81XWH-08-1-0037 (Laurie K. McCauley); and the U. S. National Cancer Institute Program Project Grant P01CA093900 (Laurie K. McCauley).

AUTHOR CONTRIBUTIONS

L. K. M. supervised all experiments and manuscript preparation. S. I. P. and L. K. M. designed the experiments and analyzed the data. S. I. P. performed the experiments and wrote the manuscript.

ACKNOWLEDGEMENTS

The authors thank Janice E. Berry, Amy J. Koh and Matthew Eber for their assistance with preparation of this manuscript, and Thomas J. Rosol for providing the Ace-1 prostate cancer cells.

REFERENCES

Aarts MM, Levy D, He B, Stregger S, Chen T, Richard S & Henderson JE 1999 Parathyroid hormone-related protein interacts with RNA. *J Biol Chem* **274** 4832-4838.

Amling M, Neff L, Tanaka S, Inoue D, Kuida K, Weir E, Philbrick WM, Broadus AE & Baron R 1997 Bcl-2 lies downstream of parathyroid hormone-related peptide in a signaling pathway that regulates chondrocyte maturation during skeletal development. *J Cell Biol* **136** 205-213.

Bhatia V, Mula RV, Weigel NL & Falzon M 2009a Parathyroid hormone-related protein regulates cell survival pathways via integrin alpha6beta4-mediated activation of phosphatidylinositol 3-kinase/Akt signaling. *Mol Cancer Res* **7** 1119-1131.

Bhatia V, Saini MK & Falzon M 2009b Nuclear PTHrP targeting regulates PTHrP secretion and enhances LoVo cell growth and survival. *Regul Pept* **158** 149-155.

Deftos LJ, Barken I, Burton DW, Hoffman RM & Geller J 2005 Direct evidence that PTHrP expression promotes prostate cancer progression in bone. *Biochem Biophys Res Commun* **327** 468-472.

Dougherty KM, Blomme EA, Koh AJ, Henderson JE, Pienta KJ, Rosol TJ & McCauley LK 1999 Parathyroid hormone-related protein as a growth regulator of prostate carcinoma. *Cancer Res* **59** 6015-6022.

Downey SE, Hoyland J, Freemont AJ, Knox F, Walls J & Bundred NJ 1997 Expression of the receptor for parathyroid hormone-related protein in normal and malignant breast tissue. *J Pathol* **183** 212-217.

Frisch SM & Francis H 1994 Disruption of epithelial cell-matrix interactions induces apoptosis. *J Cell Biol* **124** 619-626.

Henderson JE, Amizuka N, Warshawsky H, Biasotto D, Lanske BM, Goltzman D & Karaplis AC 1995 Nucleolar localization of parathyroid hormone-related peptide enhances survival of chondrocytes under conditions that promote apoptotic cell death. *Mol Cell Biol* **15** 4064-4075.

Hiraki A, Ueoka H, Bessho A, Segawa Y, Takigawa N, Kiura K, Eguchi K, Yoneda T, Tanimoto M & Harada M 2002 Parathyroid hormone-related protein measured at the time of first visit is an indicator of bone metastases and survival in lung carcinoma patients with hypercalcemia. *Cancer* **95** 1706-1713.

Iddon J, Bundred NJ, Hoyland J, Downey SE, Baird P, Salter D, McMahon R & Freemont AJ 2000 Expression of parathyroid hormone-related protein and its receptor in bone metastases from prostate cancer. *J Pathol* **191** 170-174.

Iwamura M, di Sant'Agnese PA, Wu G, Benning CM, Cockett AT, Deftos LJ & Abrahamsson PA 1993 Immunohistochemical localization of parathyroid hormone-related protein in human prostate cancer. *Cancer Res* **53** 1724-1726.

Jemal A, Bray F, Center MM, Ferlay J, Ward E & Forman D 2011 Global cancer statistics. *CA Cancer J Clin* **61** 69-90.

Langley RR & Fidler IJ 2011 The seed and soil hypothesis revisited--the role of tumor-stroma interactions in metastasis to different organs. *Int J Cancer* **128** 2527-2535.

LeRoy BE, Thudi NK, Nadella MV, Toribio RE, Tannehill-Gregg SH, van Bokhoven A, Davis D, Corn S & Rosol TJ 2006 New bone formation and osteolysis by a metastatic, highly invasive canine prostate carcinoma xenograft. *Prostate* **66** 1213-1222.

Li X, Koh AJ, Wang Z, Soki FN, Park SI, Pienta KJ & McCauley LK 2011 Inhibitory effects of megakaryocytic cells in prostate cancer skeletal metastasis. *J Bone Miner Res* **26** 125-134.

425 Liao J, Li X, Koh AJ, Berry JE, Thudi N, Rosol TJ, Pienta KJ & McCauley LK 2008 Tumor
426 expressed PTHrP facilitates prostate cancer-induced osteoblastic lesions. *Int J Cancer* **123** 2267-
427 2278.
428 Liao J & McCauley LK 2006 Skeletal metastasis: Established and emerging roles of parathyroid
429 hormone related protein (PTHrP). *Cancer Metastasis Rev* **25** 559-571.
430 Minard ME, Ellis LM & Gallick GE 2006 Tiam1 regulates cell adhesion, migration and
431 apoptosis in colon tumor cells. *Clin Exp Metastasis* **23** 301-313.
432 Moseley JM, Kubota M, Diefenbach-Jagger H, Wettenhall RE, Kemp BE, Suva LJ, Rodda CP,
433 Ebeling PR, Hudson PJ, Zajac JD, et al. 1987 Parathyroid hormone-related protein purified from
434 a human lung cancer cell line. *Proc Natl Acad Sci U S A* **84** 5048-5052.
435 Park SI, Kim SJ, McCauley LK & Gallick GE 2011a Pre-Clinical Mouse Models of Human
436 Prostate Cancer and their Utility in Drug Discovery. *Curr Protoc Pharmacol* **51** 14 15-14 15 27.
437 Park SI, Soki FN & McCauley LK 2011b Roles of Bone Marrow Cells in Skeletal Metastases:
438 No Longer Bystanders. *Cancer Microenviron*. (Epub ahead of print). doi: 10.1007/s12307-011-
439 0081-8
440 Ratcliffe WA, Norbury S, Heath DA & Ratcliffe JG 1991 Development and validation of an
441 immunoradiometric assay of parathyrin-related protein in unextracted plasma. *Clin Chem* **37**
442 678-685.
443 Sakamoto S & Kyprianou N 2010 Targeting anoikis resistance in prostate cancer metastasis. *Mol*
444 *Aspects Med* **31** 205-214.
445 Sakamoto S, McCann RO, Dhir R & Kyprianou N 2010 Talin1 promotes tumor invasion and
446 metastasis via focal adhesion signaling and anoikis resistance. *Cancer Res* **70** 1885-1895.

Schneider A, Kalikin LM, Mattos AC, Keller ET, Allen MJ, Pienta KJ & McCauley LK 2005 Bone turnover mediates preferential localization of prostate cancer in the skeleton. *Endocrinology* **146** 1727-1736.

Shen X, Mula RV, Evers BM & Falzon M 2007a Increased cell survival, migration, invasion, and Akt expression in PTHrP-overexpressing LoVo colon cancer cell lines. *Regul Pept* **141** 61-72.

Shen X, Rychahou PG, Evers BM & Falzon M 2007b PTHrP increases xenograft growth and promotes integrin alpha6beta4 expression and Akt activation in colon cancer. *Cancer Lett* **258** 241-252.

Suva LJ, Winslow GA, Wettenhall RE, Hammonds RG, Moseley JM, Diefenbach-Jagger H, Rodda CP, Kemp BE, Rodriguez H, Chen EY, et al. 1987 A parathyroid hormone-related protein implicated in malignant hypercalcemia: cloning and expression. *Science* **237** 893-896.

Thudi NK, Martin CK, Murahari S, Shu ST, Lanigan LG, Werbeck JL, Keller ET, McCauley LK, Pinzone JJ & Rosol TJ 2011 Dickkopf-1 (DKK-1) stimulated prostate cancer growth and metastasis and inhibited bone formation in osteoblastic bone metastases. *Prostate* **71** 615-625.

Toribio RE, Brown HA, Novince CM, Marlow B, Hernon K, Lanigan LG, Hildreth BE, 3rd, Werbeck JL, Shu ST, Lorch G, et al. 2010 The midregion, nuclear localization sequence, and C terminus of PTHrP regulate skeletal development, hematopoiesis, and survival in mice. *FASEB J* **24** 1947-1957.

Weilbaecher KN, Guise TA & McCauley LK 2011 Cancer to bone: a fatal attraction. *Nat Rev Cancer* **11** 411-425.

468 Yawata A, Adachi M, Okuda H, Naishiro Y, Takamura T, Hareyama M, Takayama S, Reed JC
469 & Imai K 1998 Prolonged cell survival enhances peritoneal dissemination of gastric cancer cells.
470 *Oncogene* **16** 2681-2686.
471
472

FIGURE LEGENDS

FIGURE 1 Generation of PC-3 prostate cancer cells expressing varying levels of PTHrP

PTHrP expression was reduced in PC-3^{Luc} cells via lentiviral shRNA. **A.** PTHrP protein levels were measured from the culture supernatant by immuno-radiometric assay. Data are average of two measurements ± standard deviation (Std. Dev.) Assays were repeated more than three times, and one set of representative data is shown. **B.** *In vitro* doubling time of the PC-3 clones expressing varying levels of PTHrP was calculated by enumeration of viable cells at 24, 48, 72 and 96 hour time points (n=3 each). Data are mean ± standard deviation. NS stands for 'not significant.' **C.** *In vivo* tumor size was measured by bioluminescence imaging. Subcutaneous tumors were grown for 20 days (n=10 per group). Five representative mice are shown. Tumor incidence was 100% in all three groups, determined by microscopic examination of tumor cells upon necropsy.

FIGURE 2 Reduction of PTHrP expression sensitized PC-3 cells to detachment-induced apoptosis

PC-3 cells expressing varying levels of PTHrP were induced to undergo anoikis, followed by flow cytometric analyses of apoptotic cells. Cells were seeded on regular 6-well dishes as a control, or on agarose-covered dishes to induce anoikis (n=6 each). **A–E.** Representative flow cytometric dot plots are shown. Annexin V^+PI^- cells (marked with boxes in the upper left quadrants) indicate apoptotic cells. **F.** Average percentage of apoptotic cells is shown graphically. Data are mean ± standard deviation. $P<0.05$ by Student's t-test was considered statistically significant. N.S. stands for 'not significant.'

FIGURE 3 Ectopic expression of PTHrP rescued Ace-1 prostate cancer cells from anoikis

Ace-1 prostate cancer cells (expressing undetectable basal PTHrP) were engineered to express full-length PTHrP or control vector (pcDNA3.1), followed by anoikis assay. **A–C.** Representative flow cytometric dot plots are shown. Annexin V^+PI^- cells (marked with boxes in the upper left quadrants) indicate apoptotic cells. **D.** Average percentage of apoptotic cells is shown graphically (n=6). Data are mean ± standard deviation. P<0.05 by Student's t-test was considered statistical significant.

FIGURE 4 Exogenous PTHrP failed to rescue PC-3 cells from anoikis

PTHrP-knockdown PC-3 cells were induced to undergo anoikis in combination with recombinant PTHrP (1-34) or conditioned media from the PC-3 cell culture, followed by flow cytometric analyses of apoptotic cells. **A–E.** Representative flow cytometric dot plots are shown. Annexin V^+PI^- cells (marked with boxes in the upper left quadrants) indicate apoptotic cells. **F.** Average percentage of apoptotic cells is shown. Data are mean ± standard deviation. P<0.05 by Student's t-test was considered statistical significant. NS stands for 'not significant.'

FIGURE 5 Full-length PTHrP, but not nuclear localization signal-defective PTHrP, protected prostate cancer cells from anoikis

LNCaP prostate cancer cells were transfected with pcDNA 3.1 (control), full-length PTHrP overexpression vector (PTHrP OE) or nuclear localization signal-defective PTHrP expression vector (PTHrP ΔNLS), followed by anoikis assay. **A–E.** Representative flow cytometric dot plots are shown. Annexin V^+PI^- cells (marked with boxes in the upper left quadrants) indicate

apoptotic cells. **F.** Average percentage of apoptotic cells is shown (*n*=6). Data are mean ± standard deviation. *P*<0.05 by Student's t-test was considered statistical significant. N.S. stands for 'not significant.' **G**. Western blotting analyses shows high nuclear PTHrP in the PTHrP overexpressing clone and very low nuclear PTHrP in the PTHrP ΔNLS clone. Total cellular and nuclear lysates were prepared from the PTHrP OE, PTHrP ΔNLS and pcDNA control cells, and PTHrP expression was detected by Western blotting.

FIGURE 6 Nuclear localization signal-defective PTHrP failed to decrease *TNFA* in response to detachment

A. LNCaP cells were transfected with empty pcDNA3.1 (pcDNA3.1), full-length PTHrP overexpressing (PTHrP OE) or nuclear localization signal-defective PTHrP (PTHrP ΔNLS) vectors, and stable clones were selected. Cells were grown on regular tissue-culture dishes (control) and on agarose-covered dishes to induce anoikis (*n*=3 each). Total RNA was prepared, followed by reverse transcription and quantitative PCR for *TNFA* and *GAPDH* (for normalization). Normalized *TNFA* gene expression from detached cells divided by normalized *TNFA* expression from attached cells is shown graphically. Data are mean ± standard deviation. *P*<0.05 by Student's t-test was considered statistical significant. **B**. PC-3 empty vector control cells were seeded on agarose-covered dishes to induce anoikis (*n*=5 each), followed by treatment with human recombinant TNF-α (0 to 200 ng/ml, as indicated). Apoptotic cells were quantified by flow cytometric analyses of Annexin V^+PI^- cells. Data are mean ± standard deviation. *P*<0.05 by Student's t-test was considered statistically significant. **C.** PTHrP-knockdown (Clone 10) or empty-vector control PC-3 cells were seeded on agarose-covered 6-well dishes to induce anoikis (*n*=5 each). Anti-human TNF-α antibody (0.6μg/ml) was added to neutralize

TNF-α in the culture supernatant. Apoptotic cells were quantified by flow cytometric analyses of Annexin V^+PI^- cells. Data are mean ± standard deviation. $P<0.05$ by Student's t-test was considered statistically significant.

FIGURE 7 Reduction of PTHrP expression decreased prostate cancer skeletal metastasis **A.** PTHrP knockdown (clone No. 10) or empty-vector control PC-3^{Luc} cells were inoculated into the systemic circulation to compare skeletal metastasis in male athymic mice (n=14 for empty-vector transfected group and n=11 for PTHrP knockdown clone 10 group). Development of metastatic lesions was determined by bioluminescence imaging. Hind limbs emitting more than 1×10^5 photon/second were considered metastases, and mice carrying one or more metastatic hind limbs were counted and presented. There was a statistically significant difference ($P<0.01$ by Fisher's exact test) in the incidence of hind limb metastatic lesions between the two groups. The whole body bioluminescence images of all mice in the experiment are shown. Note that not all metastatic lesions appear in colors, because of the normalization of pseudocoloring to the highest bioluminescence signals (mostly mandibular lesions in the control group). **B.** A representative microscopic image of a metastatic lesion in the proximal tibia of PC-3Luc empty vector cells. "T"=tumor cells; "B"=bone; and "BM"=bone marrow.

TABLE 1

Gene	Detachment-induced genes (Fold)		C. Fold Changes (A/B)
	A. PTHrP-KD PC-3	B. EV-control PC-3	
TNF	**4.829922**	**1.182631**	**4.08**
CD40LG	1.571345	0.547906	2.87
BAK1	1.285206	0.693515	1.85
TNFSF8	1.134455	0.688725	1.65
GADD45A	1.387031	0.865737	1.60
BIRC8	2.891865	1.830198	1.58
PYCARD	0.612168	1.126619	0.54
HRK	1.118837	2.993846	0.37
CIDEA	0.53663	1.45599	0.37
TP73	0.185823	0.890076	0.21

PC-3^{Luc} cells were transfected with *PTHRP*-targeting shRNA or empty lentiviral vectors, and stable clones were selected (designated PTHrP-KD and EV-control, respectively). Cells were grown on a regular tissue-culture dish (control) and on agarose-covered dish to induce anoikis. Total RNA was prepared, followed by reverse transcription and quantitative PCR apoptotic gene array. Detachment-induced genes and fold induction in PTHrP knockdown PC-3 cells were shown in column **A** (i.e. detachment effects in the PTHrP-knockdown clone = Detached PTHrP-KD / Attached PTHrP-KD), and those in empty-vector control PC-3 cells (i.e. detachment effects in the control clone = Detached EV-control / Attached EV-control) were shown in column **B**. To identify the anoikis genes altered by PTHrP reduction, fold changes comparing PTHrP-knockdown and control PC-3 cells were shown in column **C**.

A. **Immunoradiometric Assay**

PTHrP (pg ml^{-1} 1×10^{6}cells^{-1} 48 hours^{-1})	Average	Std. Dev.
PC-3^{Luc} Parental	2349.4	38.0
Empty Vector Control	1453.94	29.4
PTHrP Knockdown Clone 5	961.8	12.8
PTHrP Knockdown Clone 10	457.8	4.1

B. **Doubling Time *in vitro***

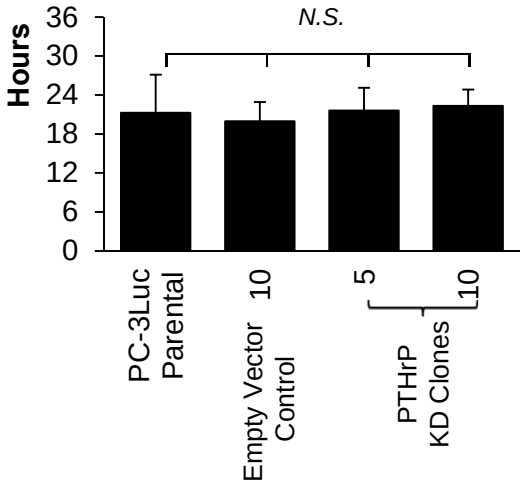

C.

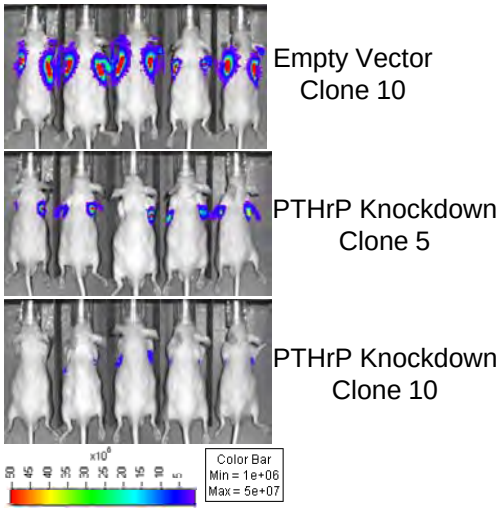

Figure 2

SI Park and LK McCauley

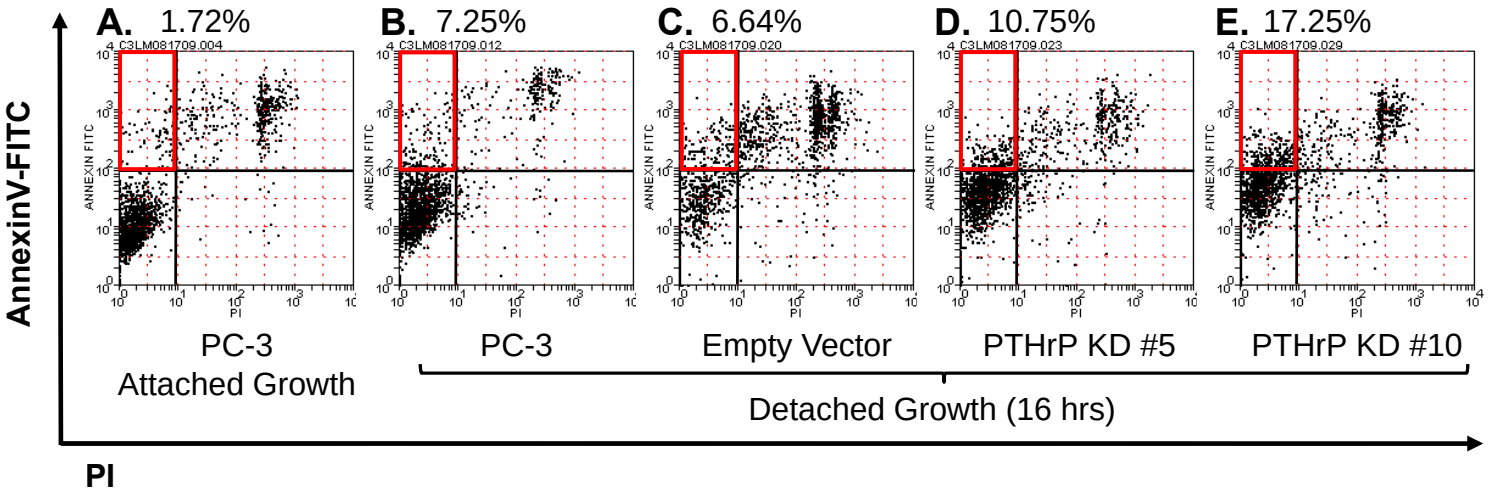

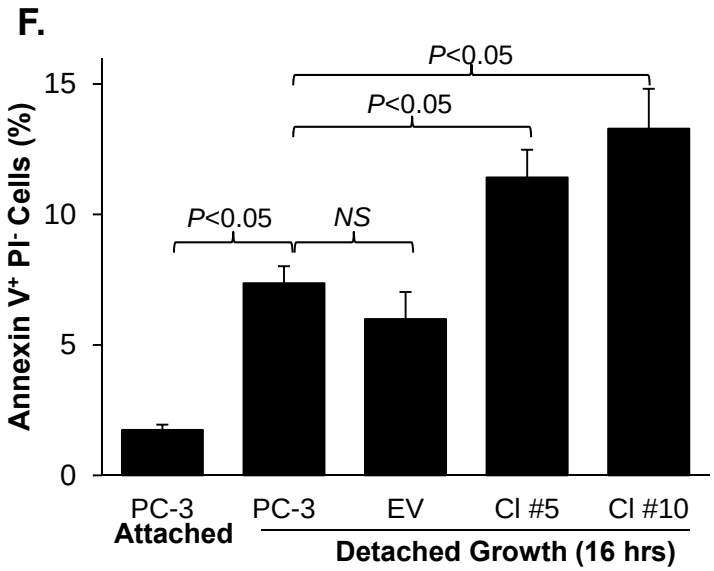

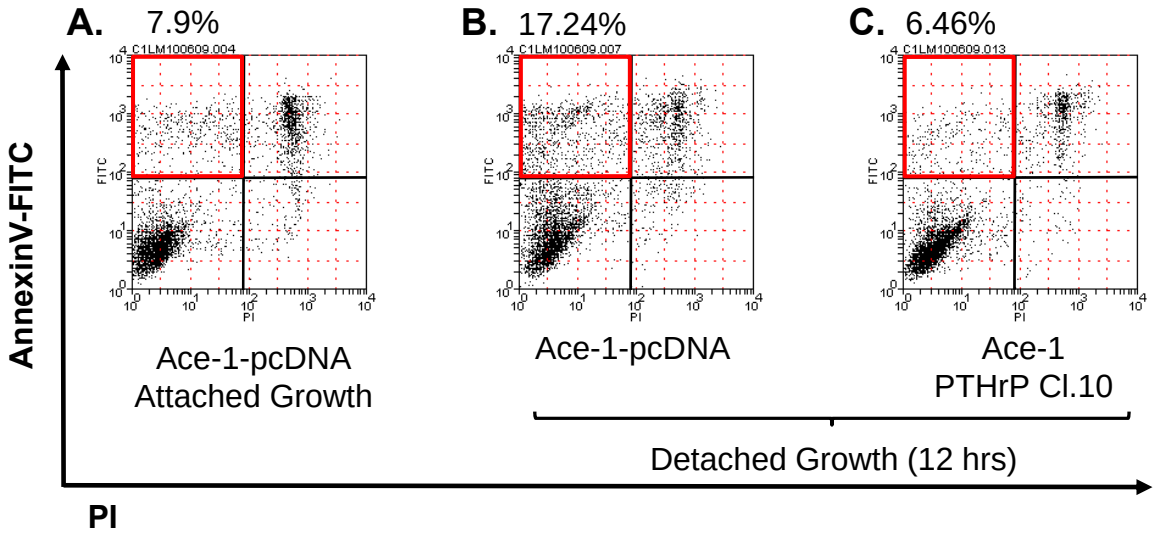
A. 7.9%
B. 17.24%
C. 6.46%
AnnexinV-FITC
PI
Ace-1-pcDNA
Attached Growth
Ace-1-pcDNA
Ace-1
PTHrP Cl.10
Detached Growth (12 hrs)

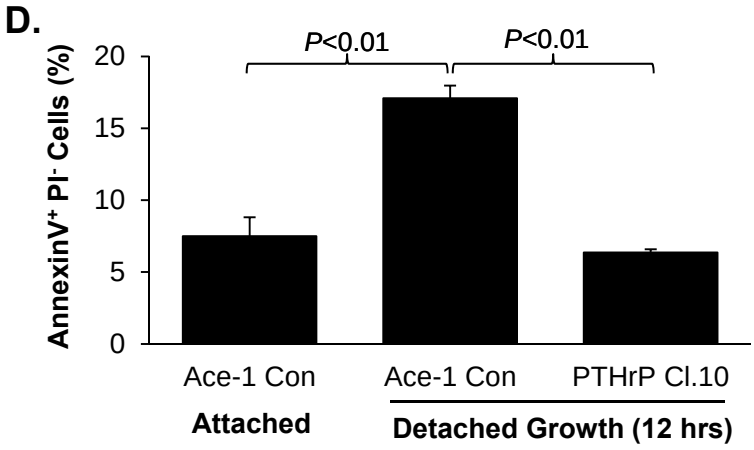
D.
P<0.01
P<0.01
AnnexinV+ PI- Cells (%)
20
15
10
5
0
Ace-1 Con
Ace-1 Con
PTHrP Cl.10
Attached
Detached Growth (12 hrs)

Figure 4

SI Park and LK McCauley

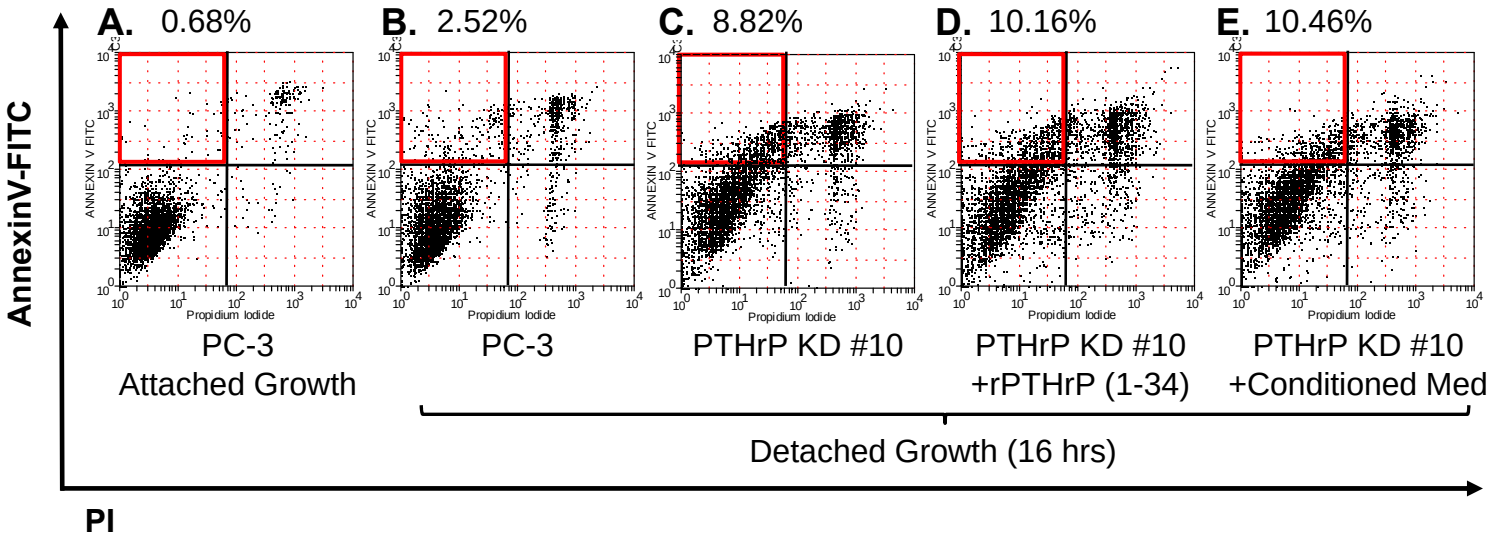

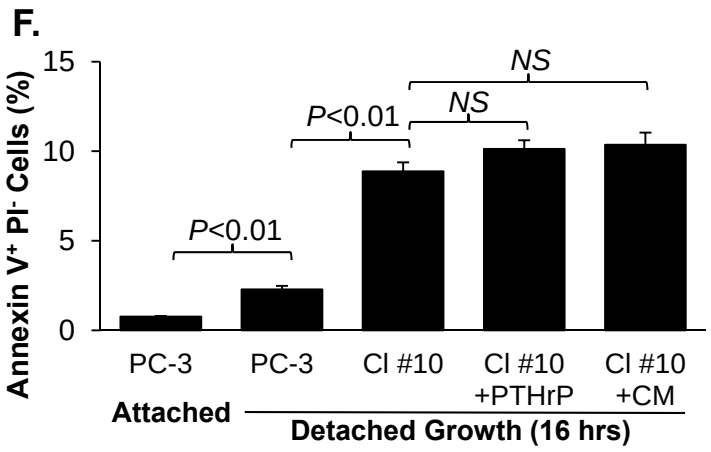

Figure 5

SI Park and LK McCauley

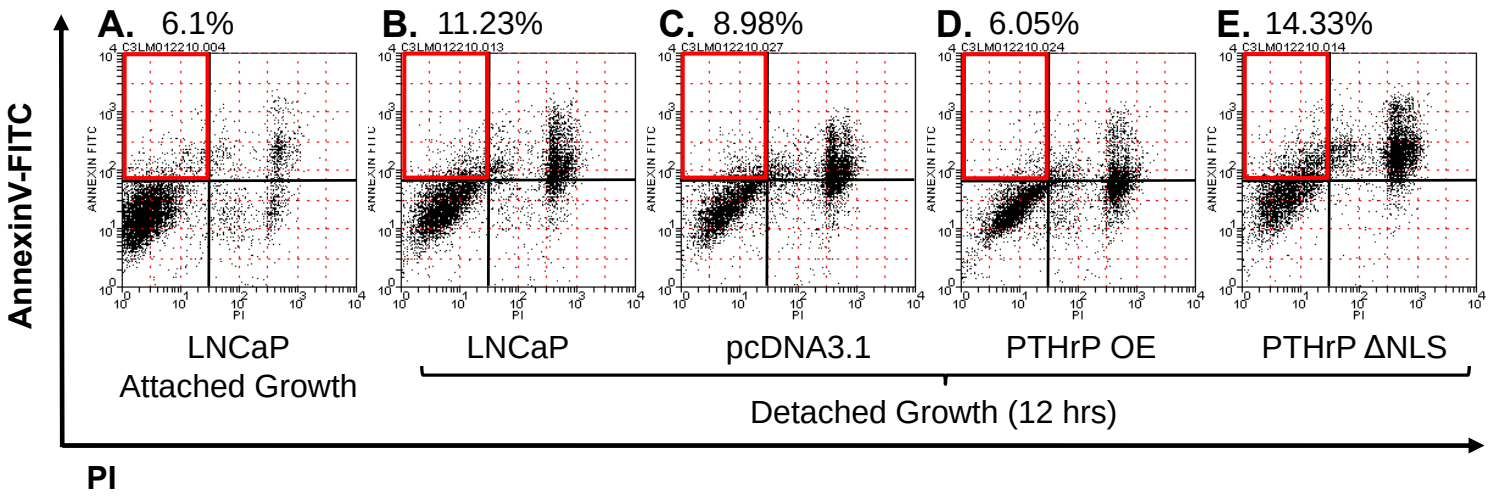

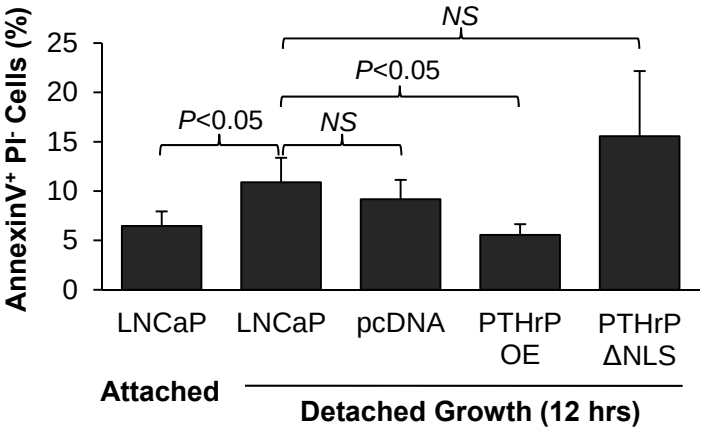

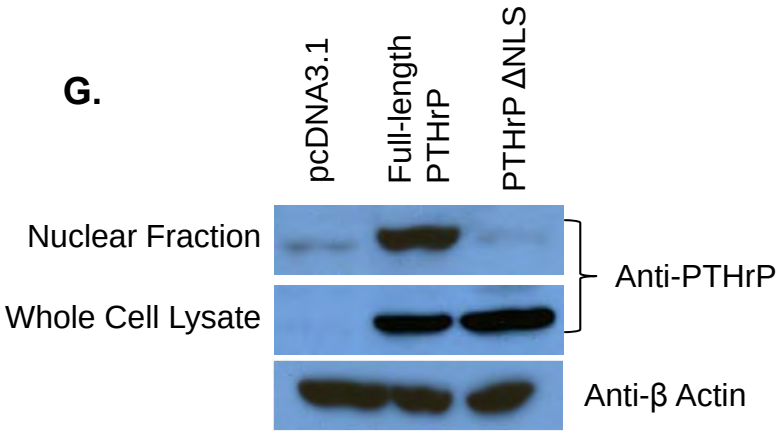

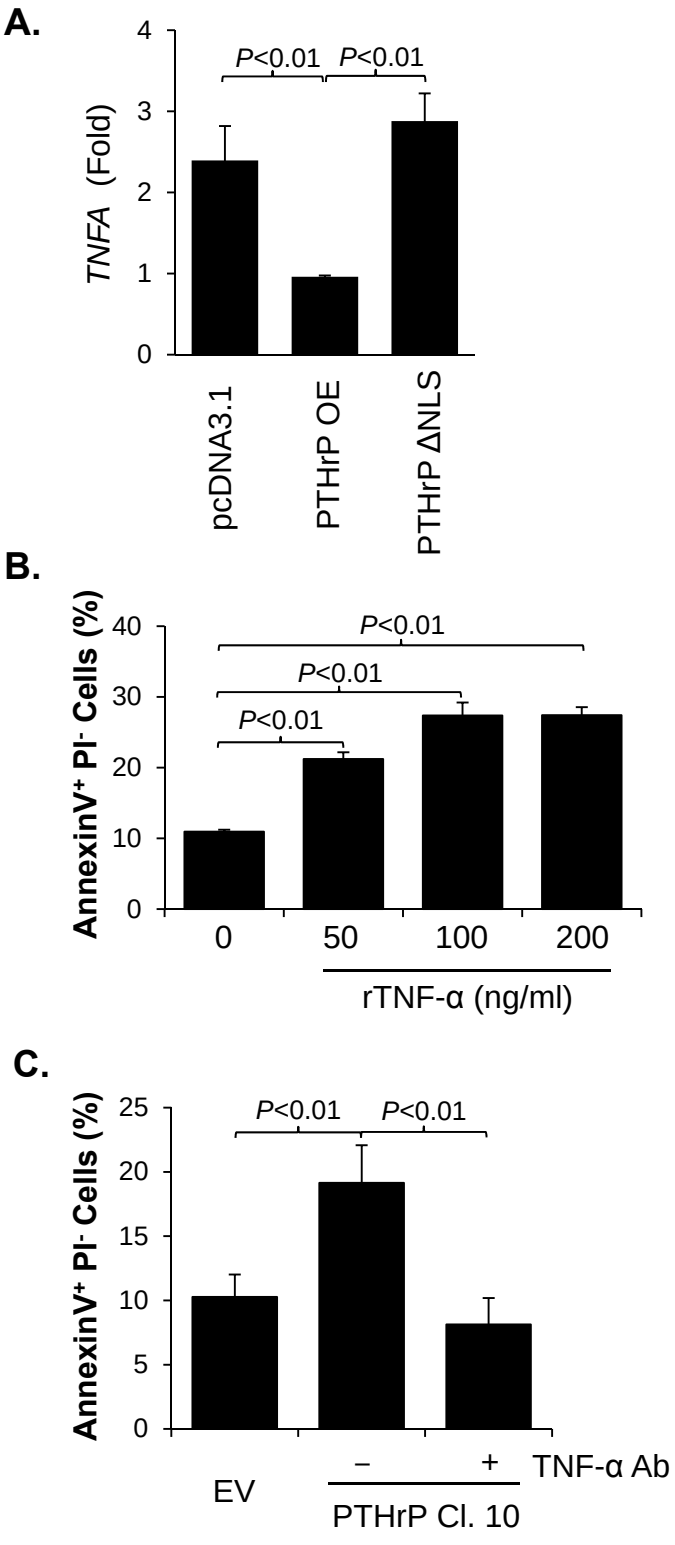
A.
P<0.01
P<0.01
TNFA (Fold)
0
1
2
3
4
pcDNA3.1
PTHrP OE
PTHrP ΔNLS
B.
AnnexinV+ PI- Cells (%)
P<0.01
P<0.01
P<0.01
0
10
20
30
40
0
50
100
200
rTNF-α (ng/ml)
C.
AnnexinV+ PI- Cells (%)
P<0.01
P<0.01
0
5
10
15
20
25
EV
–
+
TNF-α Ab
PTHrP Cl. 10

A.

Cells	Hind Limb Tumor Incidence	5 weeks after Intra-cardiac inoculation
PC-3^{Luc} Empty Vector	**14 / 14**	
PC-3^{Luc} PTHrP Cl.10	**3 / 11**	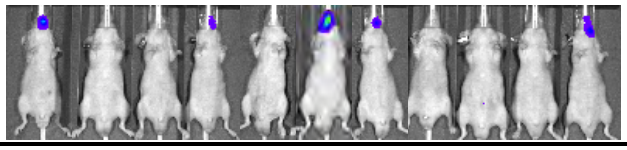

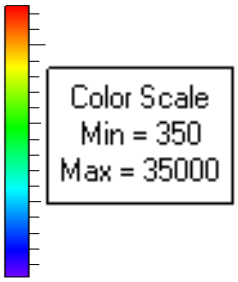

B.

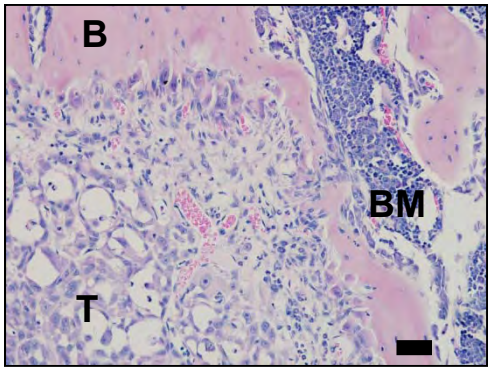

50µm

American Society for Bone and Mineral Research (ASBMR) Meeting Abstracts September 2011

[FR0139] The Impact of Macrophage Depletion on Bone Homeostasis and Prostate Tumor Growth

Fabiana Soki, University of Michigan School of Dentistry, USA; Sun Wook Cho, University of Michigan School of Dentistry, USA; Amy Koh, University of Michigan, USA; Serk In Park, University of Michigan, USA; Laurie McCauley, University of Michigan, School of Dentistry, USA.

Bone contains a population of resident macrophages termed osteomacs, which play a role in bone remodeling, repair and hematopoietic stem cell niche maintenance. Macrophages are recruited to tumors where they contribute to growth, progression and metastasis in different types of cancer. The link between macrophages residing in different compartments and their functions under various environmental stimuli remain elusive. The role of macrophages in bone and tumor growth was investigated using the macrophage fas-induced apoptosis (MAFIA) mouse model. Administration of a synthetic dimerizer (AP20187) activates a suicide gene downstream of the c-fms promoter, leading to Fas-mediated apoptosis of myeloid cells. AP20187(AP,10mg/kg) or vehicle was administered to 16 week female MAFIA mice for 3 consecutive days for initial macrophage ablation and every third day (1mg/kg) for up to 4wks. Macrophage depletion treatment resulted in splenomegaly and a 20% reduction of total bodyweight. Bone marrow flow cytometric analysis (FACS) revealed a 22% reduction of macrophages (c-fms+CD11b+F4/80+) in AP-treated mice vs. vehicle. Serum TRAP was significantly decreased (50%) after 3d of AP injection and tended to remain suppressed for 4 weeks. Bone histomorphometric analysis revealed an osteopenic phenotype with loss of bone marrow adipocytes in macrophage depleted mice. To analyze the role of macrophages in prostate cancer tumor growth, 16wk male MAFIA mice were injected with AP or vehicle for 3d (10mg/kg) and every third day (5mg/kg) for 2wks. RM-1 (mouse prostate cancer) cells were seeded subcutaneously in MAFIA mice either by injection with Matrigel or co-implanted in single vertebral bodies dissected from 7 day old C57BL/6 mice (vossicles). Macrophage (CD11b+F4/80+) numbers in Matrigel RM-1 tumors were significantly decreased in AP treated mice. FACS confirmed an 80% macrophage suppression with an increase in CD11b+ Gr1+ myeloid derived suppressor cells (MDSCs) in the bone marrow of macrophage ablated mice. RM-1 cell tumors in matrigel or vossicles showed a trend of being smaller in macrophage depleted mice. In conclusion, macrophage depletion for 4wks altered the bone phenotype and bone marrow populations. Macrophage recruitment to tumors was reduced in macrophage ablated mice and tumors were marginally smaller. These findings demonstrate the importance of macrophages in normal bone remodeling and suggest a role for macrophages in the tumor microenvironment.
Disclosure(s): Fabiana Soki has nothing to disclose.

Date: Friday, September 16, 2011
Session Info: Plenary Sessions: Welcome Reception & Plenary Poster Session (5:45 PM-7:00 PM)
Presentation Time: 5:45 pm
Room: Hall GH - San Diego Convention Center

[1088] Parathyroid Hormone-Related Peptide (PTHrP) Up-Regulates Myeloid-Derived Suppressor Cells (MDSC) in the Bone Marrow, Contributing to Prostate Cancer Growth and Angiogenesis

Serk In Park, University of Michigan, USA; William Sadler, University of Michigan, USA; Amy Koh, University of Michigan, USA; Fabiana Soki, University of Michigan, USA; Laurie McCauley, University of Michigan, School of Dentistry, USA.

The tumor microenvironment consists of primary tumor cells mixed with multiple types of stroma, in which a significant fraction originates from the bone marrow. Among those bone marrow-derived cells, $CD11b^{+}Gr1^{+}$ cells (MDSCs) correlate with tumor progression. MDSCs compromise the T cell-mediated host immune response, and serve as a predominant source of pro-tumorigenic factors such as matrix metalloproteinases (MMP). However, regulation of MDSCs in their organ of origin (i.e. bone marrow) by distant solid tumors remains unclear. PTHrP is functionally homologous with PTH, and is expressed by solid tumors including prostate cancer (PCa) that has a strong affinity for bone. This study addressed the hypothesis that PCa-derived PTHrP regulates MDSCs in the bone marrow, contributing to tumor growth and angiogenesis. Two PCa cell lines, PC-3 (expressing high basal PTHrP) and Ace-1 (expressing undetectable PTHrP), were used. PTHrP gene expression was targeted via shRNA in PC-3 cells (resulting in $PTHrP^{Hi}$ and $PTHrP^{Lo}$ PC-3 clones), whereas PTHrP was overexpressed in Ace-1 cells (resulting in Ace-1^{PTHrP} and Ace-1^{pcDNA}). Stable clones were selected and grown subcutaneously in male athymic mice. As PTHrP is a known mitogen, low-PTHrP expressing tumors were grown for a longer period, resulting in tumors of similar size between groups. Tumor tissues were then analyzed by flow cytometry, immunostaining and quantitative PCR. PCa-derived PTHrP levels correlated with MDSC recruitment in the tumor tissue and also with tumor microvessel density, potentially mediated by MDSC-derived MMP-9 expression, but not by tumor-derived VEGF. In addition, administration of recombinant PTHrP (1-34) to mice carrying Ace-1^{pcDNA} tumors expanded MDSCs both in both the tumor tissue and in bone marrow, with increased angiogenesis. Furthermore, MDSCs were sorted out by flow cytometry from the bone marrow of Ace-1^{PTHrP} or Ace-1^{pcDNA} tumor-bearing mice, followed by co-injection with tumor cells. Interestingly, tumors co-injected with MDSCs from mice bearing PTHrP-expressing tumors were significantly larger than the tumors co-injected with MDSCs from non-PTHrP tumor mice. In summary, PCa-derived PTHrP circulates to expand and potentiate MDSCs in the bone marrow, which then return to the tumor tissue contributing to tumor angiogenesis and growth. These data suggest that tumors positively regulate the bone marrow microenvironment via PTHrP expression to promote tumor angiogenesis and immune suppression.
Disclosure(s): Serk In Park has nothing to disclose.

Date: Sunday, September 18, 2011
Session Info: Oral Presentations: Concurrent Oral Session 15: Cancer and Bone (9:30 AM-11:00 AM)
Presentation Time: 10:15 am
Room: Room 32AB - San Diego Convention Center

- # Assessment of Alterations in Internal Bone Vascularity – A Three Dimensional Approach

Category: Osteoporosis - Treatment (Preclinical)

Poster Sessions, Presentation Number: SU0434
Session: Poster Session II & Poster Tours
Sunday, October 17, 2010 11:00 AM - 1:00 PM, Metro Toronto Convention Centre, South Building, South Building: Hall E

*** Jan Berry, University of Michigan, USA, Benjamin Sinder, University of Michigan, USA, Kenneth Kozloff, University of Michigan Department of Orthopaedic Surgery, USA, Robert Guldberg, Parker H. Petit Institute for Bioengineering and Bioscience , USA, Serk In Park, University of Michigan, USA, Xin Li, University of Michigan, USA, Fabiana Soki, University of Michigan, USA, Laurie McCauley, University of Michigan School of Dentistry, USA**

The vascular supply to tissues and organs is central to function and homeostasis, and also to the support of pathophysiologic conditions. A variety of techniques exist for the analysis of angiogenesis and vascular changes in extraskeletal sites, most of which are not feasible or are difficult to perform in skeletal tissues. Alterations in vascularity within the marrow cavity are strong modifiers of bone remodeling and regeneration. Three dimensional imaging through microCT analysis has provided valuable insights into osseous structure and function. Such analyses can be extended to dimensional studies of the vasculature within the bone. The purpose of this study was to analyze the impact of various bone active agents on changes in the internal bone vasculature. A perfusion technique using the radiopaque silicone rubber injection agent Microfil ™ followed by microCT analysis was utilized. Mice treated with vehicle or various agents that cause changes in the bone microenvironment (PTH, zoledronic acid, cyclophosphamide) were administered either acutely (cyclophosphamide) or over a 1-4 week period (PTH, zoledronic acid). At sacrifice, mice were perfused with lactated Ringer's solution containing 150 U/ml heparin, followed by 10% neutral buffered formalin, and then with Microfil ™ compound (1.04 specific gravity mixed 4:1 with the 0.92 specific gravity diluent). Femurs, tibiae and spleens were dissected and fixed, and bones were decalcified. Samples were analyzed by microradiography for gross differences in vascular morphology. Following radiography, bone samples were scanned in water using cone beam microCT, and reconstructed at 18-micron voxel size. Regions of interest were defined for both central bone vascularity and vascular regions near the growth plate, and quantitative differences in vessel numbers and sizes were determined using the stereology package of commercially available software. No significant quantitative changes were found in the volume of vasculature for PTH treated mice. Qualitative changes of altered vascular spaces were noted in femurs of mice treated with cyclophosphamide or zoledronic acid, however changes in spleens of these mice were not observed. This technique is valuable in providing another criteria for measuring changes in the bone microenvironment.

Invited presentation, Cancer Induced Bone Disease (CIBD) meeting, Chicago, IL December 2, 2011

Title: Bone marrow derived myeloid cells set the stage for prostate cancer (PCa) skeletal metastasis

Authors: Serk In Park, Fabiana N. Soki, Janice E. Berry, Amy J. Koh, Xin Li, Matthew R. Eber, Sudha Sud, Kenneth J. Pienta and Laurie K. McCauley

Abstract:
Bone, the congenial soil for prostate metastasis, has a complex microenvironment with multiple cell types. Prostate cancer (PCa) localizes preferentially to bones with high marrow cellularity. Recent work suggests bone marrow derived myeloid lineage cells support tumor growth, but their role in skeletal metastasis is unclear. Perturbation of myeloid cells was used as a platform to analyze an altered microenvironmental impact on skeletal metastasis using multiple approaches. The bone marrow suppressive chemotherapeutic cyclophosphamide (CY) was administered and flow cytometric analysis of CD11b+ cells performed. CD11b+ cells were decreased at 3 and 15d, and expanded at 7 and 10d after CY administration. Luciferase-labeled PCa cells ($PC\text{-}3^{Luc}$) were cardiac inoculated 3,7,and 15 days after CY, and followed 6wks by bioluminescence imaging. Mice primed with CY had increased incidence of bone metastasis, with larger histologic bone tumors than controls. When tumors were inoculated when myeloid lineage cells were most highly suppressed (d15) fewer metastasis positive mice were found, and when tumors were inoculated when myeloid lineage cells were high (d7) there were greater numbers of metastasis positive mice. Cytokines with myelogenic potential including C-C chemokine ligand 2 (CCL2/MCP-1), IL-6 and VEGF, were significantly increased in the serum of CY primed mice at 7d and were implicated in the increased tumor burden. Specific macrophage depletion was also orchestrated with the macrophage Fas-induced apoptosis (MAFIA) mouse model via administration of a synthetic dimerizer that targets $c\text{-}fms^{+}$ cells. Macrophage depletion resulted in splenomegaly, a 22% reduction in bone marrow c-fms+CD11b+F4/80+ cells and osteopenia. Murine prostate cancer cells implanted subcutaneously with or without vossicles (neonatal vertebrae) demonstrated significantly reduced macrophage recruitment to tumors as well as altered growth in depleted mice. In a third model system, PCa cell lines with altered PTHrP levels were shown to facilitate tumor angiogenesis and immune suppression by circulating from the primary tumor to expand myeloid lineage cells in the bone marrow which in turn contributed to tumor growth. In summary, altering the bone marrow microenvironment via chemotherapy, macrophage ablation or endocrine mediators provides evidence for the roles of myeloid lineage cells in PCa skeletal metastasis, and supports consideration of targeted clinical intervention.

Characters with spaces = 2491